PACIFIC EARTHQUAKE ENGINEERING RESEARCH CENTER

An Evaluation of Seismic Energy Demand: An Attenuation Approach

Chung-Che Chou
Chia-Ming Uang
University of California, San Diego

PEER 2000/04
FEB. 2000

An Evaluation of Seismic Energy Demand: An Attenuation Approach

Chung-Che Chou
Graduate Research Assistant

and

Chia-Ming Uang
Associate Professor of Structural Engineering
Department of Structural Engineering
University of California, San Diego

Final Report to the National Science Foundation and to
the Pacific Earthquake Engineering Research Center

PEER Report 2000/04
Pacific Earthquake Engineering Research Center
College of Engineering
University of California, Berkeley
February 2000

ABSTRACT

As a first step for the development of an energy-based procedure for seismic design and verification, establishing seismic demand in the form of absorbed energy spectra for an inelastic single-degree-of-freedom system was the main objective of this research. The absorbed energy (E_a), not the input energy or hysteresis energy, was selected as the key demand parameter because it is not only related to the yield strength but also directly attributed to the damage of the structure. Furthermore, expressing E_a in its equivalent velocity form ($V_a = \sqrt{2E_a / m}$, where m = mass), V_a converges to pseudo-velocity (V) in the special case when the structure responds elastically. Thus, the proposed V_a parameter bridges the seismic demands for both the energy-based and force-based design methods.

Based on 273 strong ground motion records from 15 earthquakes in California, an attenuation relationship was used to relate V_a to the earthquake magnitude, source-to-site distance, and site class. V_a, which represents the equivalent velocity of the geometric mean of E_a values for two randomly oriented components of each record, was computed at 27 periods (0.1 sec to 3.0 sec) for 3 ductility levels (2, 4, and 6).

The V_a spectra constructed from the attenuation relationship showed that the V_a and V spectra had similar shapes, but V is a poor index to estimate the energy demand in an inelastic system. V_a is insensitive to strain hardening, but it is significantly affected by the site class. Energy-based site amplification factors (F_a' and F_v') at short (T = 0.2 sec) and intermediate (T = 1.0 sec) periods were also developed. A comparison was also made between the V_a spectra with those of other energy quantities reported by previous researchers. An attenuation relationship for the normalized absorbed energy, defined as E_a divided by the strain energy at yield, was also developed. Finally, it is shown that the attenuation relationship developed in this study would significantly underestimate the energy demand produced by a near-field ground motion. An alternative procedure remains to be established.

ACKNOWLEDGMENTS

This work was supported by the Pacific Earthquake Engineering Research Center through the Earthquake Engineering Research Centers Program of the National Science Foundation under Award number EEC-9701568. The authors would like to acknowledge Drs. W. B. Joyner and D. M. Boore at the U.S. Geological Survey and Dr. M. Huang of the California Division of Mines and Geology for providing processed strong ground motion data.

CONTENTS

LIST OF FIGURES

LIST OF TABLES

NOMENCLATURE

$\boldsymbol{\alpha}$	Dummy vector with components equal to one for earthquake and zero otherwise
$\boldsymbol{\gamma}$	n x1 vector of ones
ξ	General predictor vector
$\boldsymbol{\beta}$	General coefficient vector
δ	Coefficient difference vector between each iteration
λ	Step factor
σ^2	Variance
σ_r^2	Variance of stage-one regression analysis
σ_1^2	Variance of nonlinear regression analysis
σ_c^2	Variance correction factor
σ_e^2	Variance of stage-two regression analysis
w	Earthquake weight for stage-two regression analysis
$\boldsymbol{\varepsilon}_r$	Random error of stage-one regression analysis
$\boldsymbol{\varepsilon}_e$	Random error of stage-two regression analysis
$\boldsymbol{\psi}_1$	Coefficient vector for stage-one regression analysis
$\boldsymbol{\psi}_2$	Coefficient vector for stage-two regression analysis
μ	Ductility factor
ν_g	Ground displacement
ν_t	Total displacement
ν	Relative displacement
R_i	Number of records for each earthquake event i
$\mathbf{e}_2$	Vector of deviations for the component $\boldsymbol{\varepsilon}_e$
F_a'	Energy-based site amplification at period equal to 0.2 sec
F_v'	Energy-based site amplification at period equal to 1.0 sec
$\widehat{Y}$	Predicted response value
A	Pseudo-acceleration
c	Viscous damping coefficient
C_y	Normalized yield force of an SDOF system (= yield force/weight)
D	Closest distance (km),
E_ξ	Damping energy
e_1	Vector of deviations for the component $\boldsymbol{\varepsilon}_r$
E_a	Absorbed energy
E_i	Absolute input energy
E_k	Kinetic energy
E_y	Maximum strain energy for an elasto perfectly plastic SDOF system

F_a	NEHRP site amplification at $T = 0.2$ sec
f_s	Restoring force
F_v	NEHRP site amplification at $T = 1.0$ sec
g	Gravitational acceleration
G_c	Dummy variable for site class C
G_d	Dummy variable for site class D
h	Fictitious depth (km)
M	Earthquake magnitude
m	Mass of system
N	Total number of earthquakes,
n	Total number of records for all earthquakes
N_a	Normalized absorbed energy
p	Total number of coefficients
S_D	Spectral displacement
T	Period of system
V	Pseudo-velocity
V_2	Variance-covariance matrix for stage-two regression analysis
V_a	Equivalent velocity (cm/sec) of absorbed energy
V_h	Equivalent velocity (cm/sec) of hysterisis energy
V_i	Equivalent velocity (cm/sec) input energy
X_1	Predictor vector for stage-one regression analysis
X_2	Predictor matrix for stage-two regression analysis
Y	Response value, and
Y_2	Response for stage-two regression analysis

1 Introduction

1.1 STATEMENT OF PROBLEM

Modern seismic provisions (FEMA 1997; ICBO 1997) adopt a force-based design procedure. Seismic demand in the form of an elastic design spectrum (either pseudo-acceleration, A, or pseudo-velocity, V) is first established. To consider the contribution from ductility in a structure, a seismic force reduction factor is used to reduce the elastic force demand to the design level. The seismic force reduction factor accounts for, among other characteristics, the ductility capacity and the system overstrength of a structure (Uang 1991). However, it is difficult to include the effect of duration-related cumulative damage in this design procedure. A displacement-based design procedure is being developed (Moehle 1992; Priestley 1997), but the same difficulty exists.

Early in the late fifties, an alternative energy-based design approach was first proposed by Housner (1956). The absorbed energy (E_a) in an elastic system is equal to the recoverable strain energy, which is related to the pseudo-velocity (V) as $E_a = 1/2 mV^2$. In an inelastic system, the absorbed energy is composed of the recoverable elastic strain energy, E_s, and the irrecoverable hysteretic energy, E_h. Housner postulated that the pseudo-velocity also be applicable for estimating the energy demand in an inelastic system. Based on 3 earthquake records, Akiyama (1985) demonstrated this assumption to be acceptable for an inelastic case, except for structures in the short period range. Expressing E_a in an equivalent velocity form, $V_a = \sqrt{2E_a/m}$, Joshi (1994) adopted an attenuation approach and used 346 records from 5 earthquakes to establish the V_a spectra for a single-degree-of-freedom (SDOF) system at several ductility levels. Based on 123 records from 10 earthquakes, Lawson (1996) also used an attenuation approach to relate a number of inelastic response parameters (e.g., strength reduction factor, maximum displacement, hysteresis energy) to the earthquake magnitude, source-to-site distance, and site class. Chapman (1999) established an attenuation relationship for the total input energy for an elastic system; a total of 303 records from 23 earthquakes in western North America was used for the study.

1.2 OBJECTIVE AND SCOPE

The overall objective of this project is to develop an energy-based procedure as a technical basis for performance-based seismic design and verification. The premise of this approach is that the energy demand to the structure on the basis of the ground motion characteristics such as earthquake magnitude, distance, and site class during an earthquake can be established, and the energy capacity of the structure can be evaluated. The year-one research objective was focused on establishing the inelastic energy demand for a single-degree-of-freedom system. The equivalent velocity (V_a) of absorbed energy was proposed as the key parameter for representing inelastic seismic demand. An attenuation model together with a two-stage regression analysis procedure (Boore and Joyner 1993) was used to express V_a as a function of the earthquake magnitude, source-to-site distance, and site class. In addition, a normalized form of the absorbed energy was considered as an index for energy demand. From the energy perspective, the effect of near-field ground motions was also included in the study.

Chapter 2 provides a summary of ground motion records used in this study. Chapter 3 presents the concepts of the energy-based theory and nonlinear two-stage regression analysis procedure used to develop attenuation relationships for seismic demands. Chapter 4 presents the regression results; results were also compared with those reported by other researchers. Chapter 5 contains a summary and conclusions drawn from this study.

2 Strong Ground Motion Database

2.1 INTRODUCTION

Building performance during an earthquake shaking is sensitive to the ground motion, which is mainly characterized by the earthquake magnitude, source-to-site distance, and site conditions. Therefore, estimation of an attenuation for earthquake ground motion has been an important research subject in the field of engineering seismology. Assessment of the attenuation relation developed for earthquake ground motion demands is strongly influenced by the selected strong motion records. From the viewpoint of statistical analysis, one major task is to collect a large number of accelerograms to enrich the database.

2.2 GROUND MOTION DATA

A total of 273 records, each containing two mutually perpendicular horizontal acceleration time histories, from 15 significant earthquakes in California (see Appendix A) were used for the analysis. These ground motions, which were recorded either at the free field or the ground level of a structure no more than two stories in height, were processed by either the California Division of Mines and Geology (CDMG), U.S. Geological Survey (USGS), or the University of Southern California (USC).

The data set is largely composed of the corrected accelerogram processed by the individual agencies mentioned before. However, all records of the 1979 Imperial Valley earthquakes and Coyote Lake earthquakes were originally uncorrected. These data were processed in this study based on a computer program (Converse 1992) provided by the USGS. The bandpass filter in low-cut frequencies at the beginning and end of a transition band is 0.125 and 0.25 Hz. The bandpass filter in high-cut frequencies at the beginning and end of a transition band is 23 and 25 Hz. The selection of filter parameters was to insure that the low-frequency noise can be suppressed and high-frequency noise can be eliminated. This was verified by visual inspection of the integrated velocity and displacement time histories for all these data sets.

2.3 MAGNITUDE

The measure of the earthquake size used in this study is expressed by the moment magnitude (M) because it defines well the physical properties of source. The moment magnitude, defined by Hanks and Kanamori (1979), is expressed in terms of the seismic moment (M_o), which is the product of three factors: the area of the rupture surface, the average slip, and the modulus of rigidity in the source zone. Strong motion records with moment magnitude 5.5 to 7.4 were incorporated in this study. Thirteen percent and fourteen percent of the records are from earthquakes with magnitude lower than 6.0 and larger than 7.0, respectively. Seventy-three percent of the data were collected with magnitude ranged from 6.0 to 7.0, which is the range of the most concern for engineers in seismic design.

2.4 SOURCE-TO-SITE DISTANCE

Various measures of the source-to-site distance have been used in the development of relationships of the ground motion (Shakal and Bernreater 1981). R_1 and R_2 in Fig. 2.1 are the hypocentral and epicentral distances, which are easily determined after an earthquake. R_3 is the distance which measures the site to the zone of the highest energy release. R_4 and R_5 are the closest distance to the rupture zone and to the vertical projection of the fault rupture. For shorter distances, the difference between measures of distance becomes more significant.

According to Campbell (1985), a fault-distance measure would tend to underestimate the actual distance to these localized sources if the strong motions are radiated from small areas of the fault rupture surface. It may be possible to identify these fault rupture surfaces for some past earthquakes, but it is impossible to anticipate their locations for future earthquakes. For this reason, either for probabilistic or deterministic applications, use of the closest distance (R_5) as the representative distance from the hypothesized earthquake is believed to be the most meaningful definition for describing the source-to-site distance, and this definition of distance has been used to develop the attenuation relation by several researchers (Boore et al. 1993; Lawson 1996; and Chapman 1999). Therefore, the closest distance (D = R_5) is used in this study and is ranged up to 118 km over all records.

2.5 SITE CLASSIFICATION

The information to classify the local soil site includes the topography, local site geology, and local site geological maps. The local site classification of each recording station was based on the average shear-wave velocity, V_s, over up to 30 m in depth from the ground surface (Borcherdt 1992; 1994). This scheme was adopted by Boore and Joyner (1993) to classify the local site condition, shown in Table 2.1, and was also incorporated into the 1997 *NEHRP Recommended Seismic Provisions* (FEMA 1997) to determine the site classification, also shown in Table 2.1. Note that the site classification used by Boore and Joyner is not the same as the NEHRP classification. Because Boore and Joyner's site A (defined as A' in this paper for clarity) includes both "rock" and "hard rock" sites, the site A' data was grouped as site A+B in this study. Distribution of data in terms of the source-site distance, earthquake magnitude, and site classification is shown in Fig. 2.2. Only 13% of the data is from the site class A+B, and 36% and 51% of the data is collected from sites C and D, respectively.

3 Energy-Based Design and Attenuation Model

3.1 INTRODUCTION

It is well known that the structural performance during an earthquake is not only a function of the peak responses (e.g., peak acceleration, displacement, and strength demand) but also a function of the ability to absorb and dissipate energy imparted to the structure. Energy absorbed by the structure can also be viewed as an index to incorporate the duration effect of the ground motion, because longer duration usually induces a large energy demand. Owing to complexities of evaluating the energy demand for a structure at a given location, an attenuation equation that can be used to estimate the energy demand is viewed as an alternative. In this study, the two-stage regression analysis developed by Boore and Joyner (1993) is adopted because it is conceptually simpler compared to the one-stage analysis. The seismic energy concept of a single-degree-of-freedom (SDOF) system in terms of the input energy, absorbed energy, and hysteretic energy is described in Section 3.2. Section 3.3 presents the history and methodology of the two-stage regression analysis.

3.2 ENERGY EQUATIONS FOR AN SDOF SYSTEM

An energy-based design procedure was first proposed by Housner (1956). The maximum absorbed (or strain) energy, E_a, in an elastic SDOF system is directly related to the pseudo-velocity, V:

$$E_a = \frac{(mA)}{2} S_D = \frac{mAS_D}{2} = \frac{m}{2} V^2 \tag{3.1}$$

where m is the mass, and S_D is the spectral displacement. Note that the energy demand in Eq. 3.1 can be expressed in the form of an equivalent velocity:

$$V = \sqrt{\frac{2E_a}{m}} \tag{3.2}$$

Housner postulated that V can also be used to estimate the energy demand in an inelastic system.

For an inelastic SDOF system subjected to a ground motion, the differential equation of motion is

$$m\ddot{\nu}_t + c\dot{\nu} + f_s = 0 \tag{3.3}$$

where c is the viscous damping coefficient, f_s is the restoring force, ν_t and ν are the total and relative displacements, respectively. The energy equation can be derived from Eq. 3.3 as follows (Uang and Bertero 1990):

$$\frac{m(\dot{\nu}_t)^2}{2} + \int_0^t (c\dot{\nu})d\nu + \int_0^t f_s d\nu = \int_0^t (m\ddot{\nu}_t)d\nu_g \tag{3.4}$$

or

$$E_k + E_\xi + E_a = E_i \tag{3.5}$$

where ν_g is the ground displacement, E_k, E_ξ, and E_i are the kinetic energy, viscous damping energy, and "absolute" input energy, respectively. The absorbed energy, E_a, is composed of the recoverable elastic strain energy, E_s, and the irrecoverable hysteretic energy, E_h.

The equivalent velocity of E_a, $V_a = \sqrt{2E_a/m}$, is used as an index for energy demand in this study because it converges to pseudo-velocity in an elastic case, which, in the form of pseudo-acceleration, is a design parameter used in modern seismic design provisions.

3.3 ATTENUATION MODEL

Joyner and Boore (1981) proposed a method using two-stage regression analysis to predict the strong earthquake ground motion response coefficients. In the first stage, the distance dependence together with a set of amplification factors, one for each earthquake, is nonlinearly regressed. In the second stage, the amplification factors were linearly regressed against the magnitude for each earthquake. The advantage of performing this analysis is that it decouples the determination of the magnitude dependence from the determination of the distance dependence. If coefficients of magnitude, distance, and local soil site were found simultaneously by performing one-stage regression analysis only, errors in measuring the magnitude would affect other coefficients. When data of the magnitude and distance are highly correlated, the two-stage analysis procedure was viewed as a remedy to decouple this dependence (Fukushima and Tanaka 1990). In this study, the two-stage regression analysis proposed by Joyner and Boore (1993) using a weighting matrix with zero off-diagonal terms were used. Moment magnitude, closest distance, site classification, and the geometric mean of two horizontal components of the response quantity for each ground motion record were used in this study.

The general equation is

$$\log Y_i = a + b(M_i - 6) + c(M_i - 6)^2 + d\log\left(D_i^2 + h^2\right)^{1/2} + eG_{ci} + fG_{di} + \varepsilon_{ri} + \varepsilon_{ei} \tag{3.6}$$

where the logarithm was based on 10, and *Yi* is the response value (the geometric mean of two horizontal components) computed from the *i-th* record at a selected natural period, *T*. M_i is the moment magnitude of the earthquake for the *i-th* record, D_i is the closest distance (km) from the station of the *i-th* record to the vertical projection of the fault rupture. *Gci* and *Gdi* are site classifications for the *i-th* record (*Gci* = 1 for class C and zero otherwise, *Gdi* = 1 for class D and zero otherwise). For each period, unknown coefficients *a, b, c, d, e, f, h,* and variance $\sigma^2_{\log \mathbf{Y}}$ of random errors $\boldsymbol{\varepsilon}_r$ and $\boldsymbol{\varepsilon}_e$ were determined from the two-stage regression analysis.

3.3.1 Stage-One Regression

Because both magnitude and distance variables are included in Eq. 3.6, errors in measuring the magnitude would affect other coefficients if all coefficients are solved simultaneously. To minimize the biased results, Eq. 3.6 can be rearranged in vector form for both stage-one and stage-two analyses:

$$\log \mathbf{Y} = \sum_{j=1}^{N} P_j \boldsymbol{\alpha}_j + d\log\left(\mathbf{D}^2 + h^2\boldsymbol{\gamma}\right)^{1/2} + e\mathbf{G}_c + f\mathbf{G}_d + \mathbf{e}_1 \tag{3.7}$$

$$\sum_{j=1}^{N} P_j \boldsymbol{\alpha}_j = a\boldsymbol{\gamma} + b(\mathbf{M} - 6\boldsymbol{\gamma}) + c(\mathbf{M} - 6\boldsymbol{\gamma})^2 \tag{3.8}$$

where *N* is the number of earthquake events, $\boldsymbol{\gamma}$ is an $n \times 1$ vector of ones, and *n* is the total number of records for all earthquakes. M is an $n \times 1$ vector with earthquake magnitudes as the entries, and $\boldsymbol{\alpha}_j$ is an $n \times 1$ dummy vector in which components are one for earthquake j and zero for others. $\mathbf{e}_1$ is a vector of deviations for the component $\boldsymbol{\varepsilon}_r$ only. Eq. 3.7 is nonlinear in terms of the unknown coefficient *h* and can be further written in the form as

$$\log \mathbf{Y} = \mathbf{X}_1 \boldsymbol{\psi}_1 + \mathbf{e}_1 \tag{3.9}$$

$$\mathbf{X}_1 = \left\lfloor \boldsymbol{\alpha}_1, \boldsymbol{\alpha}_2, \cdots, \boldsymbol{\alpha}_N, \log\left(\mathbf{D}^2 + h^2\boldsymbol{\gamma}\right)^{1/2}, \mathbf{G}_c, \mathbf{G}_d \right\rfloor \tag{3.10}$$

$$\boldsymbol{\psi}_1 = \left(P_1, P_2, \ldots, P_N, d, e, f\right)' \tag{3.11}$$

To find the optimal coefficients $\boldsymbol{\psi}_1$, direct minimization of the sum of square-error function is carried out by iterative calculations.

An approach suggested by Gauss is to use a linear approximation to the expectation function to iteratively improve the initial guess for all coefficients until they converge. For the *i-th* of Eq. 3.9:

$$\log Y_i = f(\xi_{1i}, \xi_{2i}, \ldots, \xi_{ki}; \beta_1, \beta_2, \ldots, \beta_p) + e_{1i} = f(\boldsymbol{\xi}_i, \boldsymbol{\beta}) + e_{1i} \tag{3.12}$$

$$\boldsymbol{\xi}_i = (\xi_{1i}, \xi_{2i}, \ldots, \xi_{ki})' = (\alpha_{1i}, \alpha_{2i}, \ldots, \alpha_{Ni}, D_i, G_{ci}, G_{di})' \tag{3.13}$$

$$\boldsymbol{\beta} = (\beta_1, \beta_2, \ldots, \beta_p)' = (P_1, P_2, \ldots, P_N, d, e, f, h)' \tag{3.14}$$

where k is the total number of predictors, and p is the total number of coefficients to be determined. The components of e_1 are assumed to be independent Gaussian random variables with $E(e_1) = 0$ and $V(e_1) = \sigma_1^2$, where $E(\,)$ and $V(\,)$ mean the expectation and variance. The first-order Taylor expansion of Eq. 3.12 about the point $\hat{\boldsymbol{\beta}}^0 = (\hat{\beta}_1^0, \hat{\beta}_2^0, \ldots, \hat{\beta}_p^0)'$, which is the initial guess point to the optimal value, is

$$f(\boldsymbol{\xi}_i, \boldsymbol{\beta}) = f(\boldsymbol{\xi}_i, \hat{\boldsymbol{\beta}}^0) + \sum_{j=1}^{p} \left[\frac{\partial f(\boldsymbol{\xi}_i, \boldsymbol{\beta})}{\partial \beta_j} \right]_{\boldsymbol{\beta}=\hat{\boldsymbol{\beta}}^0} (\beta_j - \hat{\beta}_j^0) \tag{3.15}$$

Assembling all n equations from n records for Eq. 3.15 gives:

$$\eta(\boldsymbol{\beta}) = \eta(\hat{\boldsymbol{\beta}}^0) + \mathbf{Z}^0 \boldsymbol{\delta}^0 \tag{3.16}$$

where Z^0 is an $n \times p$ matrix with each entry $\mathbf{Z}_{ij}^0 = \left[\frac{\partial f(\boldsymbol{\xi}_i, \boldsymbol{\beta})}{\partial \beta_j} \right]_{\boldsymbol{\beta}=\hat{\boldsymbol{\beta}}^0}$, and $\boldsymbol{\delta}^0$ is a $p \times 1$ vector with each entry $\delta_j^0 = \beta_j - \hat{\beta}_j^0$. The residual is

$$\mathrm{S}(\boldsymbol{\beta}) = \log \mathbf{Y} - \eta(\boldsymbol{\beta}) = (\log \mathbf{Y} - \eta(\hat{\boldsymbol{\beta}}^0)) - \mathbf{Z}^0 \boldsymbol{\delta}^0 = \mathrm{S}(\hat{\boldsymbol{\beta}}^0) - \mathbf{Z}^0 \boldsymbol{\delta}^0 \tag{3.17}$$

$$\mathrm{S}(\hat{\boldsymbol{\beta}}^0) = \mathbf{Z}^0 \boldsymbol{\delta}^0 + \mathrm{S}(\boldsymbol{\beta}) \tag{3.18}$$

Note that Eq. 3.18 is a normal linear equation with response $\mathrm{S}(\hat{\boldsymbol{\beta}}^0)$, design matrix $\mathbf{Z}^0$, coefficients $\boldsymbol{\delta}^0$, and error $\mathrm{S}(\boldsymbol{\beta})$. By minimizing the sum of the residual squares of Eq. 3.18, the coefficients can be written as

$$\hat{\boldsymbol{\delta}}^0 = \left(\mathbf{Z}^{0\prime} \mathbf{Z}^0 \right)^{-1} \mathbf{Z}^{0\prime} \mathrm{S}(\hat{\boldsymbol{\beta}}^0) \tag{3.19}$$

The new estimating point, $\hat{\boldsymbol{\beta}}^1$, could be computed as

$$\hat{\boldsymbol{\beta}}^1 = \hat{\boldsymbol{\beta}}^0 + \lambda \hat{\boldsymbol{\delta}}^0 \tag{3.20}$$

where λ, called the step factor (Box 1960; Hartley 1961), is introduced to guarantee that the sum of the residual squares of Eq. 3.18 for the new estimating point, $\hat{\boldsymbol{\beta}}^1$, is smaller than that for the previous point. If the full step increment (i.e., λ = 1) increases the sum of the residual squares rather than decreases it, the step will be cut in half until the rule is satisfied. Now, the initial guess $\hat{\boldsymbol{\beta}}^0$ can be replaced by the revised estimate point $\hat{\boldsymbol{\beta}}^1$; the same procedure as were described from Eqs. 3.15 through 3.20 can be repeated to get another revised estimate $\hat{\boldsymbol{\beta}}^2$. This process, incorporated in the computer program S-Plus5 (1999), will continue until the difference of the two sets of coefficients, $\hat{\boldsymbol{\beta}}^k$ and $\hat{\boldsymbol{\beta}}^{k+1}$, in the successive iteration is smaller than the prespecified value (Bates and Watts 1988). Each predictive response then can be approximated as

$$\log \hat{Y}_i = f\left(\boldsymbol{\xi}_i, \hat{\boldsymbol{\beta}}^k\right) \tag{3.21}$$

The variance, σ_1^2, of this multivariate nonlinear function can be written as

$$\sigma_1^2 = \frac{1}{n-p}\sum_{i=1}^{n}\left(\log Y_i - \log \widehat{Y}_i\right)^2 \tag{3.22}$$

Because the geometric mean of two horizontal components instead of the randomly oriented component was used to compute the response quantity Y_i, the variance for e_1 is underestimated for the prediction of the seismic demand of the random component. To account for this difference, Boore and Joyner (1993) suggested that the variance, σ_c^2, be based on the following formula:

$$\sigma_c^2 = \frac{1}{n}\sum_{i=1}^{n}\left\{\frac{1}{2}\left(\log Y_i^1 - \log Y_i^2\right)^2\right\} \tag{3.23}$$

where Y_i^j is the *j-th* component from the *i-th* record and the summation is carried out over all records for which both components are available in the earthquake event. The variance σ_r^2 is then computed as:

$$\sigma_r^2 = \sigma_1^2 + \sigma_c^2 \tag{3.24}$$

3.3.2 Stage-Two Regression

Coefficients *a, b,* and *c* in Eq. 3.8 can be determined by using the estimates of $\widehat{P}_i$ obtained from the stage-one analysis. However, the error of estimates, $\left(\widehat{P}_i - P_i\right)$, should be considered when conducting the stage-two linear regression analysis:

$$\widehat{P}_i = a + b\left(M_i - 6\right) + c\left(M_i - 6\right)^2 + (\widehat{P}_i - P_i) + \varepsilon_{ei} \tag{3.25}$$

The preceding equation shows two different sources that contribute to the covariance matrix of $\widehat{P}_i$: one is from the error of estimate, $\left(\widehat{P}_i - P_i\right)$, and the other is from the intrinsic variability ε_{ei} of the estimated quantity. By setting

$$Y_2 = \left(\widehat{P}_1, \widehat{P}_2, \ldots, \widehat{P}_N\right)' \tag{3.26}$$

$$\psi_2 = (a, b, c)' \tag{3.27}$$

$$X_2 = \begin{bmatrix} 1 & M_1 - 6 & (M_1 - 6)^2 \\ 1 & M_2 - 6 & (M_2 - 6)^2 \\ . & . & . \\ . & . & . \\ 1 & M_N - 6 & (M_N - 6)^2 \end{bmatrix} \tag{3.28}$$

Eq. 3.25 can be rewritten as

$$\mathbf{Y}_2 = \mathbf{X}_2 \boldsymbol{\psi}_2 + \left(\widehat{\mathbf{P}} - \mathbf{P}\right) + \boldsymbol{\varepsilon}_e = \mathbf{X}_2 \boldsymbol{\psi}_2 + \mathbf{e}_2 \tag{3.29}$$

where $\mathbf{e}_2$ is a vector of deviations for the component $\boldsymbol{\varepsilon}_e$. Because the covariance matrix of $\mathbf{V}(\mathbf{e}_2)$ is composed of two parts, $\mathbf{V}\left(\widehat{\mathbf{P}} - \mathbf{P}\right)$ and $\mathbf{V}(\boldsymbol{\varepsilon}_e)$, which are independent of each other, it can then be written as

$$\mathbf{V}_2 = \mathbf{V}(\mathbf{e}_2) = \mathbf{V}\left(\widehat{\mathbf{P}} - \mathbf{P}\right) + \mathbf{V}(\boldsymbol{\varepsilon}_e) = \mathbf{V}\left(\widehat{\mathbf{P}} - \mathbf{P}\right) + \sigma_e^2 \mathbf{I} \tag{3.30}$$

where I is the identity matrix, $\sigma_e^2 \mathbf{I}$ is the covariance matrix of the vector whose components are ε_{ei}, and $\mathbf{V}\left(\widehat{\mathbf{P}} - \mathbf{P}\right)$**,** the covariance matrix of the vector whose components are $\left(\widehat{P}_i - P_i\right)$ can be obtained from the stage-one regression analysis. By minimizing the sum of the residual squares for Eq. 3.29, the estimate coefficients $\widehat{\boldsymbol{\psi}}_2$ determined with a weighting matrix $\mathbf{V}_2^{-1}$ can be written as

$$\widehat{\boldsymbol{\psi}}_2 = \left(\mathbf{X}_2 \mathbf{V}_2^{-1} \mathbf{X}_2\right)^{-1} \mathbf{X}_2' \mathbf{V}_2^{-1} \mathbf{Y}_2 \tag{3.31}$$

The difficulty for processing this linear weighting regression analysis is that σ_e^2 cannot be known in advance. But it can be shown that (Searle 1971)

$$E\left(\left(\mathbf{Y}_2 - \mathbf{X}_2\hat{\boldsymbol{\psi}}_2\right)'\mathbf{V}_2^{-1}\left(\mathbf{Y}_2 - \mathbf{X}_2\hat{\boldsymbol{\psi}}_2\right)\right) = N - 3 \tag{3.32}$$

where $N-3$ is the number of degrees of freedom, and 3 being the rank of matrix $\mathbf{X}_2$. σ_e^2 can be determined by the following iterative procedures (Joyner and Boore 1993). Assuming a trial value of σ_e, $\mathbf{V}_2$ and $\hat{\boldsymbol{\psi}}_2$ can then be solved by Eqs. 3.30 and 3.31, respectively. Substitute the computed $\mathbf{V}_2$, $\hat{\boldsymbol{\psi}}_2$, and N into Eq. 3.32 to exam whether this equation is satisfied. If not, then this process is repeated until σ_e is converged to a sufficient precision for an acceptable weighting matrix.

After a simplified weighting matrix with zero off-diagonal terms was proposed by Joyner and Boore (1988), different types of weighting matrices for the stage-two analysis have been proposed by other researchers (Fukushima and Tanaka 1990; Masuda and Ohtake 1992). Joyner and Boore used a diagonal weighting matrix with each earthquake having a weight w_i given by

$$w_i = \left(\sigma_r^2 / R_i + \sigma_e^2\right)^{-1} \tag{3.33}$$

where R_i is the number of records for each earthquake event i, and σ_e^2 can be determined by an iterative process starting with a trial value (e.g., zero). Therefore, matrix $\mathbf{V}_2$ is just the inverse of the diagonal weighting matrix. Joyner and Boore (1993) made a comparison by applying these two different weighting matrices in the form of Eqs. 3.30 and 3.33, respectively, in the stage-two analysis, and the coefficients were shown to be about the same. This indicated that the weighting does not have a significant effect for the stage-two analysis. Therefore, the weighting matrix in the form of Eq. 3.33 was used for the stage-two regression analysis in this report. The overall variance, $\sigma_{\log \mathbf{Y}}^2$, is computed by combining the variance from the stage-one and stage-two analyses:

$$\sigma_{\log \mathbf{Y}}^2 = \sigma_r^2 + \sigma_e^2 \tag{3.34}$$

3.3.3 Smoothing of Parameters

Once the coefficients *a, b, c, d, e, f, and h* were obtained for each period *T*, each coefficient was smoothed by curve-fitting a cubic polynomial in the following form (Boore et al. 1994):

$$Q = C_0 + C_1 \log\left(\frac{T}{0.1}\right) + C_2\left(\log\left(\frac{T}{0.1}\right)\right)^2 + C_3\left(\log\left(\frac{T}{0.1}\right)\right)^3 \tag{3.35}$$

where Q is the coefficient to be smoothed.

4 Energy Response Spectra for an SDOF System

4.1 INTRODUCTION

Based on the two-stage regression analysis procedure described in Chapter 3, results for the absorbed energy demand for a single-degree-of-freedom (SDOF) system are presented in this chapter. Section 4.2 presents the results of pseudo-velocity (V), and the results are compared with those obtained by using similar attenuation relationships proposed by other researchers in order to validate the procedure. Section 4.3 presents the absorbed energy equivalent velocity (V_a) for different ductility factors, site classes, and source-to-site distances. Section 4.4 provides similar information for the normalized absorbed energy (N_a). The effect of near-field ground motions on the energy demand is presented in Section 4.5.

4.2 PSEUDO-VELOCITY

4.2.1 Regression Results

Smoothed coefficients of Eq. 3.6 for V were calculated using the two-stage regression analysis at 5% damping for different periods, and the results are tabulated in Table 4.1. The normalized residuals for data sets at T equal to 0.5 sec, 1.0 sec, 2.0 sec, and 3.0 sec are shown in Figs. B.1 to B.4 in Appendix B. The normalized residuals were plotted to verify if they follow any kind of pattern, and no pattern was observed. One set of normalized residuals against another set of quantities of standard normal distribution is also shown in a normal quantile-quantile plot (normal qq plot). That the points in this plot cluster along a straight line means that the normalized residual distribution follows the standard normal distribution.

The regressed curves of P_i versus $(M_i - 6)$ in the stage-two analysis is shown in Fig. B.5. The relationships of period versus the unsmoothed and smoothed coefficients are shown in Fig B.6.

It shows that the cubic polynomials can capture the trend of the coefficient distribution along the period. Fig. 4.1 compares the pseudo-velocity regression spectra based on the unsmoothed and smoothed regression coefficients. The smoothed coefficients result in an average response along the ragged variations. Unless noted, results based on the smoothed coefficients are used in this report.

4.2.2 Comparison of Pseudo-Velocity with Other Studies

It is worthwhile to compare the pseudo-velocity response spectra developed in this study, Boore and Joyner (1993), and Chapman (1999). All three studies used the same attenuation model in Eq. 3.6. However, the number of records used by Chapman and Boore and Joyner were 303 and 112, respectively.

Figures 4.2 to 4.7 show the comparison of V for magnitudes 6 and 7 at four different site conditions. For a magnitude of 6, Figs. 4.3 and 4.4 show that the pseudo-velocity obtained by Boore and Joyner for site classes C and D is significantly higher in the period range larger than 1.0 sec. For a magnitude of 7, the pseudo-velocity response spectra from three studies show a good agreement.

4.3 EQUIVALENT VELOCITY OF ABSORBED ENERGY

4.3.1 Regression Results

Evaluation of the absorbed energy demand is limited to the SDOF system with 5% damping ratio and the bilinear hysteretic model with 0% and 5% strain hardening ratios. The coefficients of the predictive equation for V_a at ductility factors equal to 2, 4, and 6 are tabulated in Tables 4.2 to 4.4. Sample normalized residual plots and qq plots for ductility factors 4 at periods equal to 0.5 sec, 1.0 sec, 2.0 sec, and 3.0 sec periods are shown in Figs. C.1 to C.4 in Appendix C. The relationships of P_i versus $(M_i - 6)$ in the stage-two analysis are shown in Fig. C.5. The relationships of period versus the unsmoothed and smoothed coefficients are shown in Fig. C.6.

4.3.2 Effect of Distance and Magnitude

The V_a response spectra for a constant ductility factor (μ) of 4 for different site conditions are shown in Figs. 4.8 to 4.10. The V_a spectra ascend in the short period range, reach a peak value, and then decrease at a slow rate in the longer period range. V_a tends to decrease with an increase of distances and decrease of magnitudes. The increase of V_a from magnitudes of 6.5 to 7 is much bigger than that from magnitudes of 5.5 to 6.0. Peak values of V_a for all distances occur at periods in the neighborhood of 0.5 sec, depending on the site class. For a given magnitude and distance, V_a reaches the largest value at the site class D.

4.3.3 Effect of Ductility

The effect of ductility on the V_a spectra for a magnitude of 7 at different site classes are shown in Figs. 4.11 to 4.13. For comparison purposes, the pseudo-velocity spectra are also shown; pseudo-velocity corresponds to the elastic case ($\mu = 1$) for V_a. V_a increases with an increase of the ductility factor, especially from ductility factor 1 to 2. V_a continues to increase from the ductility factor 2 to 4 in the short period range (say, less than 1.0 sec) and converges at higher ductility levels. Insignificant difference of V_a was observed from ductility 2 to 6 in the long period range.

The ratio between V_a and V reflects the increase of energy demand when ductility develops. Figures 4.14 to 4.16 show the V_a/V ratio for different site classes. The V_a/V ratio, which is high especially in the short period range, increases with ductility and with the decrease of shear-wave velocity at the local site class. For the site class A+B, V_a tends to converge to V in the longer period with a source-to-site distance less than 20 km, shown in Fig. 4.14(b). Only under this circumstance is Housner's approach correct for estimating the maximum absorbed energy for structures based on V. For other cases, it is nonconservative to use the pseudo-velocity to estimate the absorbed energy demand in an inelastic system. Figure 4.17 shows that the V_a/V ratio increases with the distance. This implies a longer duration effect of distant earthquake ground motions; the duration effect is included in the response quantity of V_a, but not V.

4.3.4 Effect of Site Class

The site class has a significant effect on the V_a spectra. Figure 4.18 shows a comparison of V_a spectra for three site classes. It can be observed that V_a at site D is much higher than at other sites for a given period, distance, and magnitude. The increase of V_a from site A+B to sites C and D can be observed from Fig. 4.19. The increase in V_a is about 70% and 160% for sites C and D, respectively, in a wide range of period.

In the 1997 NEHRP Seismic Provisions (FEMA 1997), pseudo-acceleration spectral values for site class B are given at T equal to 0.2 sec and 1.0 sec. Two parameters, F_a and F_v, are then used to modify the spectral values for other site classes. At $T = 0.2$ sec, the site amplification factor, F_a, ranges from 1.0 to 1.2 for site class C and from 1.0 to 1.6 for site class D. Define the following energy-based site amplification factors for V_a values at $T = 0.2$ and 1.0 sec, respectively, in this study:

$$F_a' = \frac{V_a(T = 0.2\sec)}{V_{a(A+B)}(T = 0.2\sec)} \tag{4.1}$$

$$F_v' = \frac{V_a(T = 1.0\sec)}{V_{a(A+B)}(T = 1.0\sec)} \tag{4.2}$$

Figure 4.20(a) shows that the amplification factor F_a' is insensitive to the ductility level, and average values of 1.5 and 1.7 can be used for site classes C and D, respectively. At T= 1.0 sec, the NEHRP values of F_v range from 1.3 to 1.7 for site class C and 1.5 to 2.4 for site class D. Figure 4.20(b) shows that the average F_v' values are 1.7 to 2.6 for site classes C and D, respectively. The values of energy-based site amplification factors are generally higher than those specified in the NEHRP Provisions.

4.3.5 Effect of Strain Hardening

Figure 4.21 shows the V_a spectra with 0% and 5% strain hardening ratio for a magnitude of 7 and two ductility levels. Irrespective of the site class, strain hardening has a negligible effect on the absorbed energy. Another study (Seneviratna and Krawinkler 1997) conducted on the total dissipated energy, which is the sum of the damping energy and hysteretic energy, also showed that the energy demand is insensitive to strain hardening.

4.3.6 Comparison of Energy Spectra with Other Studies

Based on a total of 126 ground motion records, Lawson (1996) used the same regression model, Eq. (3.6), to establish an attenuation relationship for the hysteretic energy, E_h. The larger value of two perpendicular components was used for this study rather than the geometric mean value of the response quantity. E_h can be expressed in the equivalent velocity form: $V_h = \sqrt{2E_h/m}$. (In the elastic case, V_h is equal to zero, while V_a converges to V.) Keeping in mind the differences between these two energy quantities, a comparison of V_h and V_a spectra in Fig. 4.22 do show that the trend is similar. For a ductility factor of 2, V_a is generally larger V_h than [see Fig. 4.22(a)], because the recoverable elastic strain energy, E_s, contributes more to the absorbed energy demand in relation to the hysteretic energy, E_h. This discrepancy between the V_h and V_a spectra is reduced or even reversed at the higher ductility level or larger source-to-site distance, shown in Figs. 4.22(b), (c), and (d).

Chapman (1999) established attenuation relationships of the elastic input energy spectra based on a total of 303 ground motion records. The geometric mean of two horizontal components was used for the analysis. The input energy is expressed in the equivalent velocity form, $V_i = \sqrt{2E_i/m}$. Because E_i includes both the kinetic energy (E_k) and viscously damped energy (E_ξ), Fig. 4.23 shows that V_i significantly overestimates the absorbed energy (V_a) that contributes to the damage of the structure.

4.4 NORMALIZED ABSORBED ENERGY

The absorbed energy can also be expressed in a nondimensional form, which is related to the yield force level of the system. The normalized absorbed energy, N_a, is defined as the absorbed energy divided by the recoverable strain energy at yield. (N_a converges to one in the elastic case.) For a given period, N_a can be represented by:

$$N_a = \frac{E_a}{E_y} = \frac{mV_a^2/2}{mg^2C_y^2T^2/8\pi^2} = \frac{4\pi^2}{T^2}\frac{V_a^2}{C_y^2g^2} \tag{4.3}$$

where C_y is the yield force normalized by the weight, and E_y $(= mg^2C_y^2T^2/8\pi^2)$ represents the maximum strain energy that can be stored in an elasto-perfectly-plastic SDOF system. Smoothed coefficients for the predictive equation of N_a at ductility factors of 2, 4, and 6 are given in Tables 4.5 to 4.7.

Figures 4.24 to 4.26 show the typical N_a response spectra for different site classes. In addition to the smoothed response spectra, response spectra based on the unsmoothed coefficients are also shown for comparison purposes. It is interesting to note that N_a is sensitive to the ductility level. For a given ductility, however, N_a is a very stable quantity for a wide range of period. Fig. 4.27 shows that N_a increases with the distance at a higher ductility level, but not so when the ductility is low. The N_a spectrum is not sensitive to the site class either, except when the ductility factor is larger than 4 (see Fig. 4.28). Figures 4.29 to 4.31 show the effect of strain hardening on the N_a spectra from three site classes. For a ductility factor of 2 or 4, strain hardening does not have a significant effect on N_a. But N_a for a system without strain hardening tends to be larger at a higher ductility level, especially when the distance is short.

4.5 NEAR-FIELD GROUND MOTION EFFECT

Ground motions recorded near the fault impose unusually high deformation demand to structures (Hall et al. 1995; Krawinkler and Alavi 1998). This type of ground shaking also induces higher energy demand to the structure than the far-field ground motion. Four near-field ground motion records from two California earthquakes—the 1979 Imperial Valley and 1994 Northridge events—were used in this study (see Fig. 4.32). The ground motion time histories plotted correspond to the recording directions of the instrument. For the Imperial Valley earthquake, since the 230-degree component is normal to the fault, the velocity pulse of all stations is much more noticeable than that of the other component. For the Sylmar record of the Northridge earthquake, the velocity pulse in the 360-degree component is also larger than other component. Compared with these velocity pulses, it can be seen that the Imperial Valley earthquake produced a longer period and smoother velocity pulse than the Northridge earthquake.

4.5.1 Prediction of V_a for Near-Field Ground Motions

Figures 4.33 to 4.36 show a comparison of the geometric mean of the absorbed energy spectra and those predicted by Eq. 3.6. Except for the short period range, the figures clearly show the high energy demand from the near-field ground motions. Because an insufficient number of near-field ground motion records were included in our data sets, V_a, mainly regressed based on far-field motion, and can not reflect the near-field ground motion effect. For the Imperial Valley earthquake records, the peak value of V_a occurs around structural period 3.0 sec for ductility factor 1 or 2. These ground motions produced much more energy demand in the longer period range. Maximum V_a value reduces and shifts to the lower period range for a higher ductility factor. For the Northridge earthquake, the peak V_a value occurs around structural period 2.5 sec for ductility factor 1 or 2 and then also reduces and shifts to the lower period range.

5 Summary and Conclusions

5.1 SUMMARY

As a first step for developing an energy-based design procedure, seismic demand in the form of an absorbed energy spectrum for an inelastic single-degree-of-freedom (SDOF) system was proposed. Other than input energy, the absorbed energy was selected because it is directly related to the strength of the structure. The absorbed energy (E_a) can be conveniently expressed in the form of an equivalent velocity (V_a) by Eq. 3.2. The equivalent absorbed energy velocity was selected as a design parameter because, in the special case when the system responds elastically, it converges to the pseudo-velocity (V). As pseudo-velocity, or in a transformed form as pseudo-acceleration, is the basis for estimating the demand for a force-based design procedure in modern seismic design provisions, the proposed design parameter provides a smooth transition between these two design procedures.

An attenuation-based approach was used to establish the energy demand. For a given earthquake magnitude, source-to-site distance, site class, and ductility level, the attenuation model can be used to compute the energy demand. The attenuation model and a two-stage nonlinear regression analysis procedure, proposed by Boore and Joyner (1993) were used. The analysis was based on a total of 273 ground motion records from 15 significant earthquakes in California, with magnitudes ranging from 5.5 to 7.4 (Appendix A). Regressed coefficients after smoothing for the attenuation model in Eq. 3.6 are presented in Table 4.1 for the pseudo-velocity (elastic case), Tables 4.2 to 4.4 for the equivalent velocity of absorbed energy, and Tables 4.5 to 4.7 for the normalized absorbed energy defined in Eq. 4.3. The regressed results were compared with those proposed by other researchers. The near-fault ground motion effect from the energy perspective was also investigated.

5.2 CONCLUSIONS

Based on this study, the following conclusions can be made.

(1) With the same attenuation model but different databases, pseudo-velocity (V) response spectra produced by this study were similar to those predicted by Boore and Joyner (1993) and Chapman (2000) for earthquake magnitude 7. But the Boore and Joyner model predicted a much higher pseudo-velocity values for site classes C and D in the longer period range when the magnitude is 6 (Figs. 4.3 and 4.4).

(2) V_a is a stable index for representing the seismic demand in a ductile SDOF system. Although both V_a and V spectra have the similar shape, the pseudo velocity is a poor index to estimate the energy demand in an inelastic system, especially in the short period range.

(3) V_a is insensitive to strain hardening (Fig. 4.21). But the effect of site class on the absorbed energy is very significant. Energy-based site amplification factors at short ($T = 0.2$ sec) and intermediate ($T = 1.0$ sec) periods are presented (Fig. 4.20). These factors are in general higher than F_a and F_v specified in the 1997 NEHRP provisions.

(4) The trend of equivalent velocity spectra for the hysteresis energy (Lawson 1996) was similar to that of the V_a spectra (Fig. 4.22). But the total input energy derived from an elastic system would significantly overestimate the absorbed energy demand in an inelastic system (Fig. 4.23).

(5) The normalized absorbed energy (*Na*), which is a parameter related to the yield strength of the system, is a very stable quantity for a wide range of period (Figs. 4.24 to 4.26).

(6) Near-field ground motions impose unusual demands not only on deformation but also on absorbed energy. The attenuation relationship developed in this study cannot be applied to this type of ground motions.

REFERENCES

Akiyama, H. 1985. *Earthquake-resistant limit-state design for buildings.* Tokyo: University of Tokyo Press.

Bates, D. M., and D. G. Wattes. 1988. *Nonlinear regression analysis and its applications.* New York: John Wiley & Sons.

Boore, D. M., W. B. Joyner, and T. E. Fumal. 1993. *Estimation of response spectra and peak accelerations from western North American earthquakes.* Report No. 93-509. Menlo Park, Calif.: U.S. Geological Survey.

Boore, D. M., W. B. Joyner, and T. E. Fumal. 1994. *Estimation of response spectra and peak accelerations from western North American earthquakes.* Part 2. Report No. 94-127. Menlo Park, Calif.: U.S. Geological Survey,

Borcherdt, R. D. 1992. Simplified site classes and empirical amplification factors for site-dependent code provisions. Proc. *NCEER/SEAOC/BSSC Workshop on Site Response During Earthquakes and Seismic Code Provisions.* Los Angeles: University of Southern California.

Borcherdt, R. D. 1994. Estimates of site-dependent response spectra for design (methodology and justification). *Earthquake Spectra* 10(4): 617–53.

Box, G. E. P. 1960. Fitting empirical data. Annals of the New York Academy of Sciences 86: 792–816.

Campbell, K. W. 1985. Strong motion attenuation relations: A ten-year perspective. *Earthquake Spectra* 1(4): 759–803.

Chapman, M. C. 1999. On the use of elastic input energy for seismic hazard analysis. *Earthquake Spectra* 15(4): 607–35.

Converse, A. M., and A. G. Brady. 1992. BAP: *Basic strong-motion accelerogram processing software.* Version 1.0. Report No. 92-296A. Menlo Park, Calif.: U.S. Geological Survey.

Fukushima, Y., and T. Tanaka. 1990. A new attenuation relation for peak horizontal acceleration of strong earthquake ground motion in Japan. *Bull. Seismological Society of America* 80(4): 757–78.

FEMA. *1997. NEHRP Recommended provisions for the development of seismic regulations for new buildings.* Washington, D. C.: FEMA-302.

Hall, J. F., T. H. Heaton, M. W. Halling, and D. J. Wald. 1995. Near-source ground motion and its effects on flexible buildings. *Earthquake Spectra* 11(4): 569–605.

Hanks, T. C., and T. C. Kanamori. 1979. A moment magnitude scale. *J. of Geophysical Research* 84: 2348–50.

Hartley, H. O. 1961. The modified Gauss-Newton method for the fitting of non-linear regression functions by least squares. *Technometrics* 3: 269–80.

Housner, G. W. 1956. Limit design of structures to resist earthquakes. *Proc. 1st. World Conference Earthquake Engineering.* Berkeley, Calif.: EERI,

ICBO. *Uniform Building Code.* 1997. Whittier, Calif.: International Conference of Building Officials.

Joshi, R. 1994. Two-stage regression analysis of earthquake ground motions and seismic response. Master Thesis, (advisor: C. M. Uang). Boston, Mass.: Department of Civil Engineering, Northeastern University.

Joyner, W. B., and D. M. Boore. 1981. Peak horizontal acceleration and velocity from strong-motion records including records from 1979 Imperial Valley, California, earthquake. *Bull. Seismological Society America* 71(6): 2011–38.

Joyner, W. B., and D. M. Boore. 1988. Measurement, characterization, and prediction of strong ground motion. *Proc. Conference on Earthquake Engineering and Soil Dynamics II.* GT Div/ASCE. Park City, Utah.

Joyner, W. B., and D. M. Boore. 1993. Methods for regression analysis of strong-motion data. *Bull. Seismological Society America* 83(2): 469–87.

Krawinkler, H., and B. Alavi. 1998. Development of improved design procedures for near fault ground motions. *SMIP98 Seminar on Utilization of Strong-Motion Data.* Oakland, Calif.

Lawson, R. S. 1996. Site-dependent inelastic seismic demands. Doctoral Thesis, (advisor: H. Krawinkler). Stanford, Calif.: Department of Civil Engineering, Stanford University.

Masuda, T., and M. Ohtake. 1992. Comment on “A new attenuation relation for peak horizontal acceleration of strong earthquake ground motion in Japan” by Y. Fukushima and T. Tanaka. *Bull. Seismological Society America* 82(1): 521–22.

Moehle, J. P. 1992. Displacement-based design of R/C structures subjected to earthquakes. *Earthquake Spectra* 8(3): 403–28.

Newmark, N. M., and W. J. Hall. 1981. *Earthquake resistant design considerations and seismic design spectra.* Report No. 620/N46/1981. Oakland, Calif.: EERI.

Priestley, M. J. N. 1997. Displacement-based seismic assessment of reinforced concrete buildings. *J. Earthquake Engineering* 1(1):157–92.

Searle, S. R. 1971. *Linear models.* New York: John Wiley & Sons.

Seneviratna, G. D. P. K., and H. Krawinkler. 1997. *Evaluation of inelastic MDOF effects for seismic design.* Stanford, Calif.: Department of Civil Engineering, Stanford University.

Shakal, A. F., and D. L. Bernreuter. 1981. *Empirical analysis of near-source ground motion.* Report No. NUREG/CR-2095. U. S. Nuclear Regulatory Commission.

S-Plus 5 for UNIX Guide to Statistics. 1999. Seattle, Wash.: Mathsoft, Inc.

Uang, C. M., and V. V. Bertero. 1990. Evaluation of seismic energy in structures. Earthquake Engineering and Structural Dynamics 19(1): 77–90.

Uang, C. M., 1991. Establishing R (or R_w) and C_d factors for building seismic provisions. *J. of Structural Engineering* 117(1): 19–28.

Table 2.1 Site Classifications

NEHRP Site Class	General Description	V_s (m/sec)	Boore & Joyner (1993)
A	Hard rock	$V_s > 1500$	A′
B	Rock	$1500 \geq V_s > 760$	A′
C	Very dense soil and soft rock	$760 \geq V_s > 360$	B′
D	Stiff soil	$360 \geq V_s \geq 180$	C′
E	Soil	$180 > V_s$	D′
F	Liquefiable soils, sensitive clays, collapsible cemented soils	$180 > V_s$	D′

Table 4.1 Smoothed Coefficients for Pseudo-Velocity, *V*

(5% Damping)

T (sec)	*a*	*b*	*c*	*d*	*e*	*f*	*h* (km)	$\sigma_{\log \mathbf{Y}}$
0.1	1.679	0.413	-0.200	-0.925	0.100	0.100	8.131	0.224
0.2	1.805	0.404	-0.158	-0.802	0.164	0.209	6.206	0.255
0.3	1.835	0.363	-0.083	-0.762	0.189	0.263	5.240	0.267
0.4	1.838	0.331	-0.021	-0.746	0.201	0.296	4.670	0.275
0.5	1.830	0.310	0.028	-0.740	0.208	0.319	4.311	0.280
0.6	1.818	0.298	0.065	-0.738	0.212	0.335	4.080	0.284
0.7	1.804	0.293	0.093	-0.739	0.213	0.347	3.931	0.287
0.8	1.789	0.293	0.115	-0.741	0.214	0.357	3.841	0.290
0.9	1.773	0.298	0.130	-0.744	0.213	0.364	3.793	0.293
1.0	1.758	0.305	0.142	-0.748	0.212	0.370	3.777	0.295
1.1	1.742	0.315	0.149	-0.752	0.211	0.375	3.784	0.298
1.2	1.727	0.328	0.154	-0.756	0.210	0.379	3.810	0.300
1.3	1.712	0.342	0.156	-0.760	0.208	0.382	3.851	0.302
1.4	1.698	0.357	0.156	-0.764	0.206	0.384	3.903	0.304
1.5	1.684	0.373	0.154	-0.768	0.204	0.386	3.965	0.306
1.6	1.670	0.391	0.150	-0.772	0.202	0.388	4.035	0.308
1.7	1.657	0.409	0.146	-0.776	0.199	0.389	4.111	0.310
1.8	1.644	0.428	0.140	-0.779	0.197	0.390	4.192	0.312
1.9	1.631	0.447	0.133	-0.783	0.195	0.390	4.277	0.314
2.0	1.619	0.467	0.125	-0.787	0.193	0.391	4.366	0.316
2.2	1.596	0.508	0.107	-0.794	0.188	0.391	4.553	0.319
2.4	1.573	0.550	0.087	-0.800	0.183	0.390	4.748	0.322
2.6	1.552	0.592	0.064	-0.806	0.179	0.390	4.948	0.326
2.8	1.532	0.635	0.041	-0.812	0.174	0.388	5.152	0.329
3.0	1.512	0.678	0.016	-0.817	0.170	0.387	5.359	0.332

Table 4.2 Smoothed Coefficients for V_a

(5% Damping, Ductility Factor = 2, No Strain Hardening)

T (sec)	a	b	c	d	e	f	h (km)	$\sigma_{\log \mathbf{Y}}$
0.1	1.806	0.402	-0.187	-0.882	0.113	0.119	8.734	0.228
0.2	1.862	0.406	-0.146	-0.747	0.177	0.209	5.837	0.239
0.3	1.863	0.374	-0.077	-0.704	0.203	0.266	4.756	0.245
0.4	1.850	0.348	-0.020	-0.688	0.216	0.305	4.239	0.250
0.5	1.833	0.330	0.024	-0.682	0.224	0.334	3.971	0.254
0.6	1.814	0.319	0.059	-0.681	0.229	0.355	3.834	0.257
0.7	1.795	0.314	0.086	-0.683	0.231	0.371	3.773	0.261
0.8	1.776	0.313	0.107	-0.686	0.232	0.384	3.759	0.264
0.9	1.758	0.316	0.123	-0.690	0.233	0.394	3.775	0.266
1.0	1.740	0.321	0.135	-0.694	0.232	0.402	3.812	0.269
1.1	1.723	0.329	0.143	-0.698	0.232	0.409	3.863	0.272
1.2	1.706	0.338	0.149	-0.703	0.231	0.413	3.924	0.274
1.3	1.691	0.349	0.153	-0.707	0.229	0.417	3.991	0.276
1.4	1.675	0.361	0.155	-0.712	0.228	0.420	4.064	0.279
1.5	1.660	0.374	0.155	-0.716	0.226	0.422	4.139	0.281
1.6	1.646	0.388	0.154	-0.720	0.225	0.423	4.216	0.283
1.7	1.632	0.403	0.151	-0.724	0.223	0.424	4.295	0.285
1.8	1.619	0.418	0.148	-0.728	0.221	0.424	4.374	0.287
1.9	1.606	0.434	0.144	-0.732	0.219	0.424	4.454	0.289
2.0	1.593	0.450	0.138	-0.735	0.217	0.424	4.533	0.291
2.2	1.569	0.483	0.126	-0.742	0.214	0.422	4.691	0.295
2.4	1.546	0.518	0.111	-0.749	0.210	0.419	4.847	0.298
2.6	1.525	0.553	0.095	-0.755	0.206	0.415	4.999	0.301
2.8	1.504	0.588	0.077	-0.760	0.202	0.410	5.147	0.305
3.0	1.485	0.624	0.058	-0.765	0.198	0.405	5.291	0.308

Table 4.3 Smoothed Coefficients for V_a

(5% Damping, Ductility Factor = 4, No Strain Hardening)

T (sec)	a	b	c	d	e	f	h (km)	$\sigma_{\log \mathbf{Y}}$
0.1	1.826	0.418	-0.183	-0.821	0.134	0.146	7.700	0.225
0.2	1.882	0.400	-0.106	-0.712	0.189	0.230	5.400	0.225
0.3	1.870	0.372	-0.041	-0.675	0.214	0.286	4.526	0.228
0.4	1.846	0.352	0.008	-0.659	0.227	0.326	4.111	0.231
0.5	1.819	0.340	0.044	-0.652	0.235	0.354	3.905	0.235
0.6	1.793	0.334	0.071	-0.650	0.240	0.376	3.809	0.238
0.7	1.768	0.332	0.092	-0.651	0.242	0.392	3.780	0.241
0.8	1.745	0.333	0.107	-0.653	0.243	0.404	3.791	0.244
0.9	1.723	0.337	0.120	-0.656	0.243	0.413	3.830	0.247
1.0	1.704	0.342	0.129	-0.659	0.243	0.420	3.888	0.249
1.1	1.685	0.349	0.135	-0.663	0.241	0.425	3.958	0.251
1.2	1.668	0.358	0.140	-0.667	0.240	0.429	4.037	0.254
1.3	1.652	0.367	0.143	-0.671	0.238	0.431	4.122	0.256
1.4	1.637	0.378	0.145	-0.675	0.236	0.432	4.212	0.258
1.5	1.622	0.389	0.145	-0.680	0.234	0.433	4.305	0.260
1.6	1.609	0.400	0.145	-0.684	0.231	0.433	4.399	0.262
1.7	1.596	0.412	0.143	-0.688	0.229	0.432	4.495	0.263
1.8	1.585	0.424	0.141	-0.692	0.226	0.431	4.592	0.265
1.9	1.573	0.437	0.139	-0.696	0.224	0.429	4.689	0.267
2.0	1.563	0.450	0.136	-0.700	0.221	0.427	4.785	0.268
2.2	1.543	0.476	0.128	-0.708	0.215	0.421	4.978	0.271
2.4	1.525	0.503	0.118	-0.715	0.210	0.415	5.168	0.274
2.6	1.508	0.530	0.108	-0.722	0.204	0.407	5.355	0.276
2.8	1.493	0.557	0.096	-0.729	0.198	0.400	5.538	0.279
3.0	1.480	0.585	0.084	-0.735	0.193	0.391	5.718	0.281

Table 4.4 Smoothed Coefficients for V_a

(5% Damping, Ductility Factor = 6, No Strain Hardening)

T (sec)	a	b	c	d	e	f	h (km)	$\sigma_{\log \mathbf{Y}}$
0.1	1.840	0.428	-0.178	-0.793	0.145	0.159	7.182	0.216
0.2	1.886	0.394	-0.089	-0.699	0.196	0.245	5.114	0.214
0.3	1.868	0.370	-0.026	-0.667	0.219	0.300	4.377	0.217
0.4	1.838	0.357	0.019	-0.653	0.232	0.338	4.053	0.222
0.5	1.808	0.350	0.052	-0.647	0.239	0.365	3.911	0.226
0.6	1.779	0.348	0.076	-0.645	0.243	0.384	3.862	0.230
0.7	1.752	0.349	0.095	-0.645	0.245	0.399	3.867	0.233
0.8	1.728	0.352	0.109	-0.647	0.245	0.409	3.905	0.237
0.9	1.705	0.357	0.119	-0.650	0.245	0.417	3.963	0.240
1.0	1.684	0.363	0.127	-0.653	0.244	0.423	4.035	0.242
1.1	1.665	0.371	0.133	-0.656	0.242	0.427	4.115	0.245
1.2	1.647	0.379	0.137	-0.660	0.240	0.429	4.202	0.247
1.3	1.630	0.387	0.140	-0.663	0.238	0.431	4.292	0.249
1.4	1.614	0.396	0.142	-0.667	0.236	0.431	4.384	0.251
1.5	1.600	0.406	0.142	-0.671	0.233	0.431	4.477	0.253
1.6	1.586	0.415	0.142	-0.675	0.231	0.430	4.571	0.255
1.7	1.573	0.425	0.141	-0.679	0.228	0.428	4.665	0.257
1.8	1.561	0.435	0.139	-0.683	0.225	0.426	4.758	0.258
1.9	1.550	0.446	0.137	-0.686	0.222	0.424	4.851	0.260
2.0	1.539	0.456	0.135	-0.690	0.219	0.421	4.943	0.261
2.2	1.520	0.477	0.128	-0.697	0.213	0.414	5.124	0.264
2.4	1.502	0.498	0.121	-0.704	0.207	0.407	5.300	0.266
2.6	1.486	0.519	0.112	-0.711	0.201	0.399	5.471	0.268
2.8	1.471	0.540	0.102	-0.717	0.194	0.390	5.637	0.270
3.0	1.458	0.561	0.092	-0.723	0.188	0.380	5.799	0.272

Table 4.5 Smoothed Coefficients for N_a

(5% Damping, Ductility Factor = 2, No Strain Hardening)

T (sec)	a	b	c	d	e	f	h (km)	$\sigma_{\log \mathbf{Y}}$
0.1	0.844	0.031	-0.083	0.007	-0.022	-0.050	8.860	0.299
0.2	0.575	0.057	-0.111	0.175	0.032	-0.012	17.881	0.288
0.3	0.526	0.047	-0.096	0.203	0.048	0.011	21.240	0.283
0.4	0.530	0.033	-0.076	0.199	0.053	0.027	19.684	0.279
0.5	0.551	0.020	-0.057	0.184	0.054	0.037	16.814	0.277
0.6	0.578	0.010	-0.042	0.165	0.054	0.045	13.679	0.275
0.7	0.607	0.001	-0.028	0.147	0.052	0.051	10.639	0.274
0.8	0.636	-0.007	-0.017	0.128	0.050	0.055	7.818	0.272
0.9	0.664	-0.012	-0.008	0.111	0.048	0.058	5.254	0.272
1.0	0.691	-0.017	0.000	0.094	0.046	0.060	2.946	0.271
1.1	0.716	-0.020	0.007	0.079	0.044	0.061	0.882	0.270
1.2	0.740	-0.023	0.012	0.064	0.041	0.062	0.957	0.270
1.3	0.763	-0.024	0.017	0.051	0.039	0.062	2.591	0.270
1.4	0.784	-0.025	0.020	0.038	0.037	0.062	4.039	0.269
1.5	0.805	-0.026	0.023	0.027	0.035	0.062	5.318	0.269
1.6	0.824	-0.026	0.025	0.016	0.033	0.061	6.445	0.269
1.7	0.842	-0.025	0.027	0.006	0.031	0.061	7.434	0.269
1.8	0.858	-0.024	0.028	-0.003	0.029	0.060	8.297	0.269
1.9	0.874	-0.023	0.028	-0.012	0.027	0.058	9.046	0.269
2.0	0.890	-0.022	0.029	-0.020	0.026	0.057	9.691	0.269
2.2	0.918	-0.018	0.028	-0.035	0.023	0.054	10.704	0.269
2.4	0.943	-0.013	0.026	-0.048	0.020	0.051	11.398	0.269
2.6	0.965	-0.008	0.023	-0.059	0.017	0.047	11.822	0.269
2.8	0.986	-0.002	0.020	-0.069	0.015	0.043	12.016	0.269
3.0	1.005	0.004	0.016	-0.078	0.012	0.039	12.011	0.269

Table 4.6 Smoothed Coefficients for N_a

(5% Damping, Ductility Factor = 4, No Strain Hardening)

T (sec)	a	b	c	d	e	f	h (km)	$\sigma_{\log \mathbf{Y}}$
0.1	1.308	0.086	-0.175	0.035	-0.001	-0.048	0.476	0.330
0.2	1.175	0.099	-0.131	0.158	0.052	0.002	0.163	0.309
0.3	1.149	0.065	-0.096	0.187	0.066	0.030	0.207	0.302
0.4	1.147	0.031	-0.069	0.193	0.069	0.047	0.551	0.299
0.5	1.152	0.001	-0.048	0.192	0.068	0.059	0.863	0.298
0.6	1.159	-0.023	-0.031	0.188	0.066	0.067	1.147	0.297
0.7	1.166	-0.043	-0.016	0.184	0.063	0.073	1.407	0.297
0.8	1.173	-0.058	-0.004	0.179	0.060	0.076	1.647	0.296
0.9	1.179	-0.071	0.006	0.174	0.057	0.079	1.870	0.296
1.0	1.184	-0.081	0.015	0.169	0.055	0.081	2.077	0.296
1.1	1.188	-0.089	0.023	0.165	0.052	0.082	2.273	0.296
1.2	1.192	-0.095	0.029	0.162	0.049	0.082	2.456	0.296
1.3	1.195	-0.100	0.035	0.159	0.046	0.082	2.631	0.296
1.4	1.197	-0.103	0.040	0.156	0.044	0.081	2.796	0.295
1.5	1.199	-0.105	0.045	0.153	0.042	0.081	2.953	0.295
1.6	1.200	-0.106	0.049	0.151	0.039	0.079	3.103	0.295
1.7	1.200	-0.106	0.053	0.150	0.037	0.078	3.247	0.295
1.8	1.201	-0.105	0.056	0.148	0.036	0.077	3.385	0.295
1.9	1.200	-0.104	0.059	0.147	0.034	0.075	3.518	0.294
2.0	1.200	-0.102	0.061	0.146	0.032	0.073	3.646	0.294
2.2	1.198	-0.096	0.066	0.145	0.029	0.069	3.888	0.293
2.4	1.195	-0.089	0.069	0.144	0.026	0.065	4.114	0.293
2.6	1.191	-0.081	0.071	0.145	0.024	0.060	4.327	0.292
2.8	1.186	-0.071	0.073	0.146	0.022	0.055	4.528	0.291
3.0	1.181	-0.061	0.075	0.147	0.020	0.050	4.719	0.291

Table 4.7 Smoothed Coefficients for N_a

(5% Damping, Ductility Factor = 6, No Strain Hardening)

T (sec)	a	b	c	d	e	f	h (km)	$\sigma_{\log Y}$
0.1	1.510	0.133	-0.217	0.055	0.022	-0.035	1.500	0.331
0.2	1.450	0.095	-0.150	0.164	0.056	-0.002	6.386	0.304
0.3	1.437	0.049	-0.102	0.189	0.068	0.027	6.877	0.295
0.4	1.433	0.011	-0.067	0.196	0.073	0.048	6.554	0.292
0.5	1.432	-0.019	-0.041	0.196	0.074	0.064	6.067	0.290
0.6	1.431	-0.042	-0.021	0.195	0.074	0.076	5.587	0.290
0.7	1.430	-0.060	-0.005	0.194	0.073	0.085	5.165	0.290
0.8	1.429	-0.075	0.009	0.192	0.071	0.092	4.813	0.290
0.9	1.428	-0.086	0.019	0.191	0.069	0.097	4.529	0.290
1.0	1.426	-0.095	0.028	0.191	0.067	0.101	4.309	0.290
1.1	1.424	-0.102	0.035	0.190	0.064	0.104	4.145	0.290
1.2	1.422	-0.107	0.041	0.191	0.061	0.105	4.032	0.290
1.3	1.419	-0.111	0.045	0.191	0.058	0.106	3.962	0.291
1.4	1.416	-0.113	0.049	0.192	0.056	0.107	3.932	0.291
1.5	1.413	-0.115	0.052	0.194	0.053	0.107	3.937	0.291
1.6	1.410	-0.115	0.055	0.195	0.050	0.106	3.972	0.291
1.7	1.407	-0.115	0.057	0.197	0.047	0.105	4.034	0.291
1.8	1.403	-0.114	0.058	0.200	0.044	0.104	4.121	0.291
1.9	1.399	-0.113	0.059	0.202	0.041	0.102	4.228	0.291
2.0	1.396	-0.111	0.060	0.205	0.039	0.100	4.356	0.291
2.2	1.388	-0.106	0.060	0.210	0.033	0.096	4.660	0.291
2.4	1.380	-0.100	0.059	0.217	0.028	0.091	5.020	0.291
2.6	1.371	-0.092	0.058	0.224	0.022	0.085	5.425	0.290
2.8	1.363	-0.084	0.055	0.231	0.017	0.079	5.868	0.290
3.0	1.354	-0.075	0.052	0.239	0.012	0.072	6.342	0.289

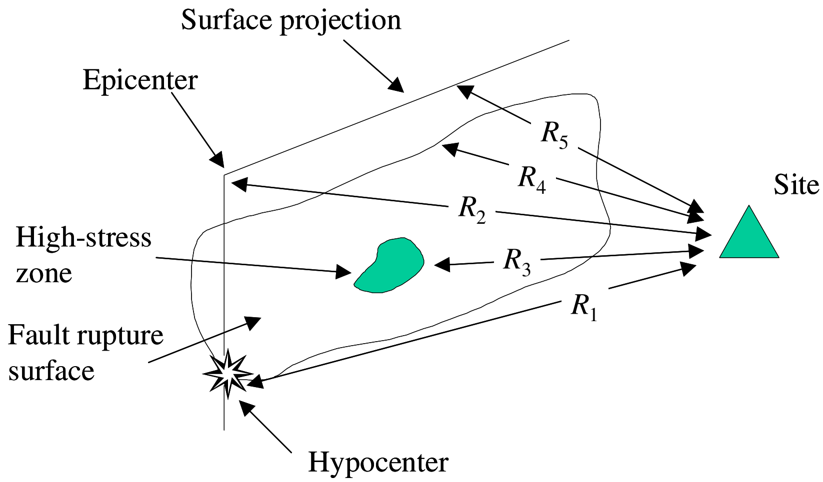

Fig. 2.1 Various Measures of Distance from Site to Fault Rupture (Shakal and Bernreuter 1981)

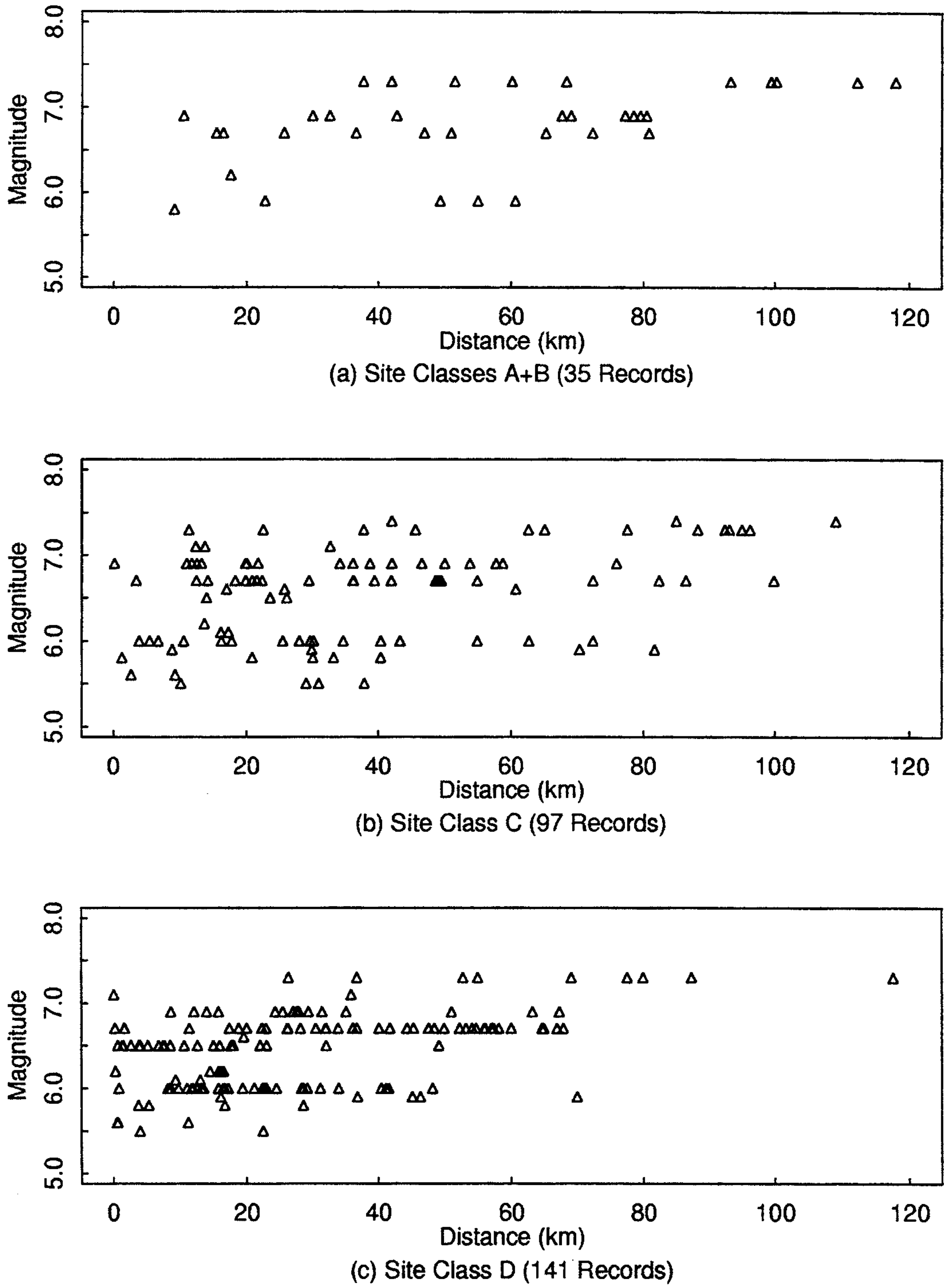

Fig. 2.2 Earthquake Magnitude versus Distance Distribution

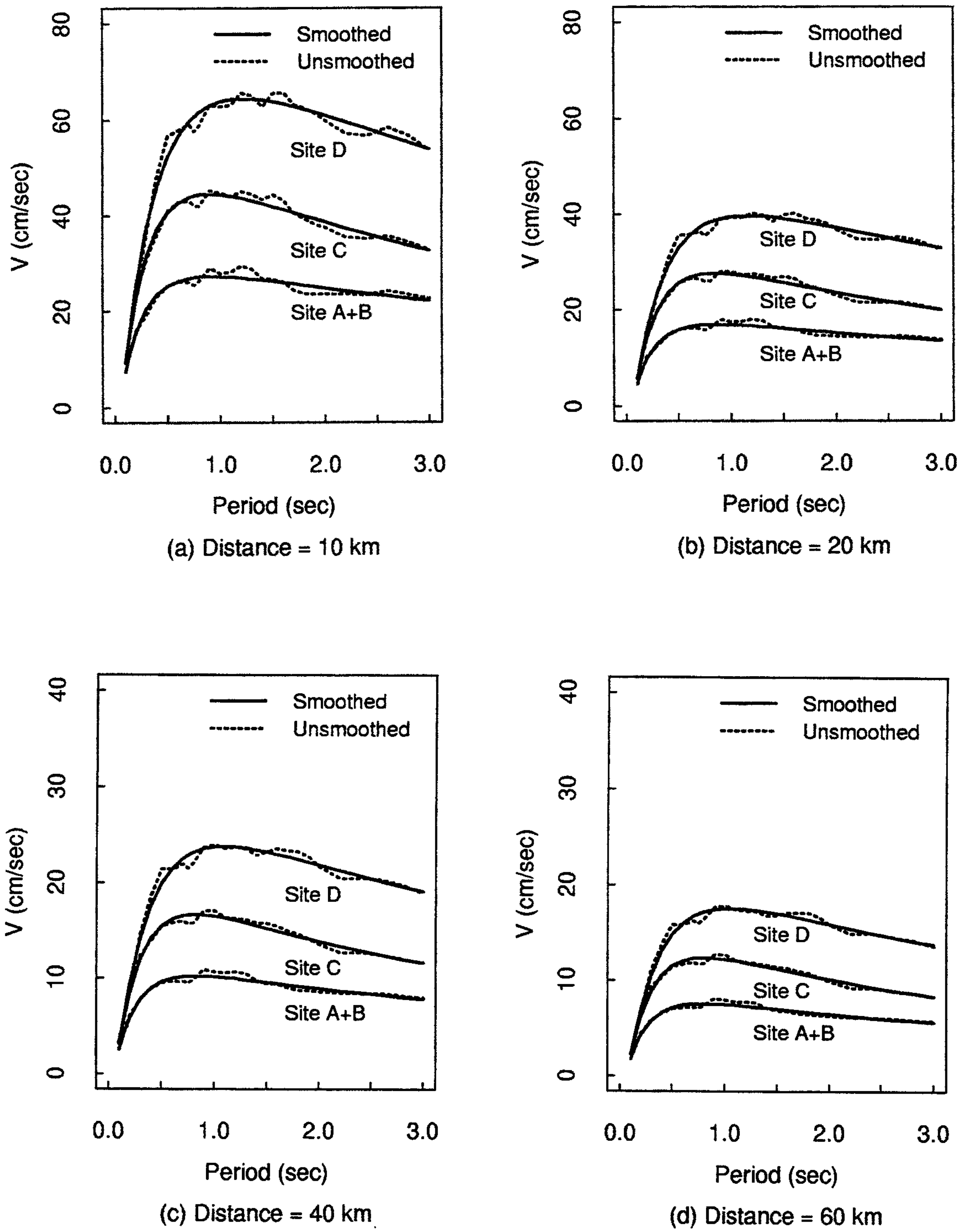

Fig. 4.1 Comparison of Smoothed and Unsmoothed Pseudo-Velocity Response Spectra (5% Damping, Magnitude = 7)

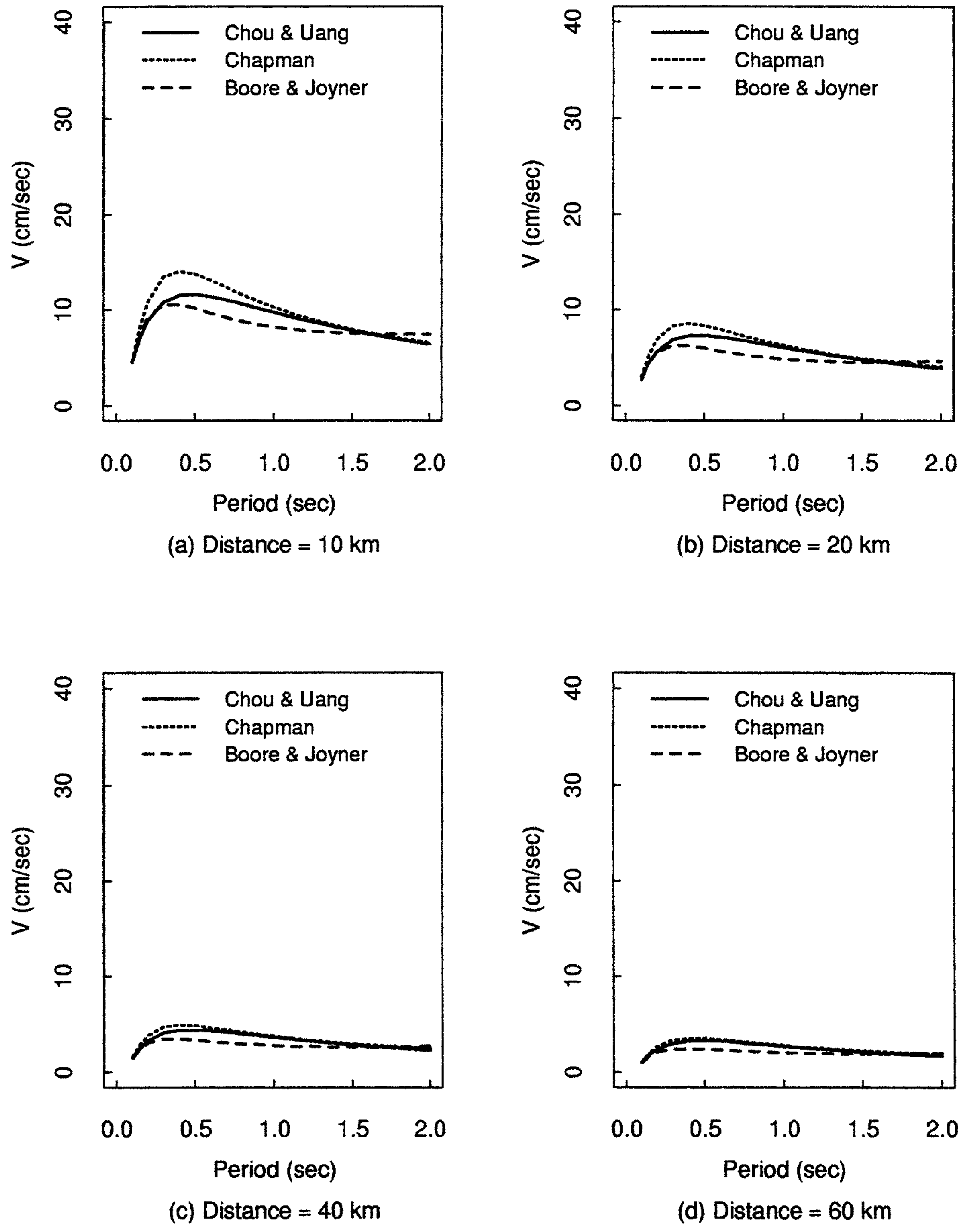

Fig. 4.2 Comparison of Pseudo-Velocity Response Spectra

(5% Damping, Magnitude = 6, Site Class A+B)

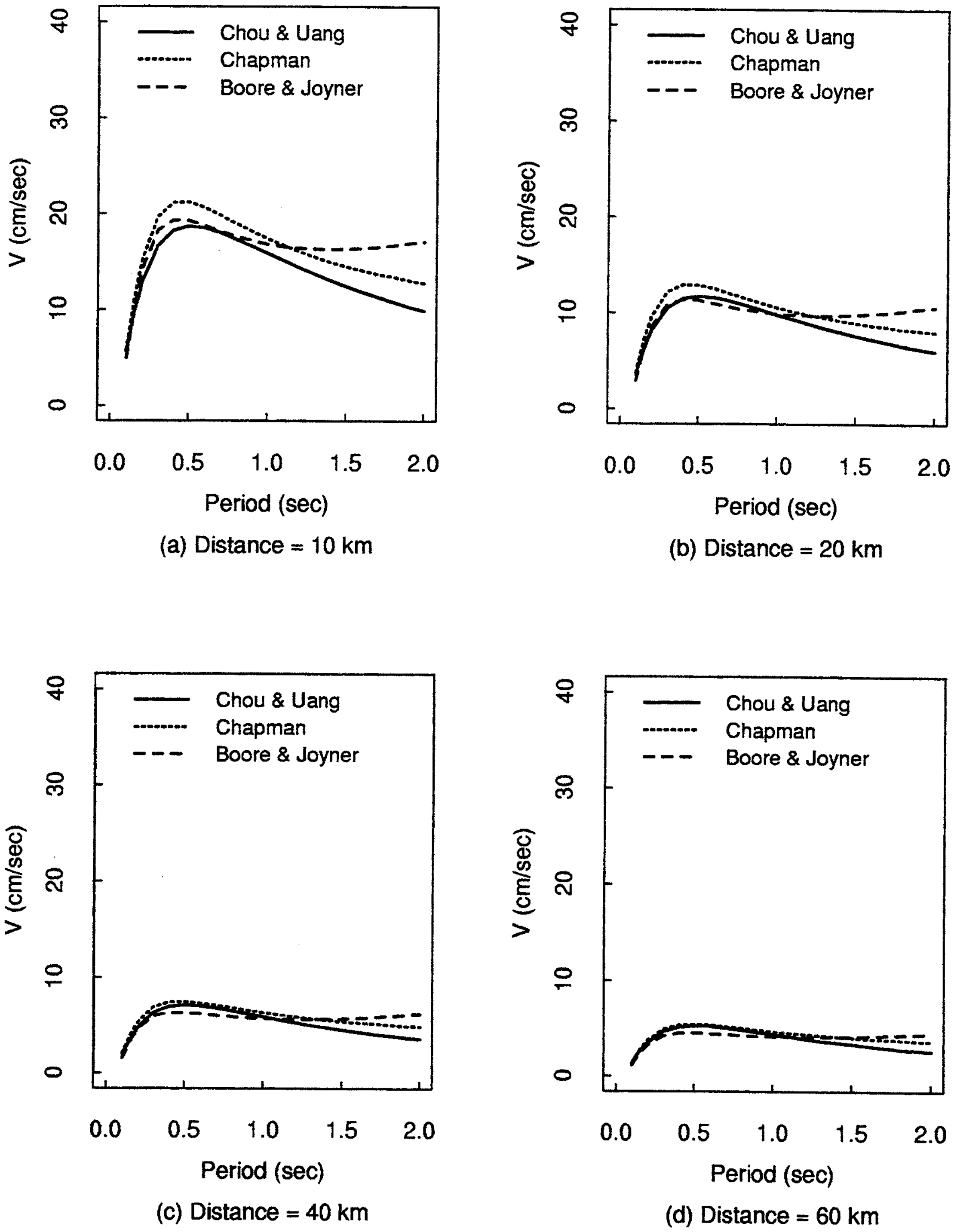

Fig. 4.3 Comparison of Pseudo-Velocity Response Spectra

(5% Damping, Magnitude = 6, Site Class C)

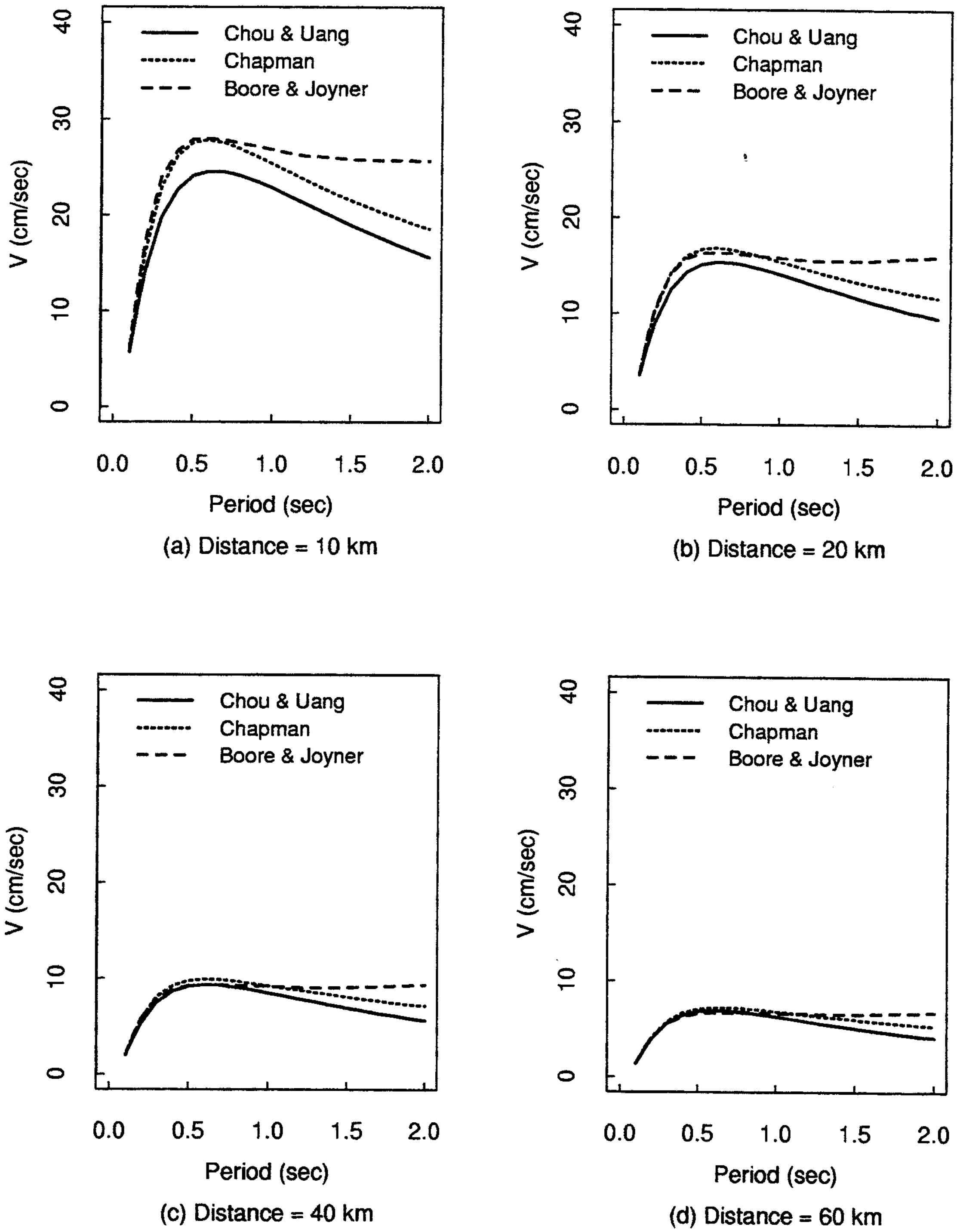

Fig. 4.4 Comparison of Pseudo-Velocity Response Spectra
(5% Damping, Magnitude = 6, Site Class D)

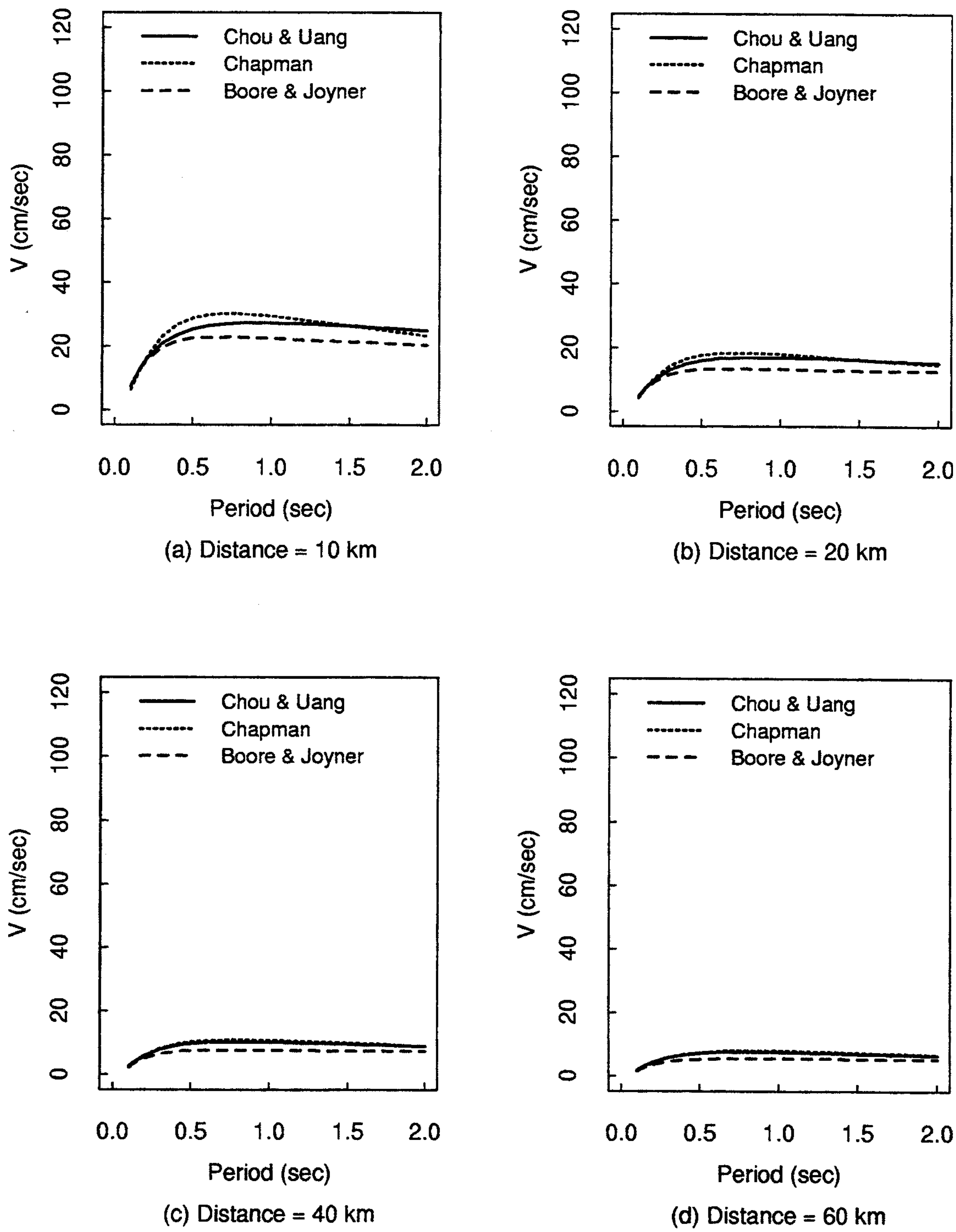

Fig. 4.5 Comparison of Pseudo-Velocity Response Spectra
(5% Damping, Magnitude = 7, Site Class A+B)

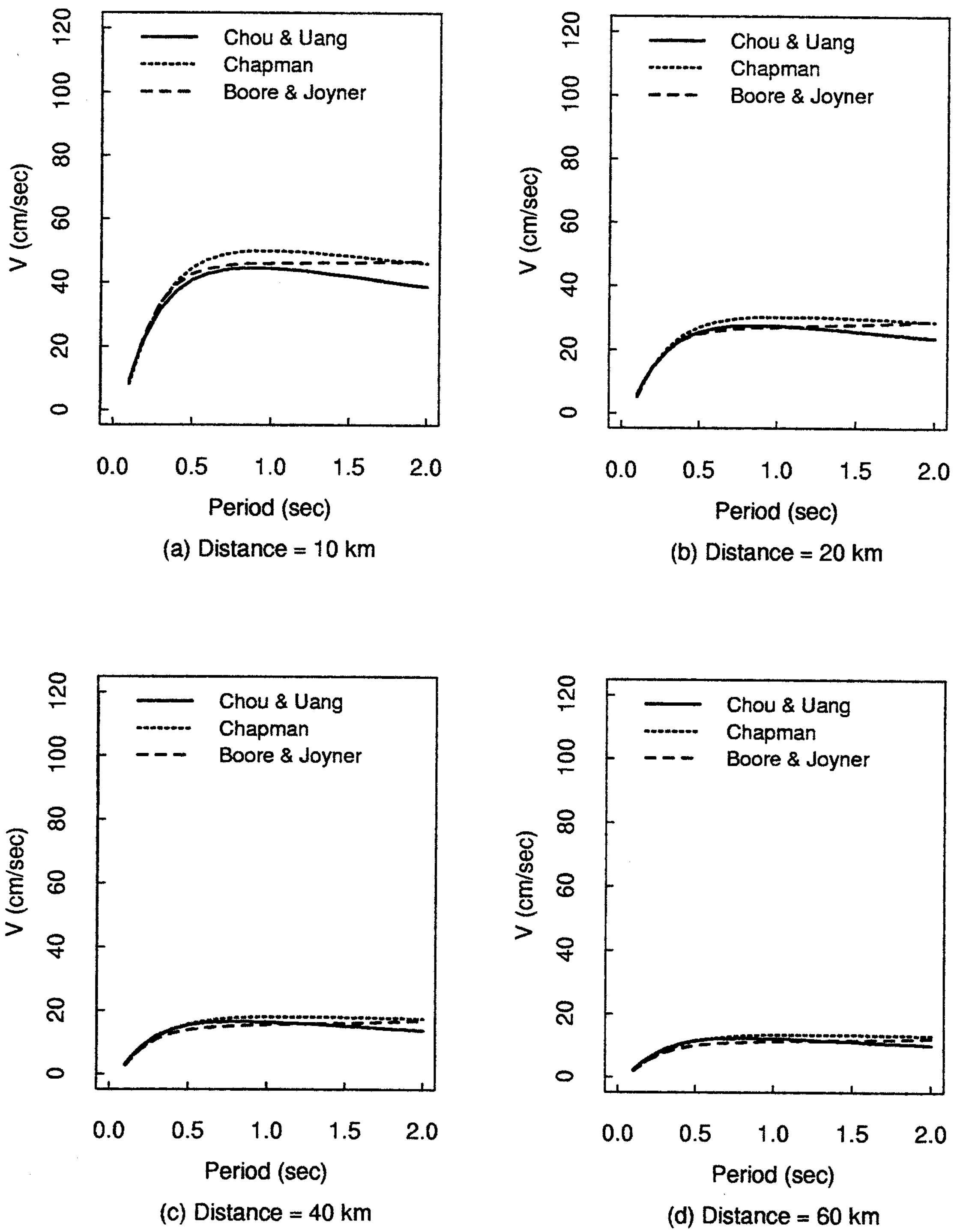

Fig. 4.6 Comparison of Pseudo-Velocity Response Spectra
(5% Damping, Magnitude = 7, Site Class C)

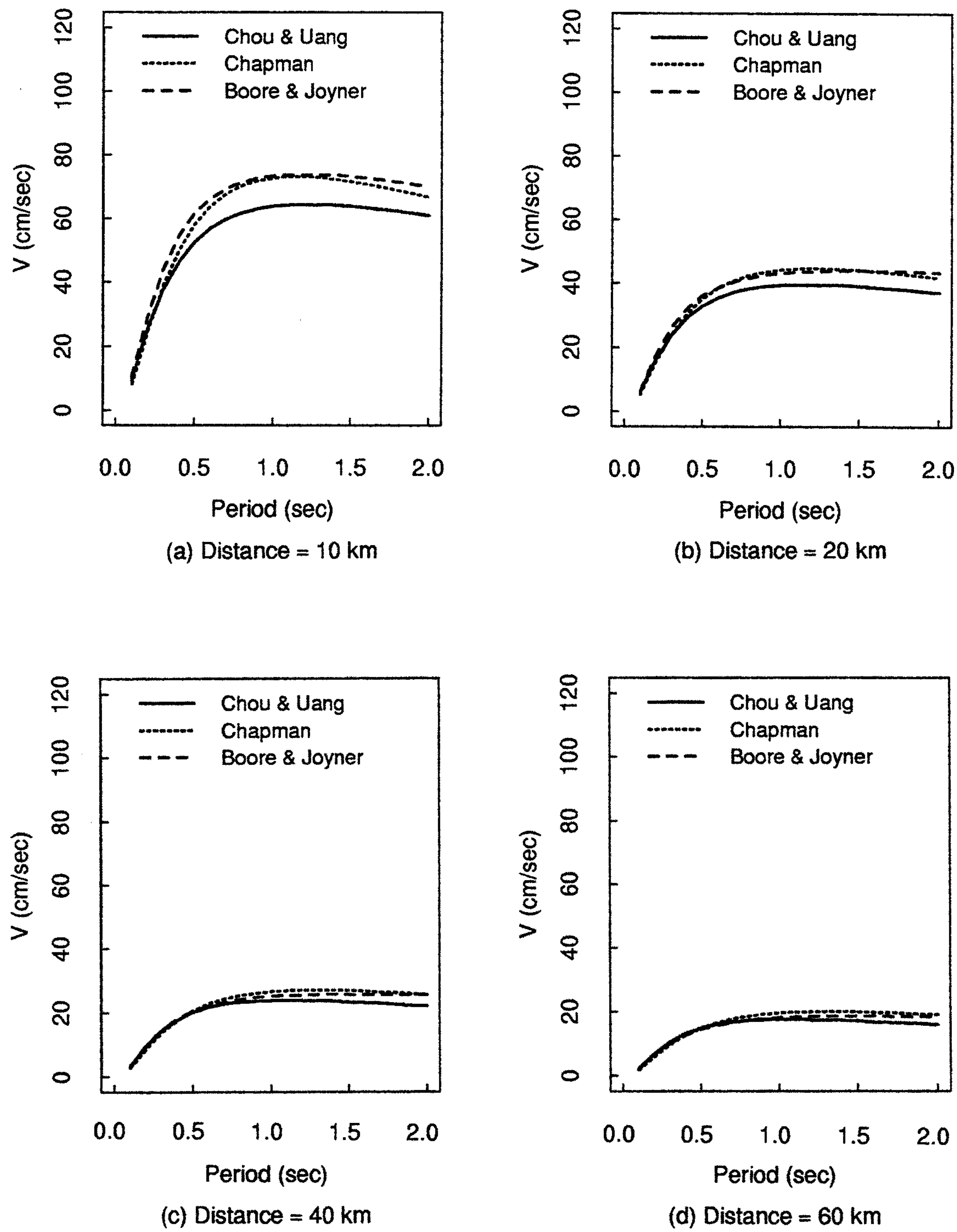

Fig. 4.7 Comparison of Pseudo-Velocity Response Spectra

(5% Damping, Magnitude = 7, Site Class D)

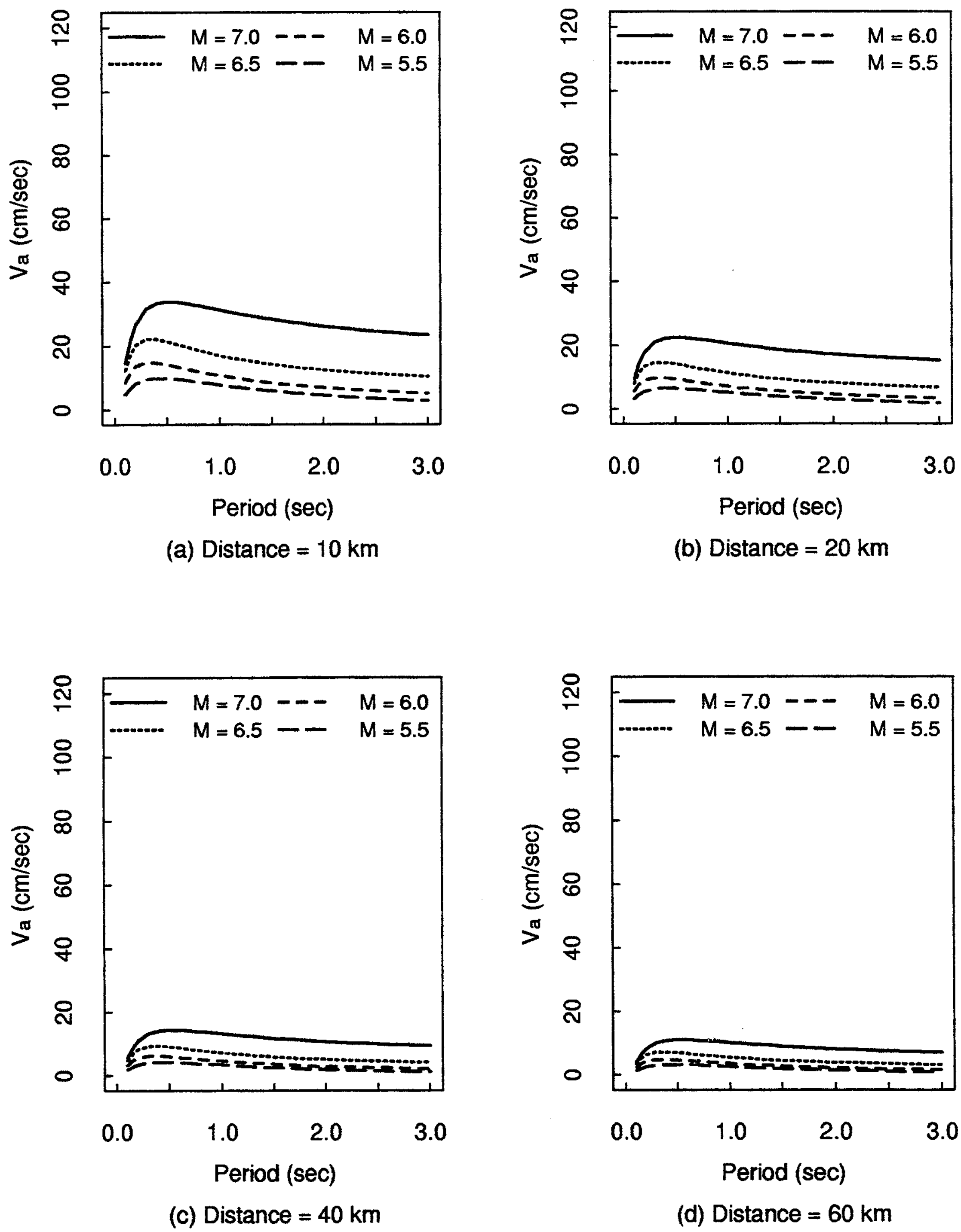

Fig. 4.8 Variations of V_a Spectra with Different Magnitudes

(5% Damping, Ductility Factor = 4, Site Class A+B)

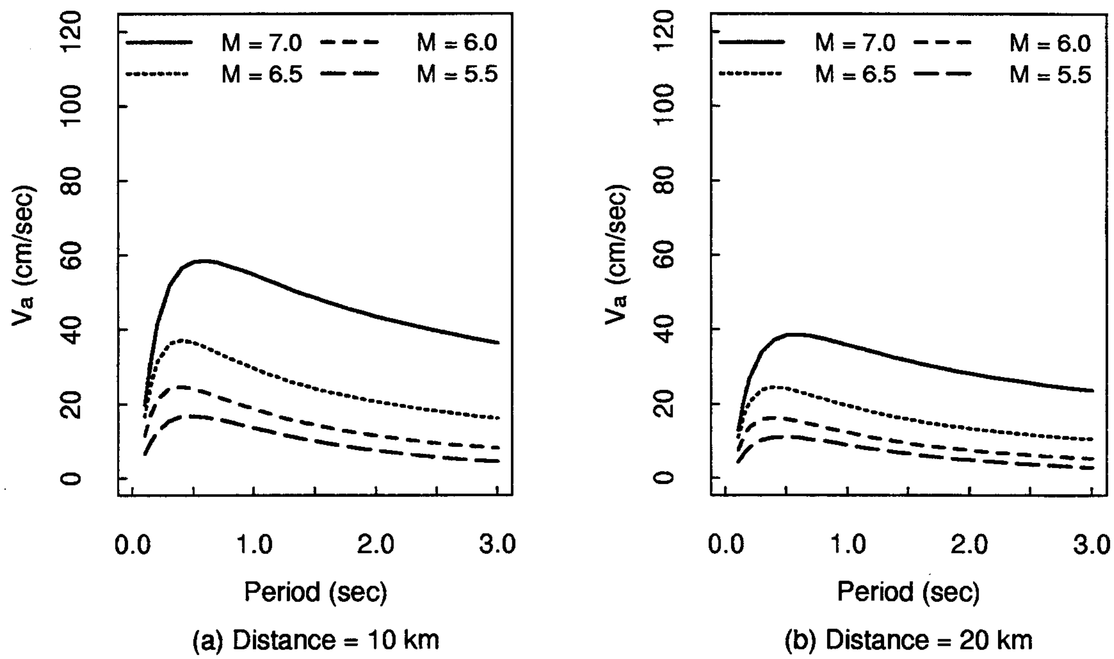

Fig. 4.9 Variations of V_a Spectra with Different Magnitudes

(5% Damping, Ductility Factor = 4, Site Class C)

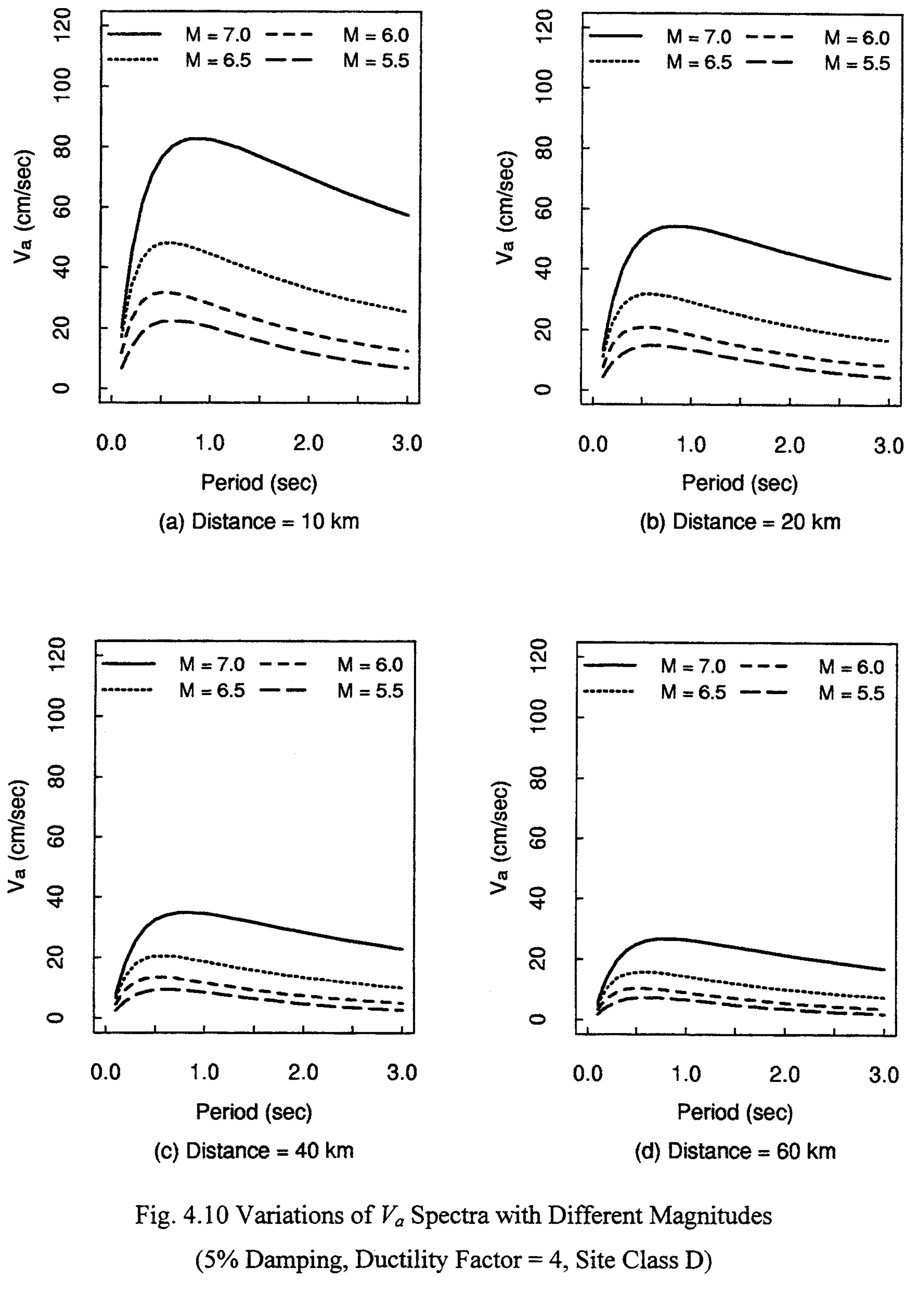

Fig. 4.10 Variations of V_a Spectra with Different Magnitudes

(5% Damping, Ductility Factor = 4, Site Class D)

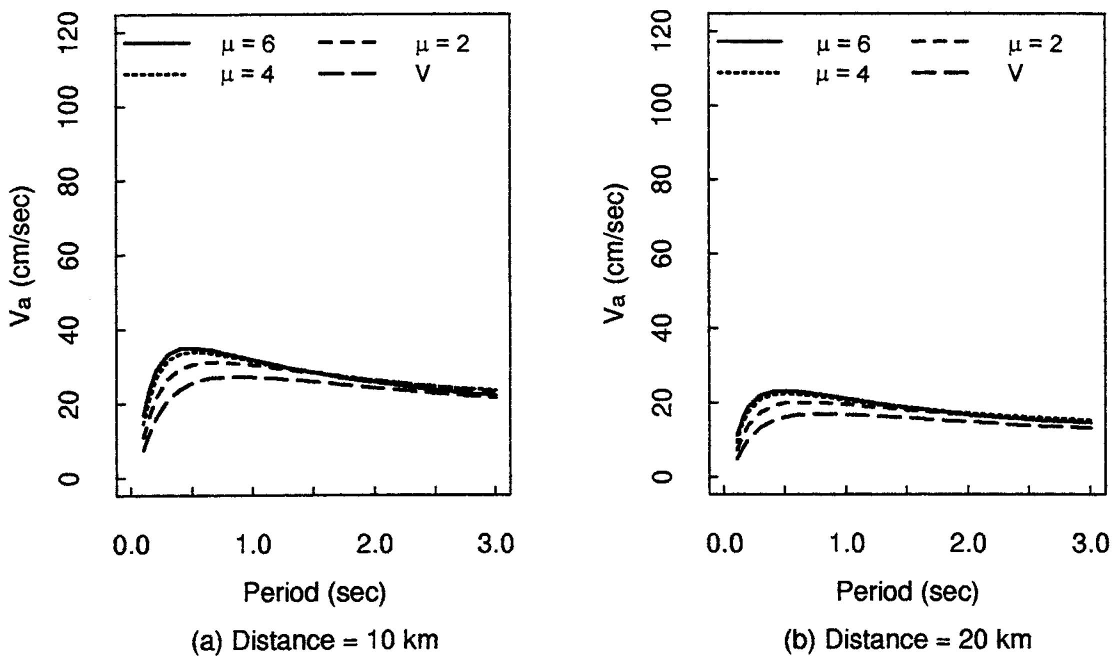

Fig. 4.11 Effect of Ductility on V_a Spectra

(5% Damping, Magnitude = 7, Site Class A+B)

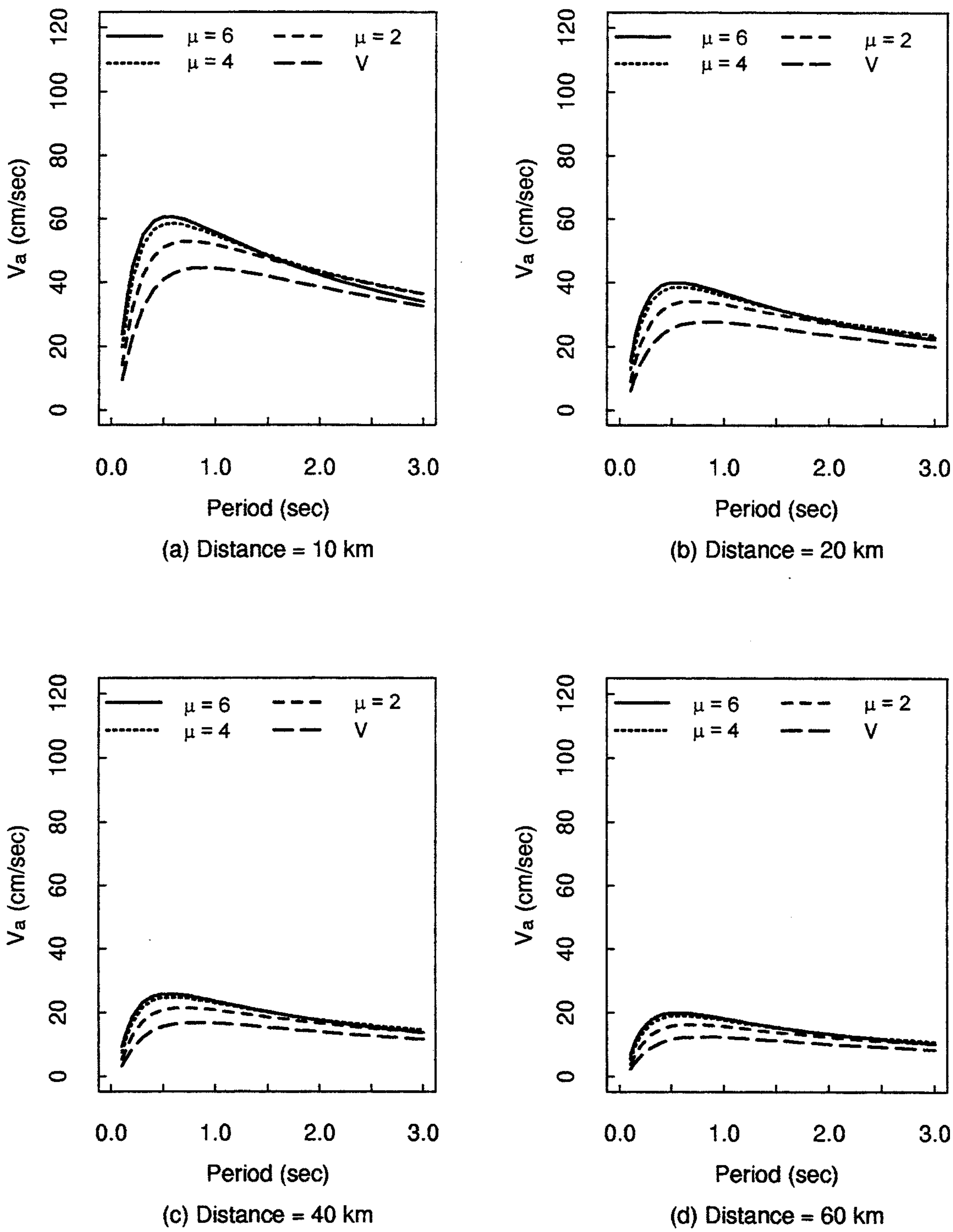

Fig. 4.12 Effect of Ductility on V_a Spectra

(5% Damping, Magnitude = 7, Site Class C)

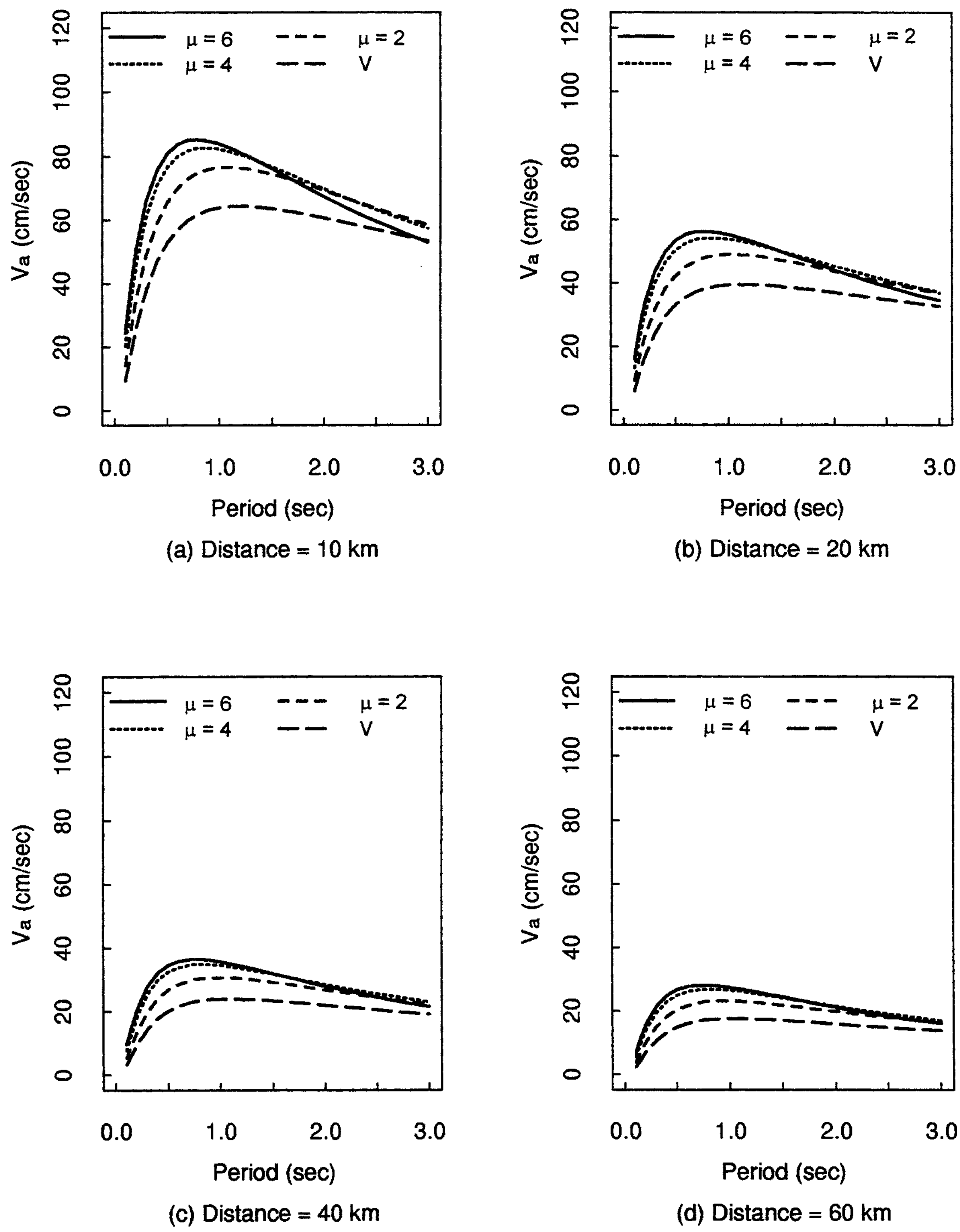

Fig. 4.13 Effect of Ductility on V_a Spectra

(5% Damping, Magnitude = 7, Site Class D)

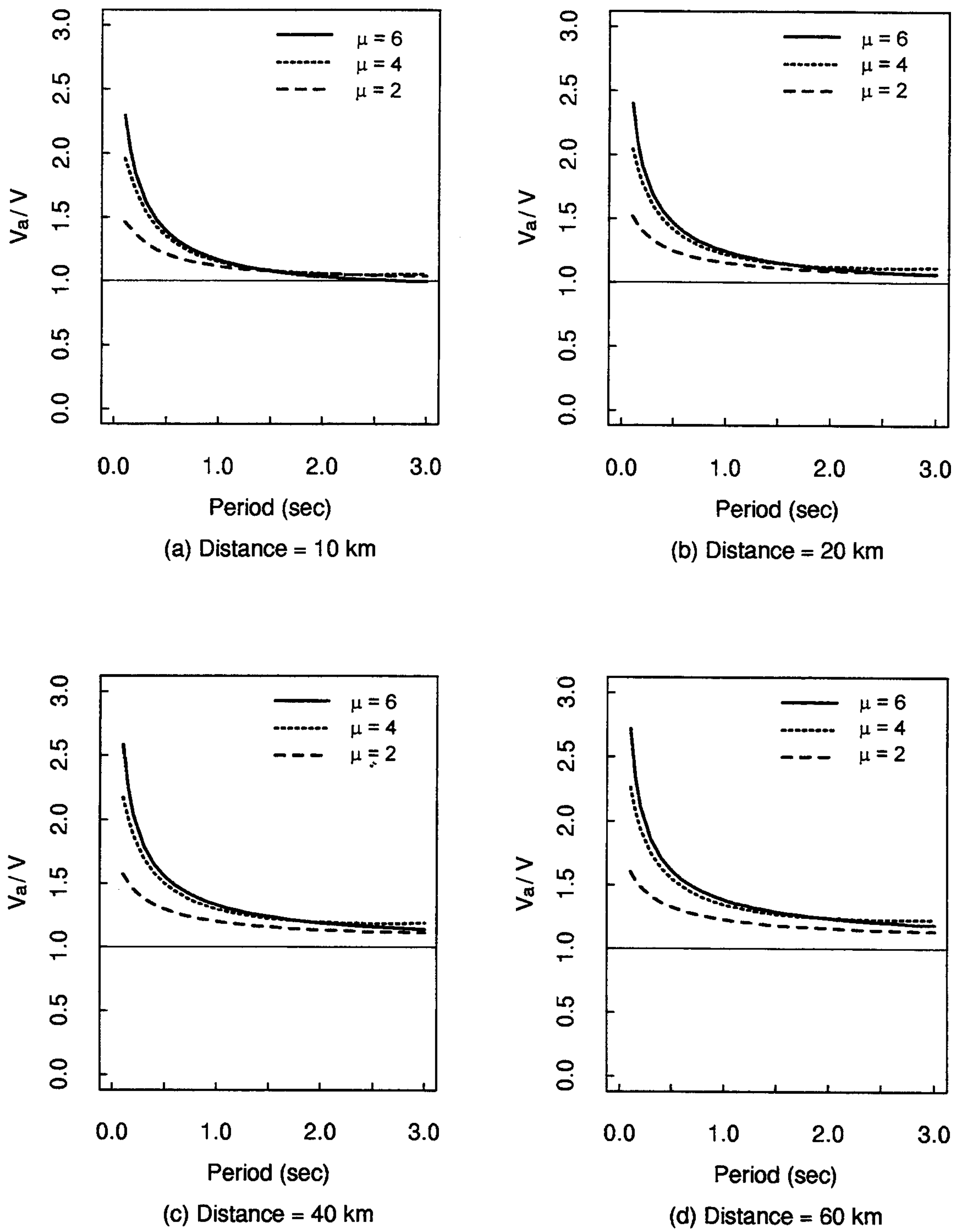

Fig. 4.14 Effect of Ductility on V_a/V Ratios

(5% Damping, Magnitude = 7, Site Class A+B)

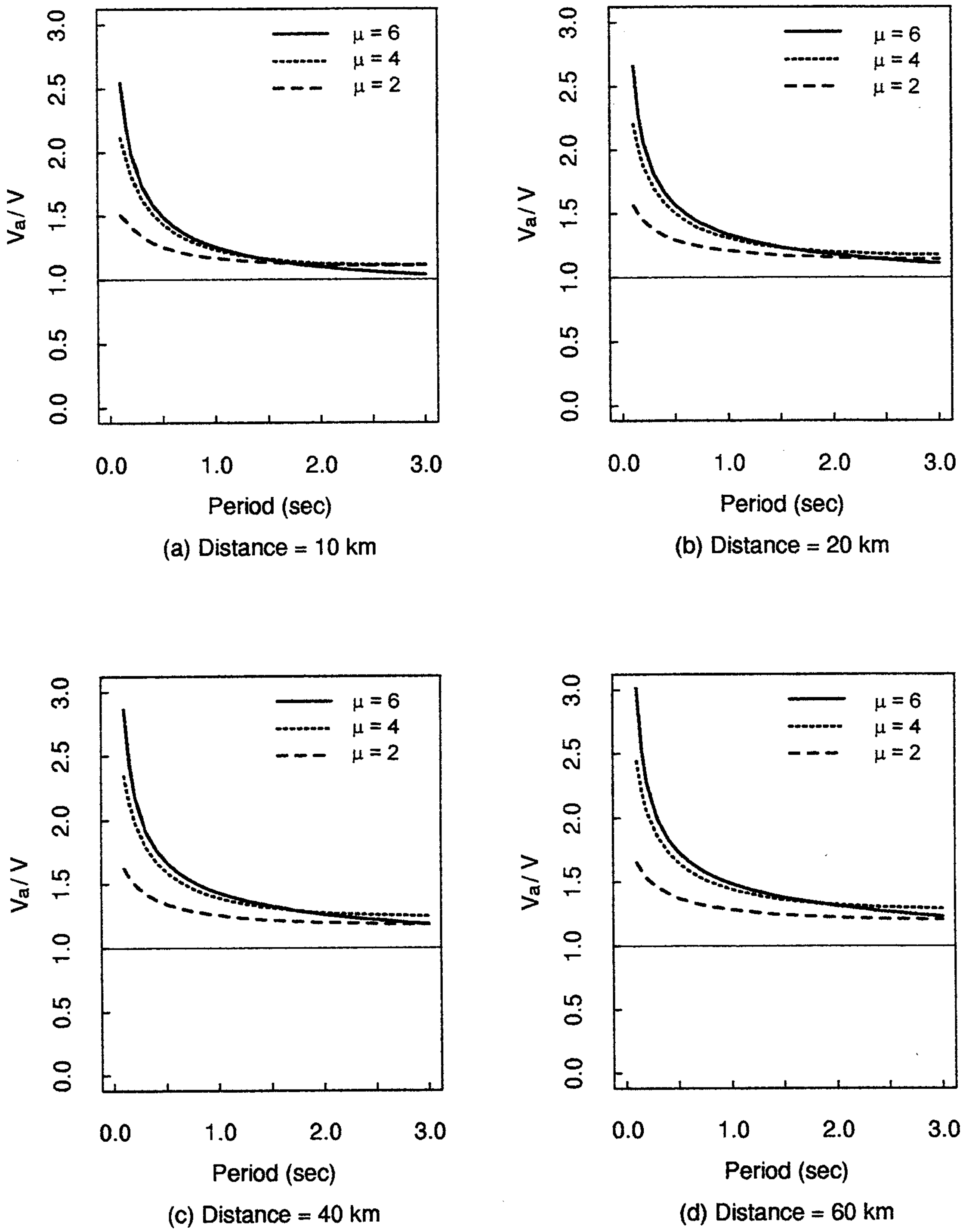

Fig. 4.15 Effect of Ductility on V_a/V Ratios

(5% Damping, Magnitude = 7, Site Class C)

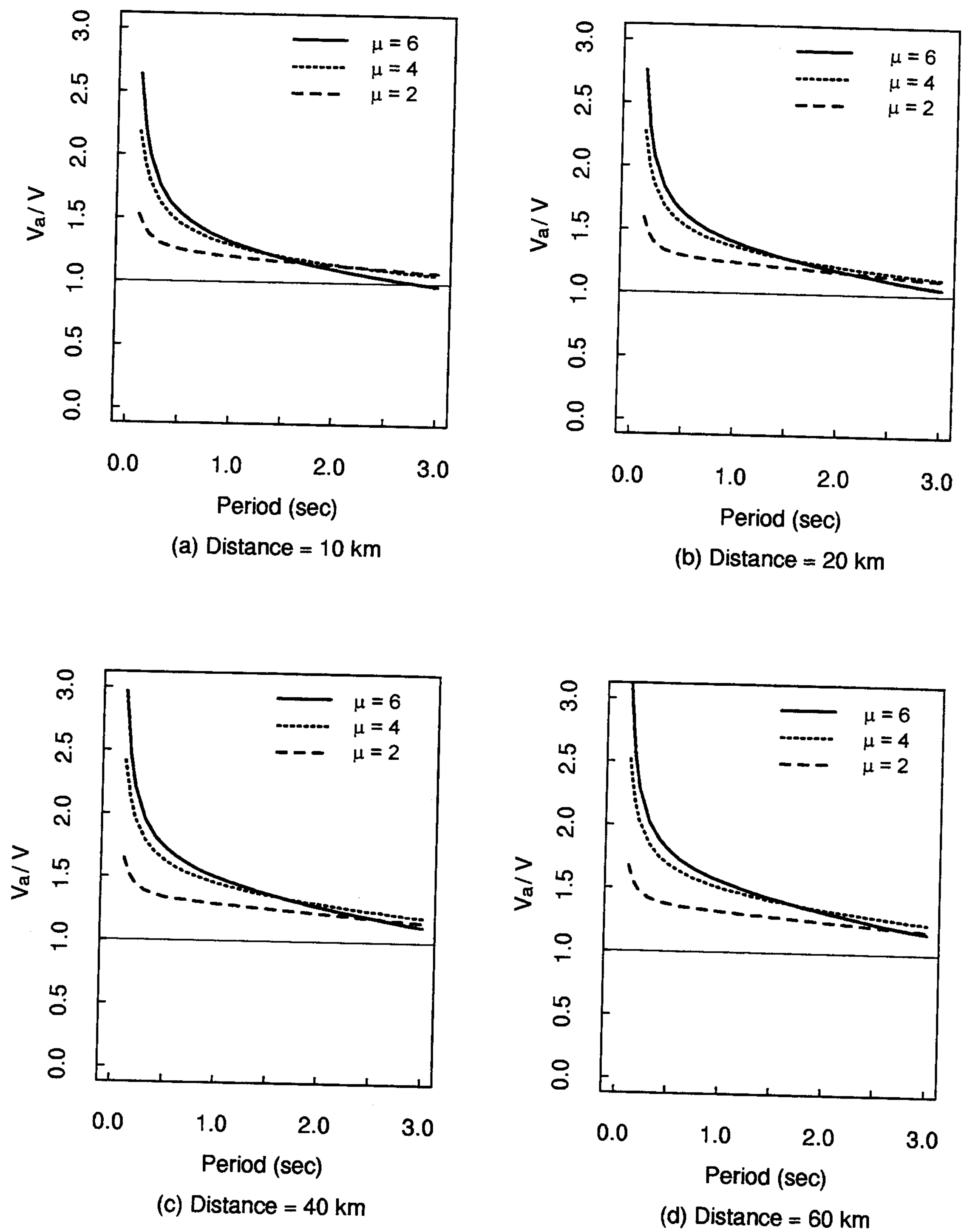

Fig. 4.16 Effect of Ductility on V_a/V Ratios

(5% Damping, Magnitude = 7, Site Class D)

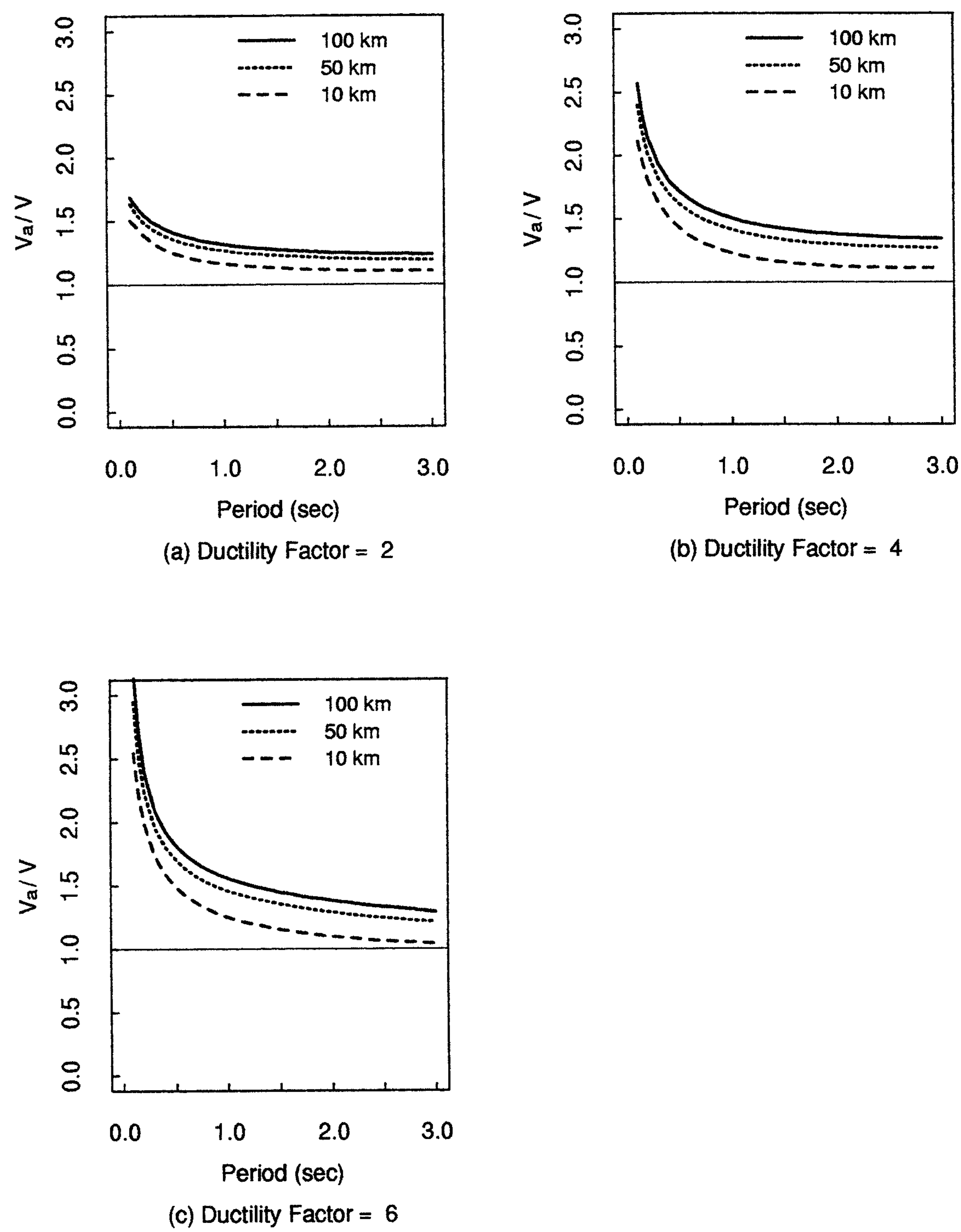

Fig. 4.17 Effect of Distance on V_a/V Ratios

(5% Damping, Magnitude = 7, Site Class C)

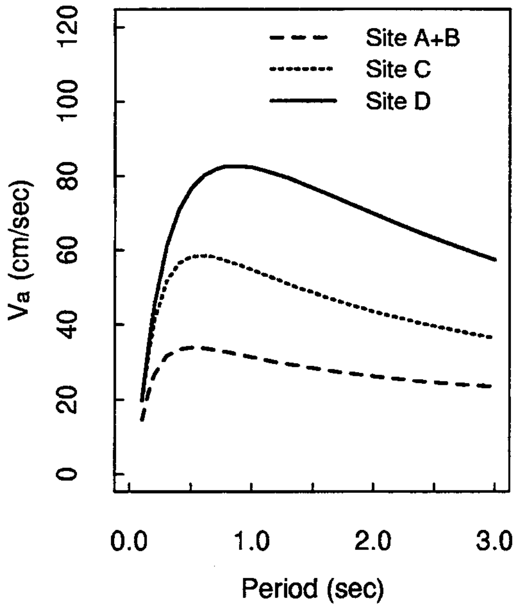

(a) Distance = 10 km

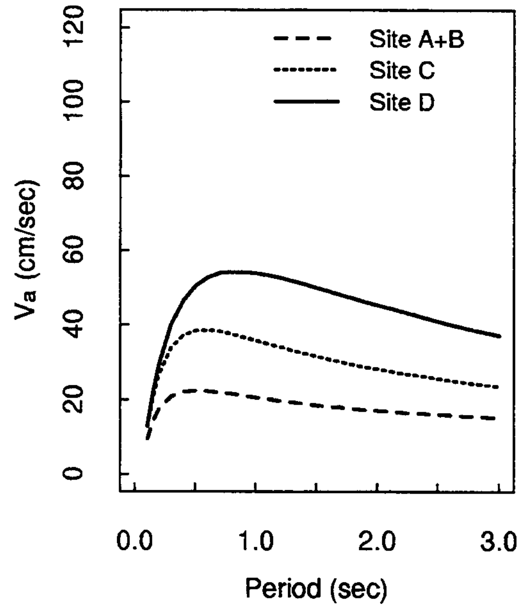

(b) Distance = 20 km

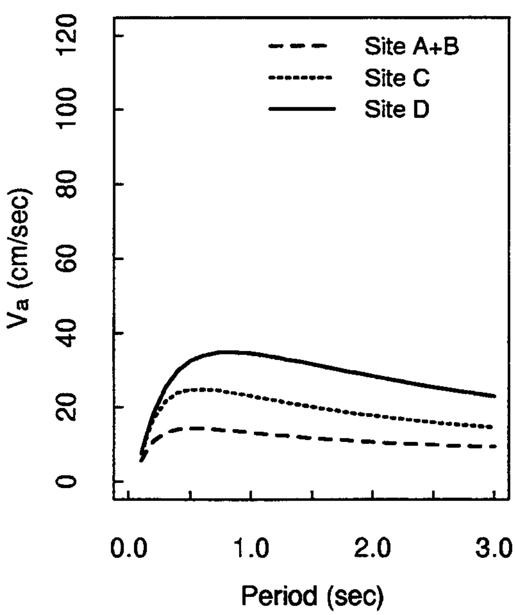

(c) Distance = 40 km

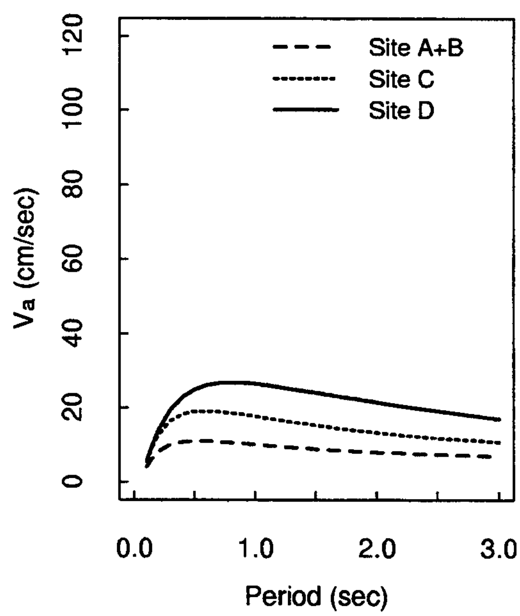

(d) Distance = 60 km

Fig. 4.18 Effect of Site Class on V_a Spectra

(5% Damping, Magnitude = 7, Ductility Factor = 4)

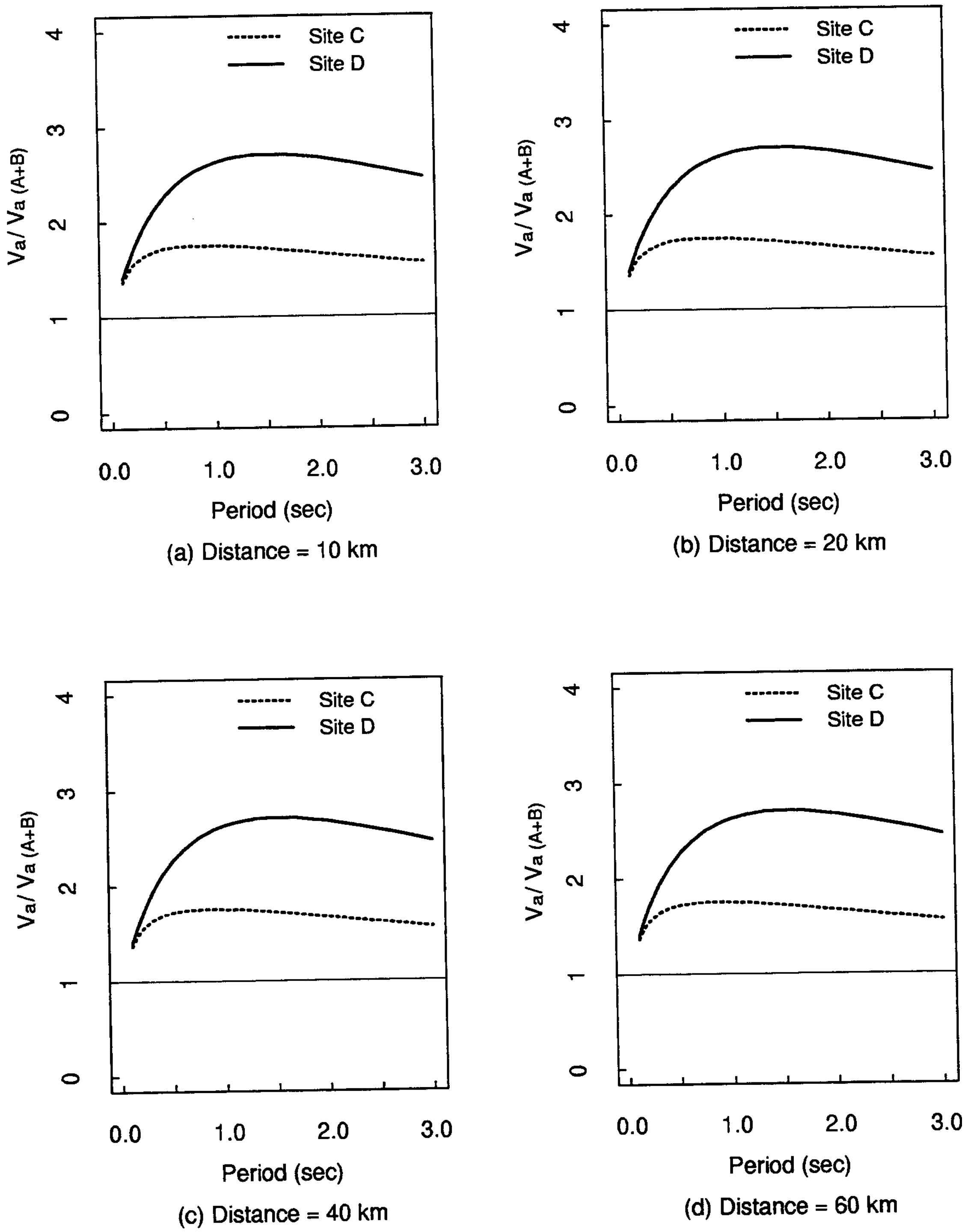

Fig. 4.19 Increase of V_a due to Site Class Effect

(5% Damping, Magnitude = 7, Ductility Factor = 4)

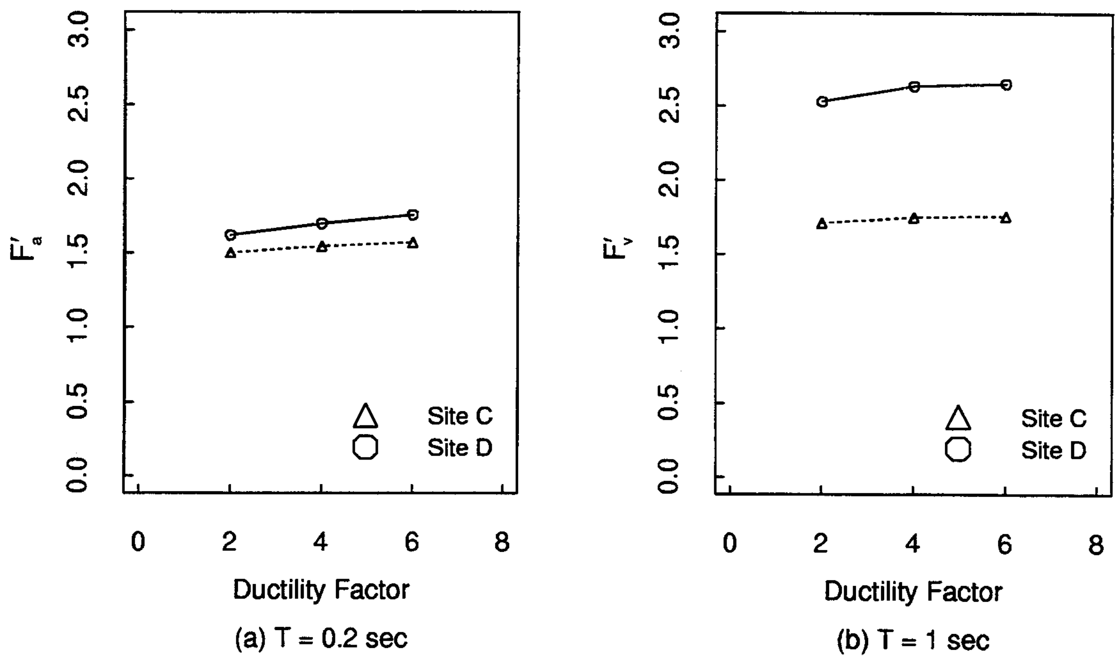

Fig. 4.20 Variations of Site Amplification Factors F'_a and F'_v

(5% Damping)

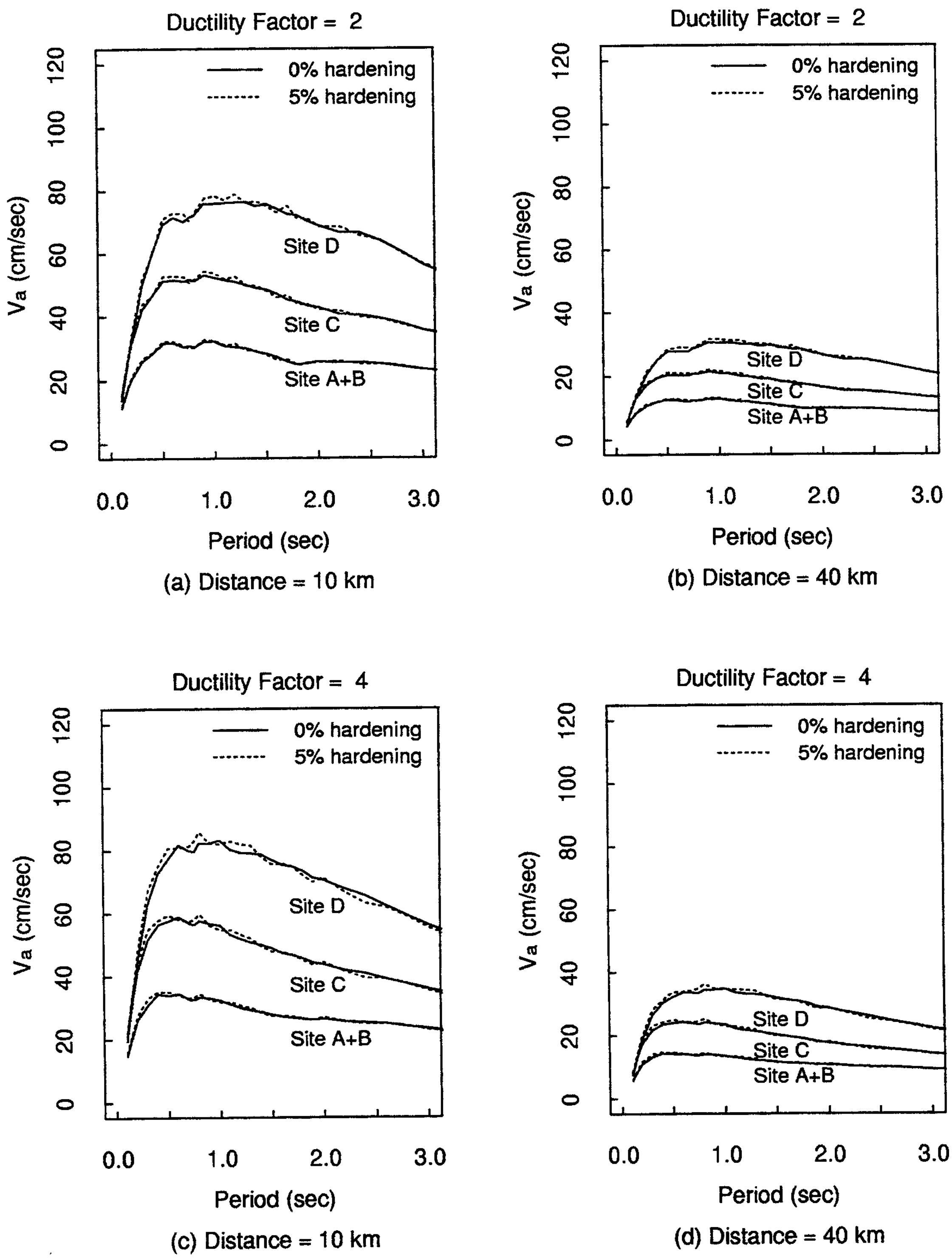

Fig. 4.21 Effect of Strain Hardening on V_a Spectra

(5% Damping, Magnitude = 7)

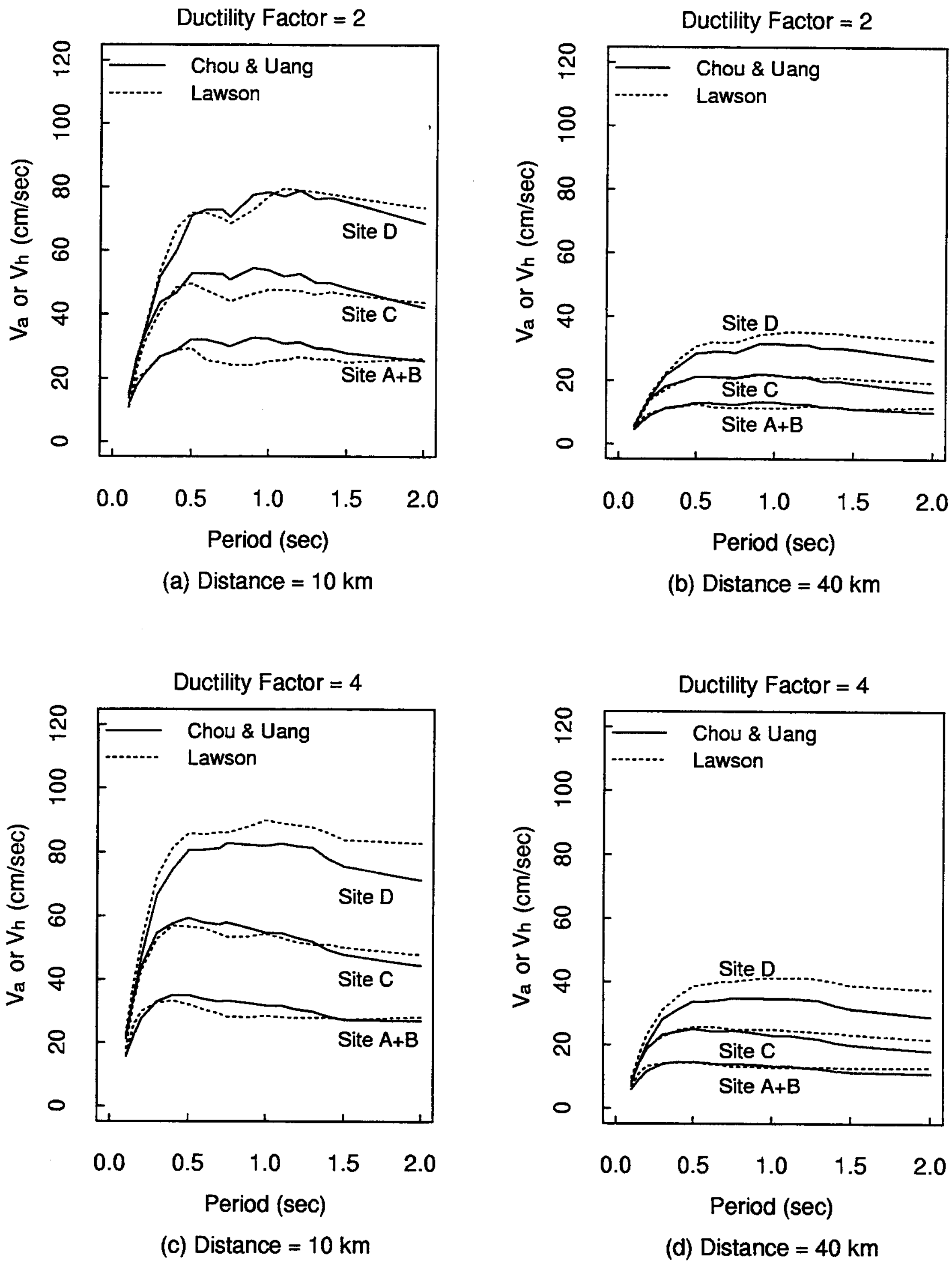

Fig. 4.22 Comparison of V_a and V_h Spectra with Unsmoothed Coefficients

(5% Damping, Magnitude = 7)

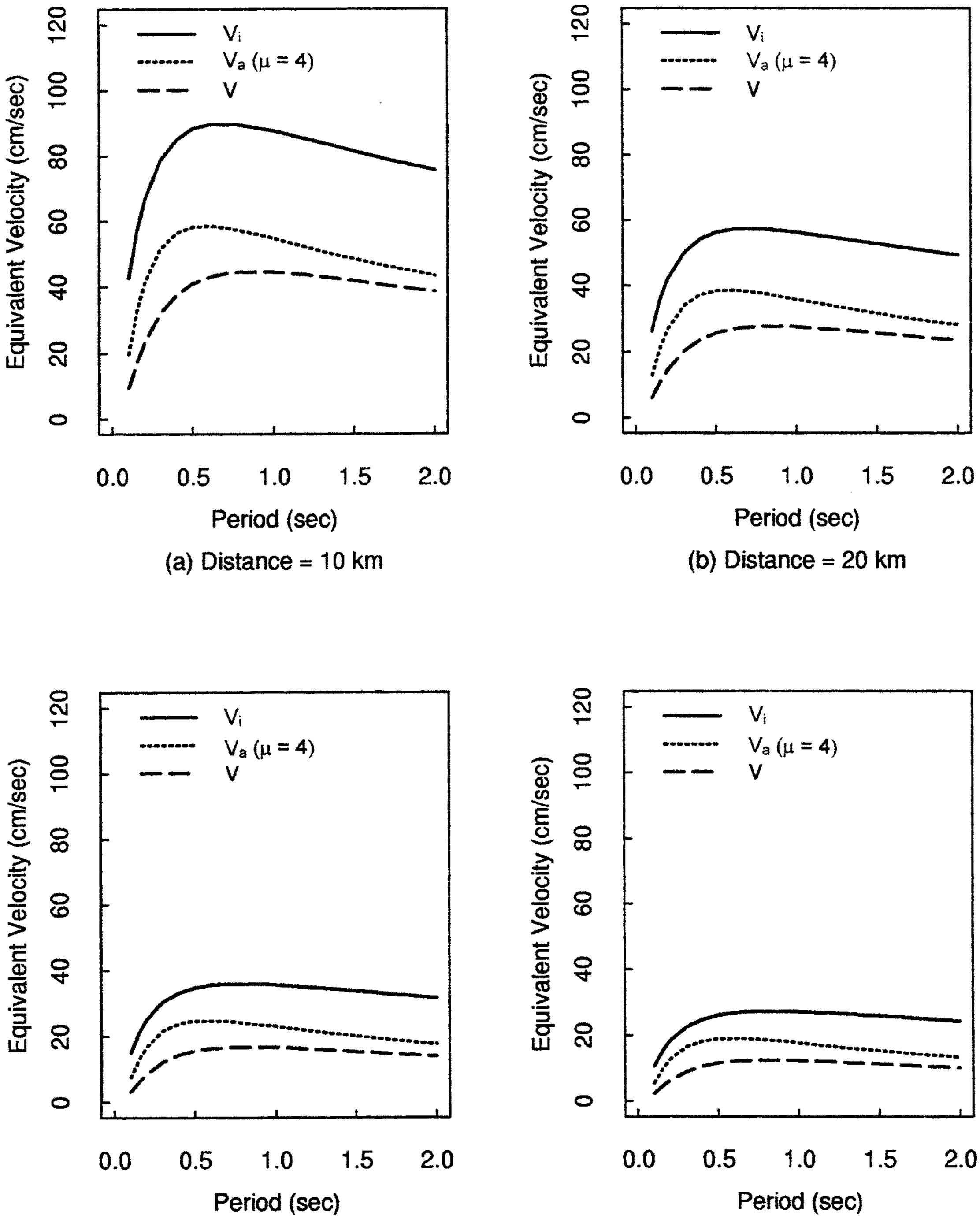

(a) Distance = 10 km

(b) Distance = 20 km

(c) Distance = 40 km

(d) Distance = 60 km

Fig. 4.23 Comparison of V_i, V_a, and V Spectra

(5% Damping, Magnitude = 7)

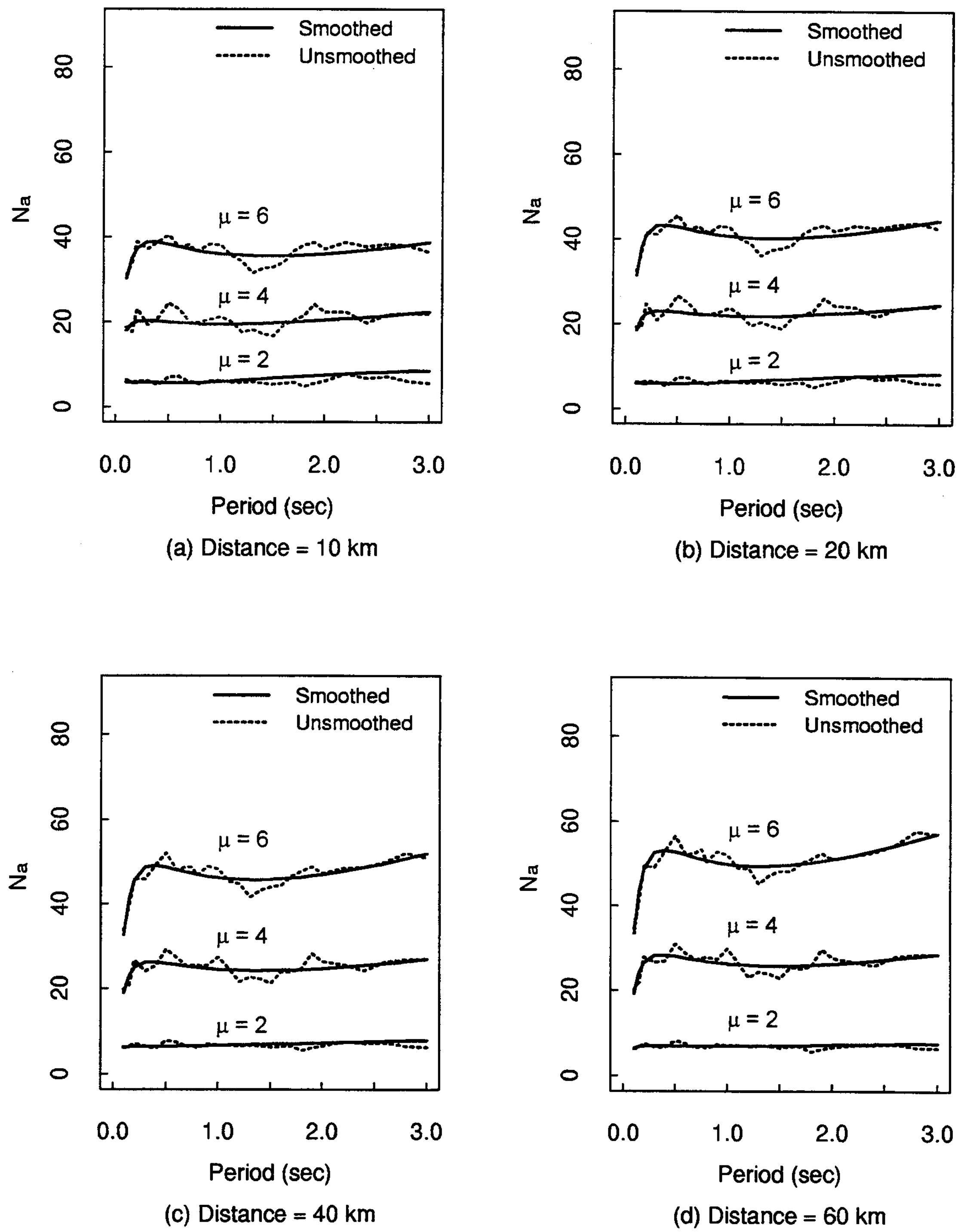

Fig. 4.24 N_a Spectra Based on Smoothed and Unsmoothed Coefficients
(5% Damping, Magnitude = 7, Site Class A+B)

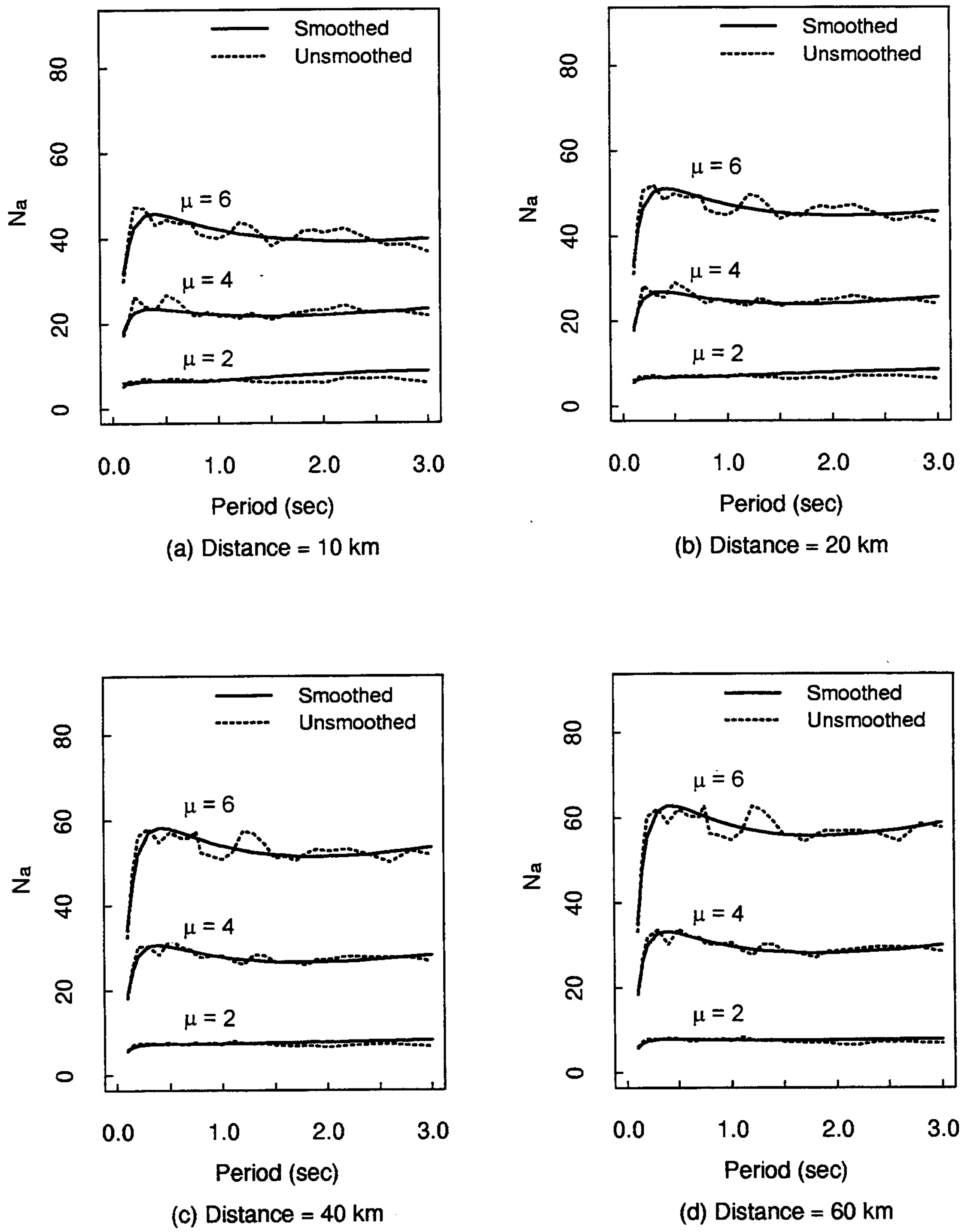

Fig. 4.25 N_a Spectra Based on Smoothed and Unsmoothed Coefficients
(5% Damping, Magnitude = 7, Site Class C)

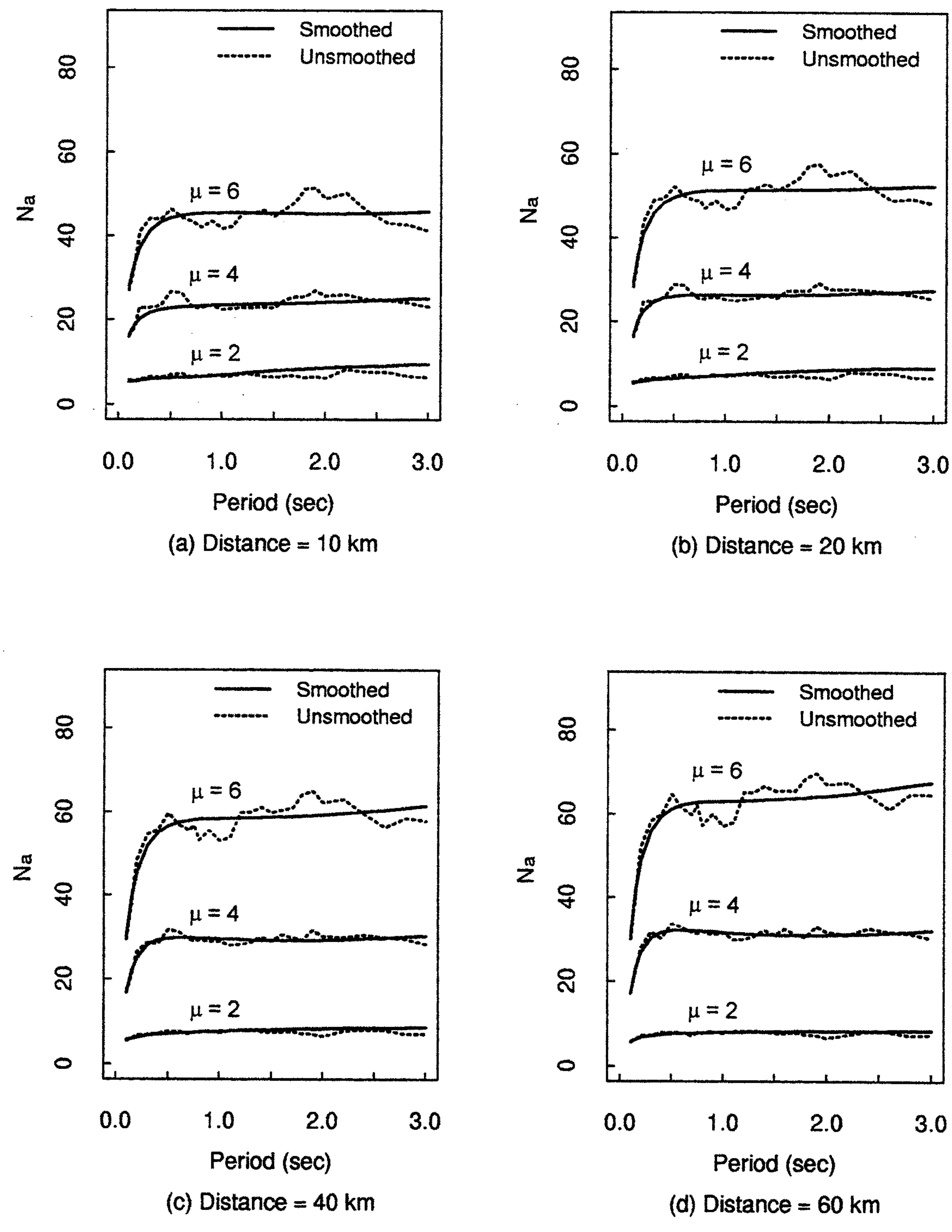

Fig. 4.26 N_a Spectra Based on Smoothed and Unsmoothed Coefficients
(5% Damping, Magnitude = 7, Site Class D)

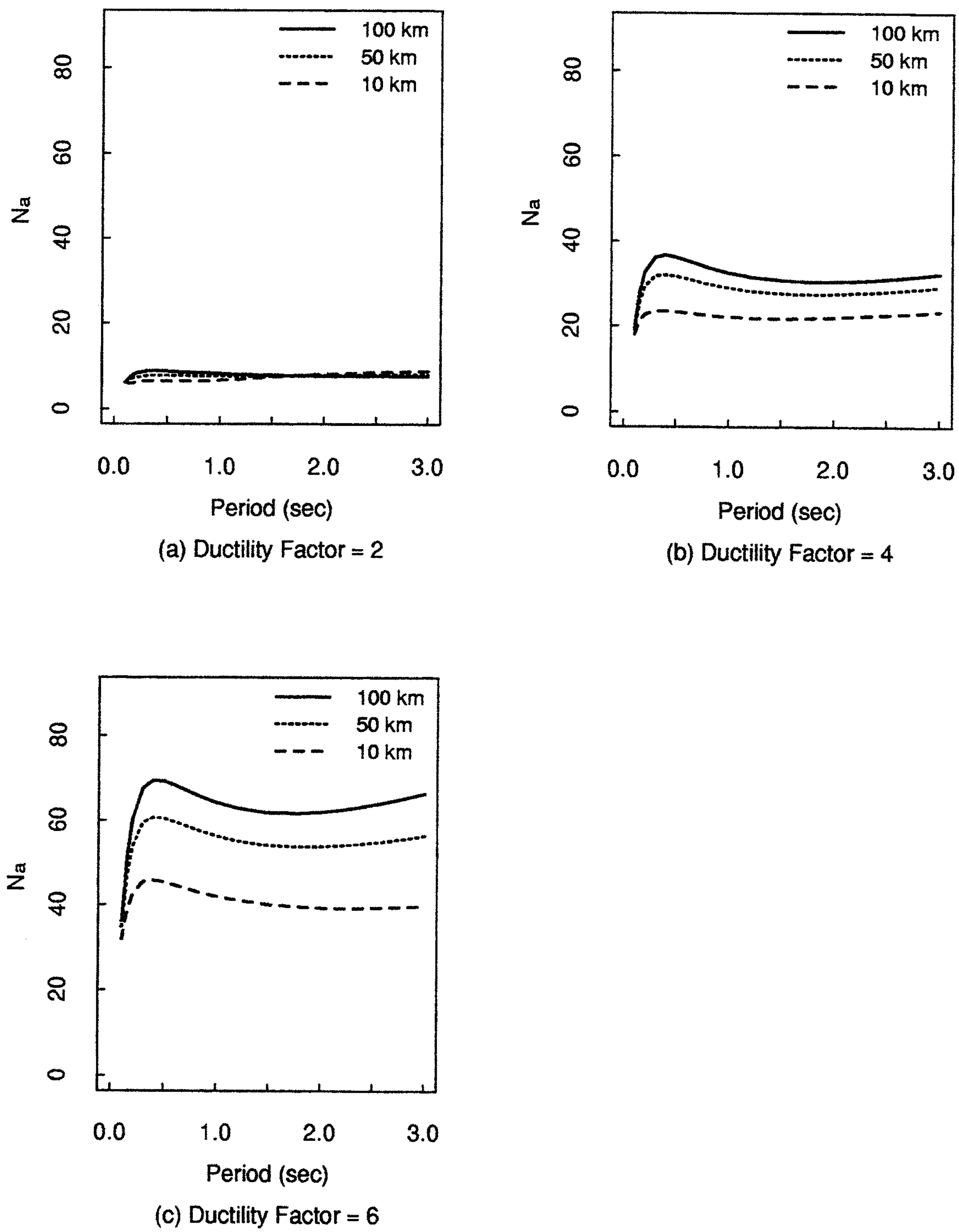

Fig. 4.27 Effect of Distance on N_a Spectra

(5% Damping, Magnitude = 7, Site Class C)

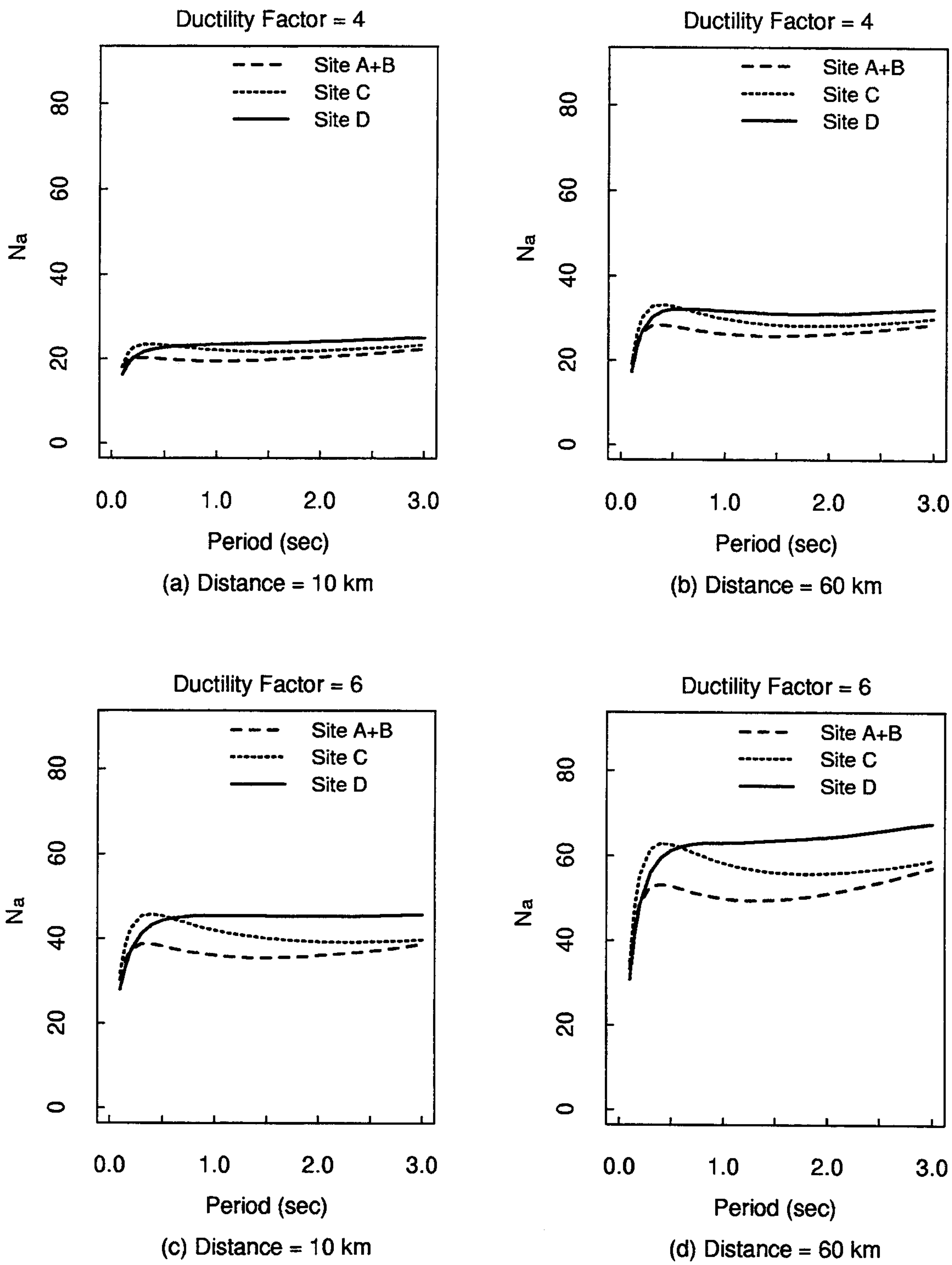

Fig. 4.28 Effect of Ductility on N_a Spectra

(5% Damping, Magnitude = 7)

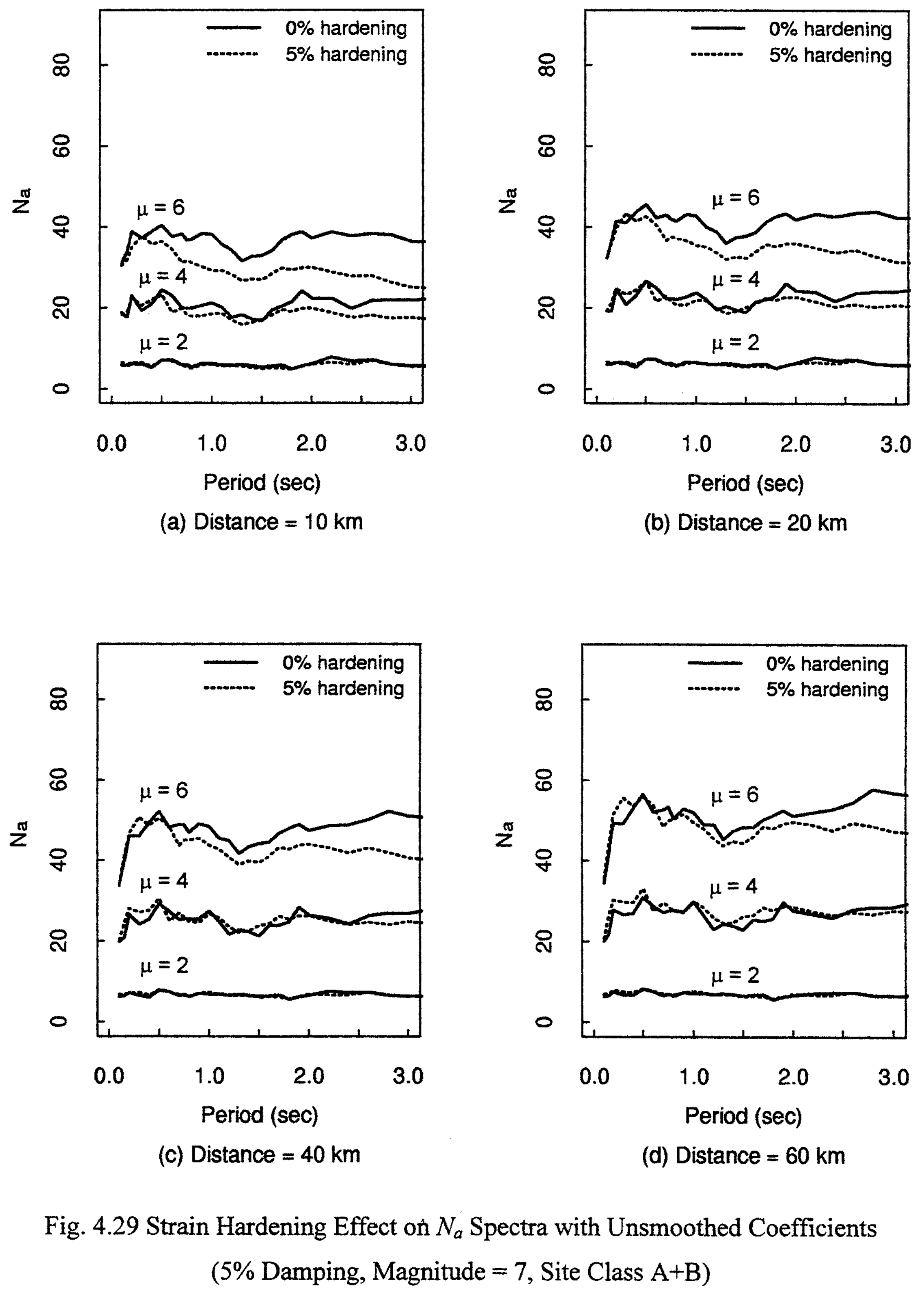

Fig. 4.29 Strain Hardening Effect on N_a Spectra with Unsmoothed Coefficients (5% Damping, Magnitude = 7, Site Class A+B)

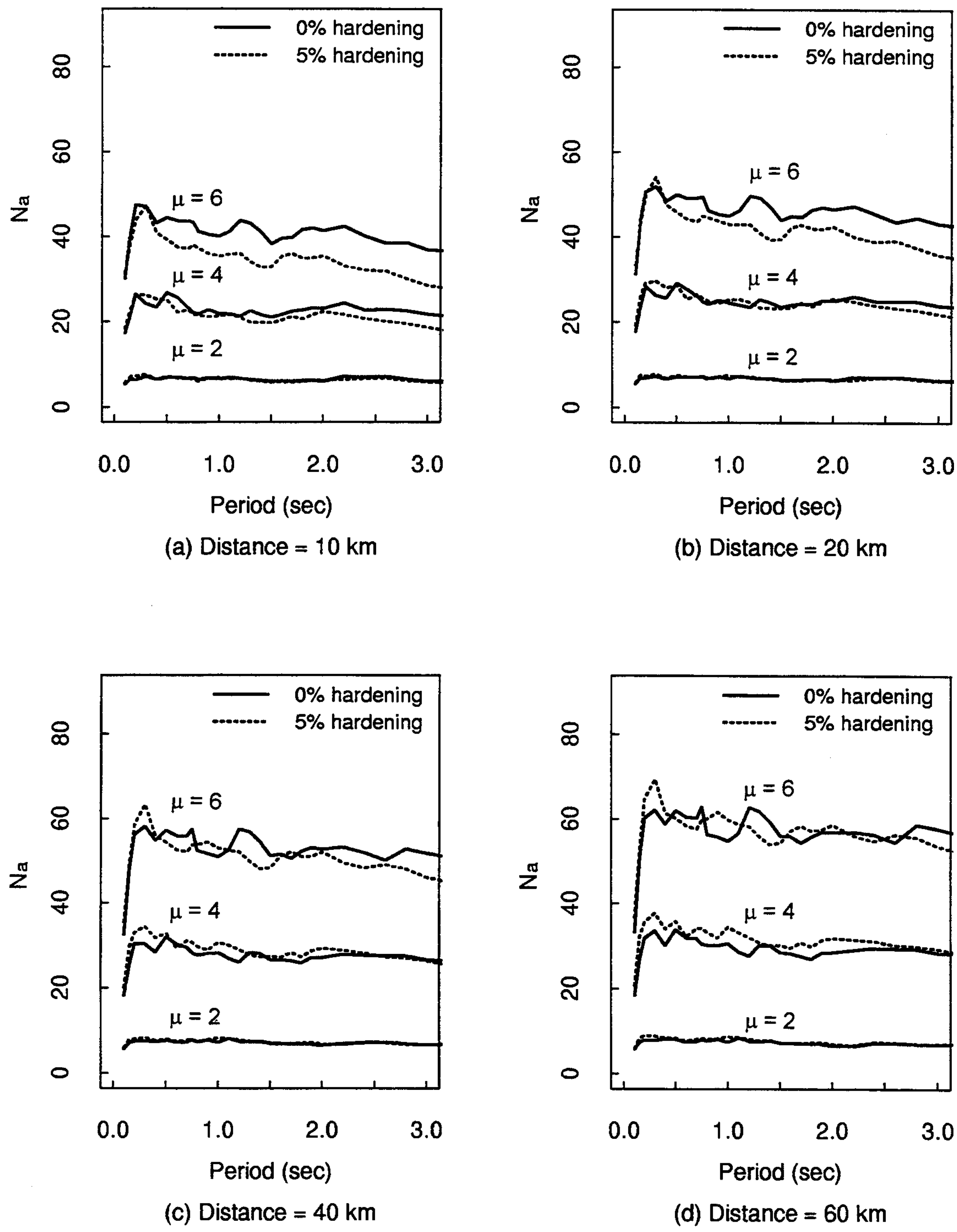

Fig. 4.30 Strain Hardening Effect on N_a Spectra with Unsmoothed Coefficients (5% Damping, Magnitude = 7, Site Class C)

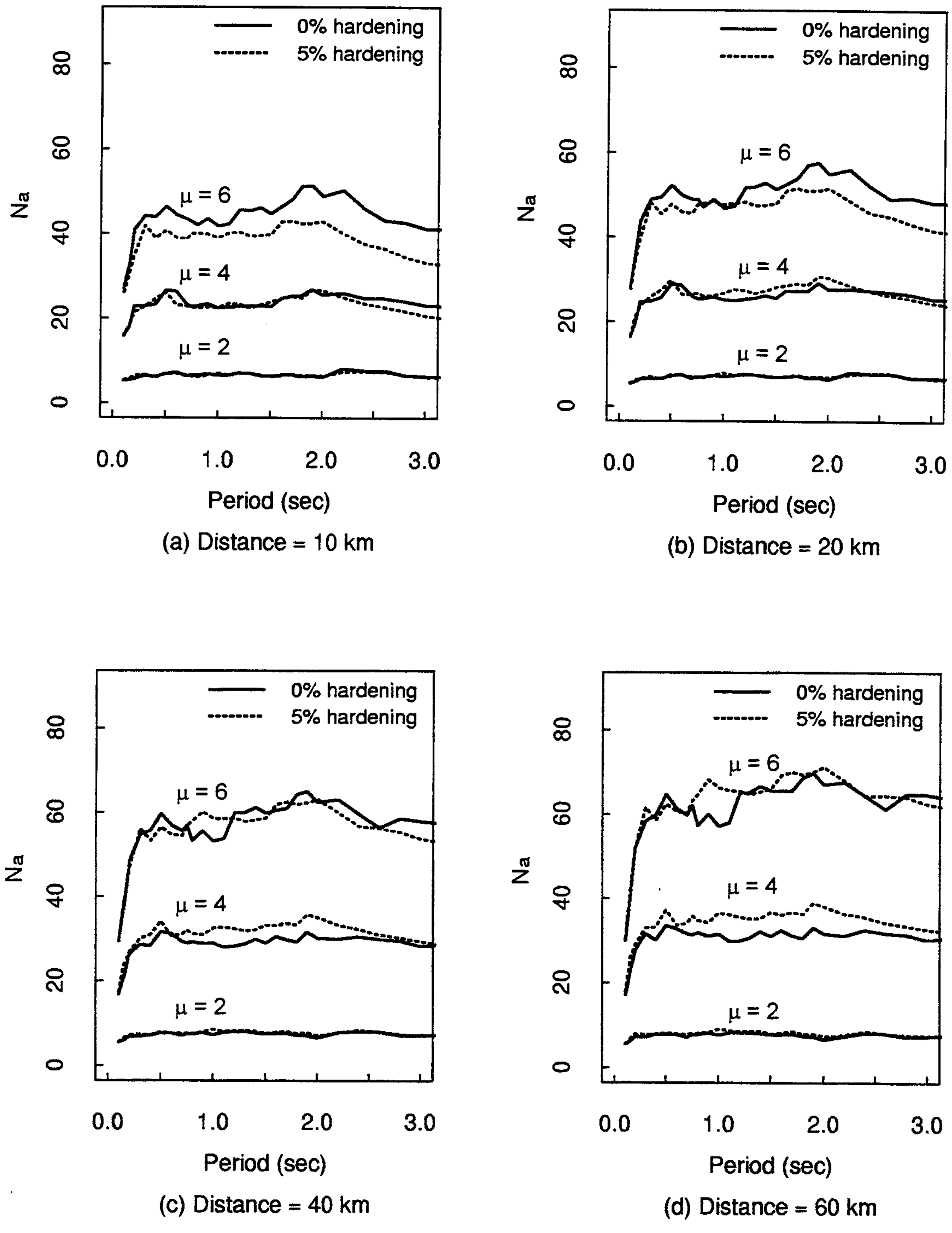

Fig. 4.31 Strain Hardening Effect on N_a Spectra with Unsmoothed Coefficients
(5% Damping, Magnitude = 7, Site Class D)

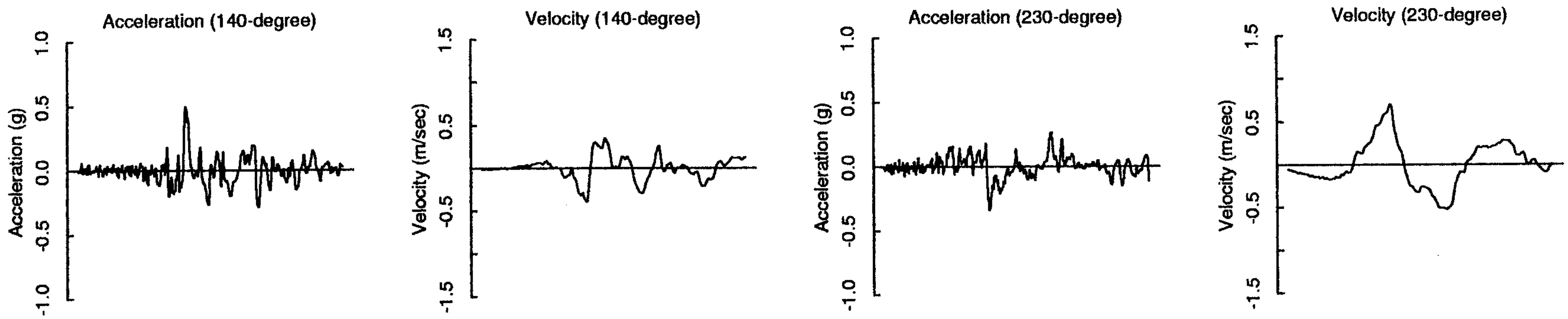

(a) Imperial Valley Earthquake (1979) - EL Centro Array #4

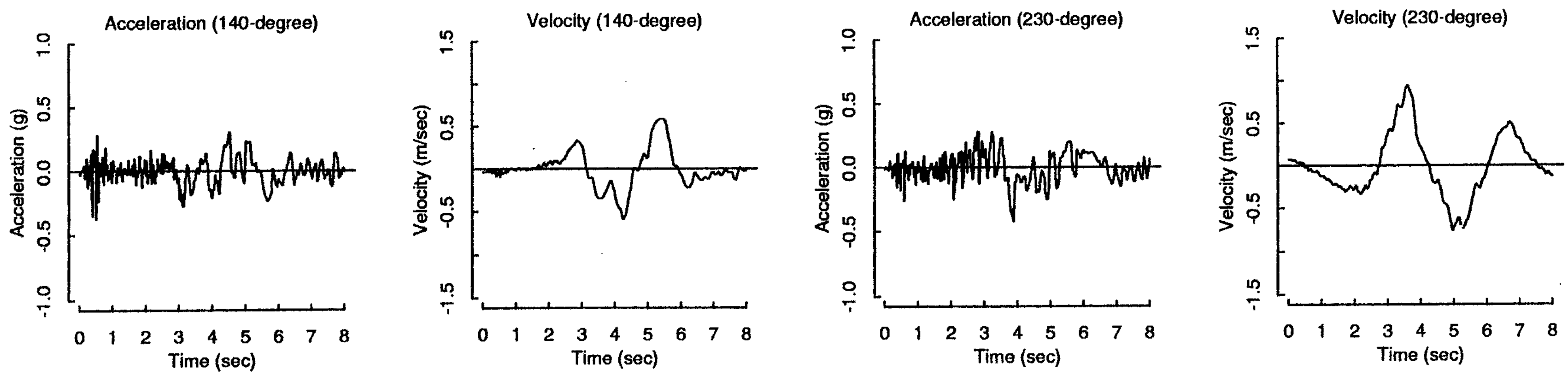

(b) Imperial Valley Earthquake (1979) - EL Centro Array #6

Fig. 4.32 Time Histories of Near-Field Ground Motions

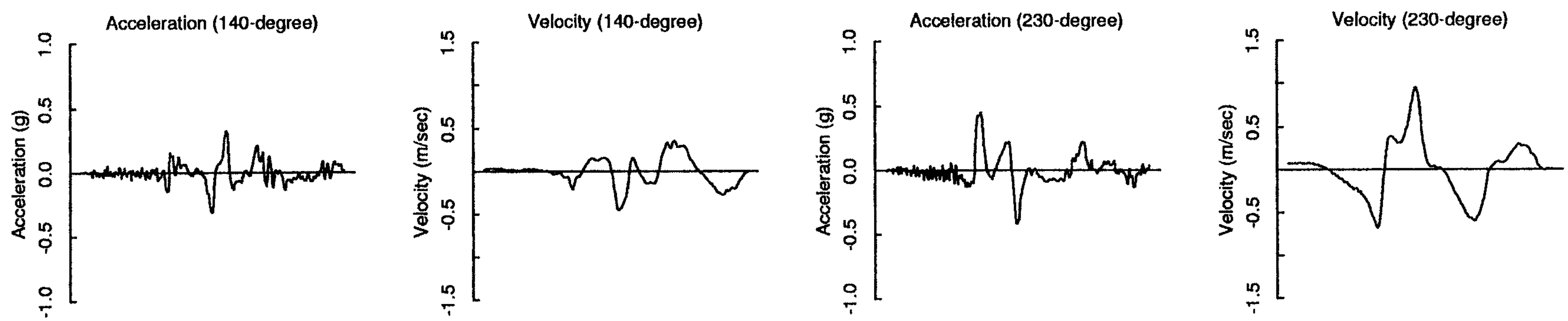

(c) Imperial Valley Earthquake (1979) - EL Centro Array #7

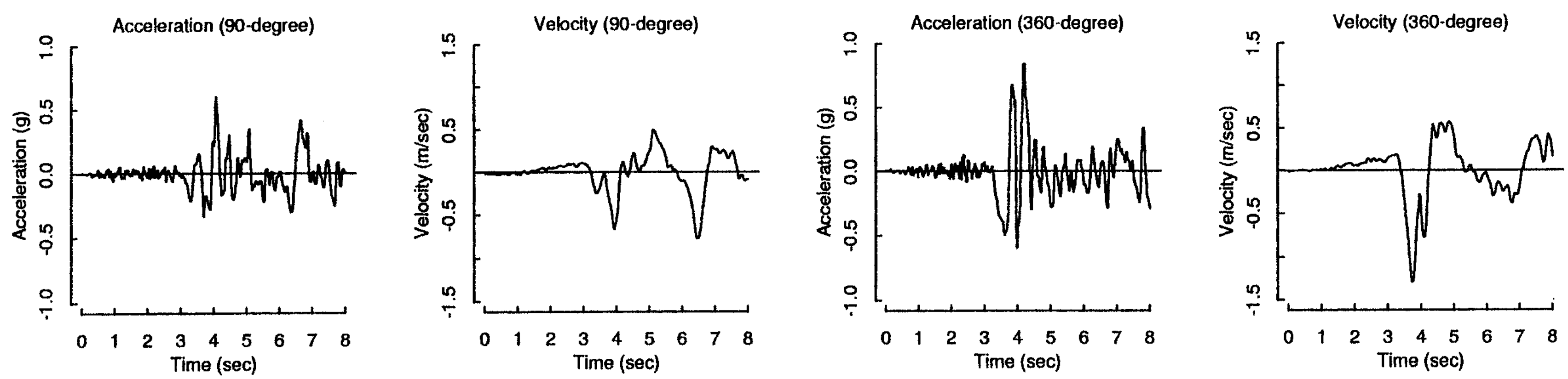

(d) Northridge Earthquake (1994) - County Hospital Parking Lot (Sylmar)

Fig. 4.32 Time Histories of Near-Field Ground Motions (continued)

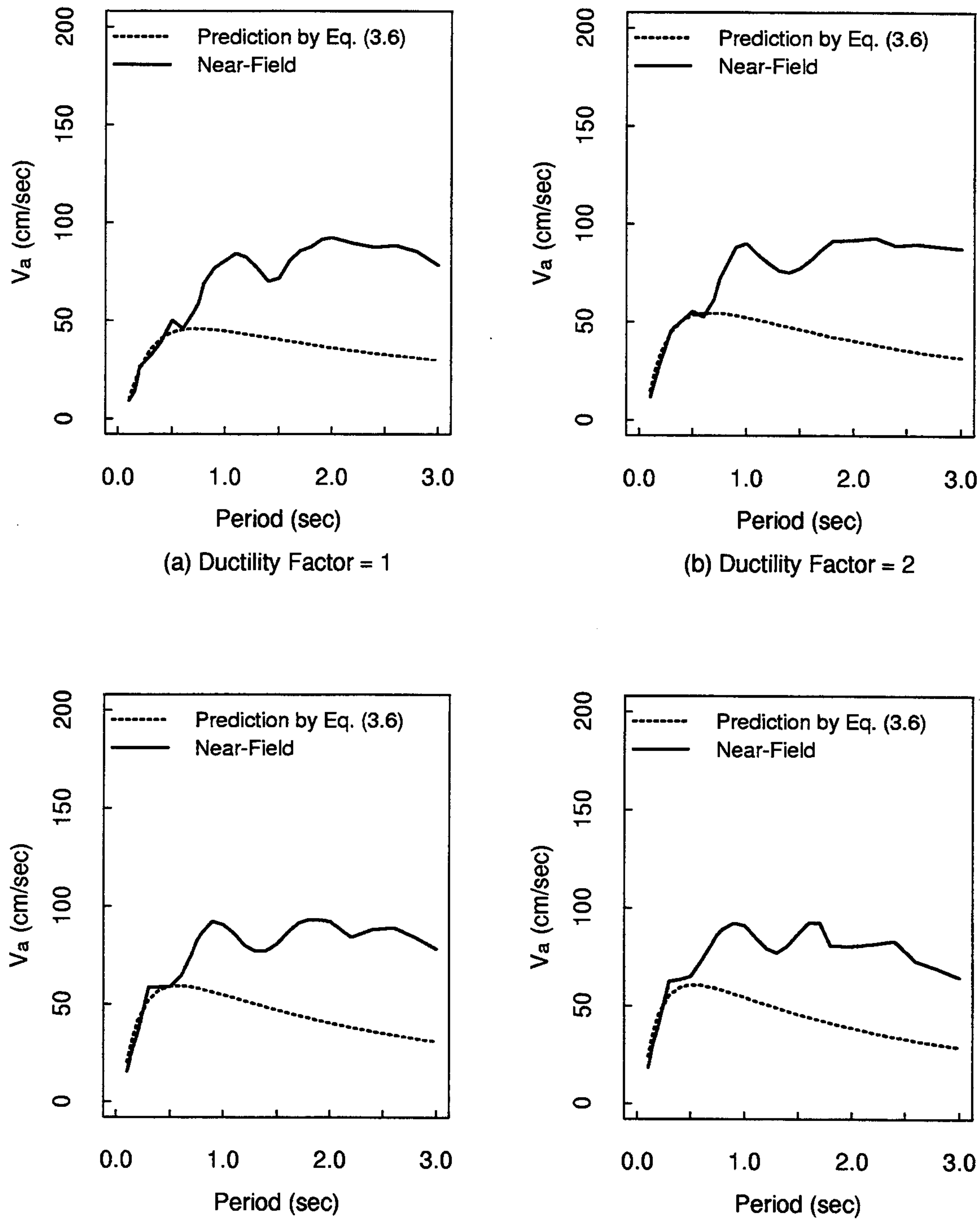

(a) Ductility Factor = 1

(b) Ductility Factor = 2

(c) Ductility Factor = 4

(d) Ductility Factor = 6

Fig. 4.33 V_a Spectra with Magnitude = 6.5, Distance = 6.8 km – Site Class D

(5% Damping, Imperial Valley-El Centro Array Station 4)

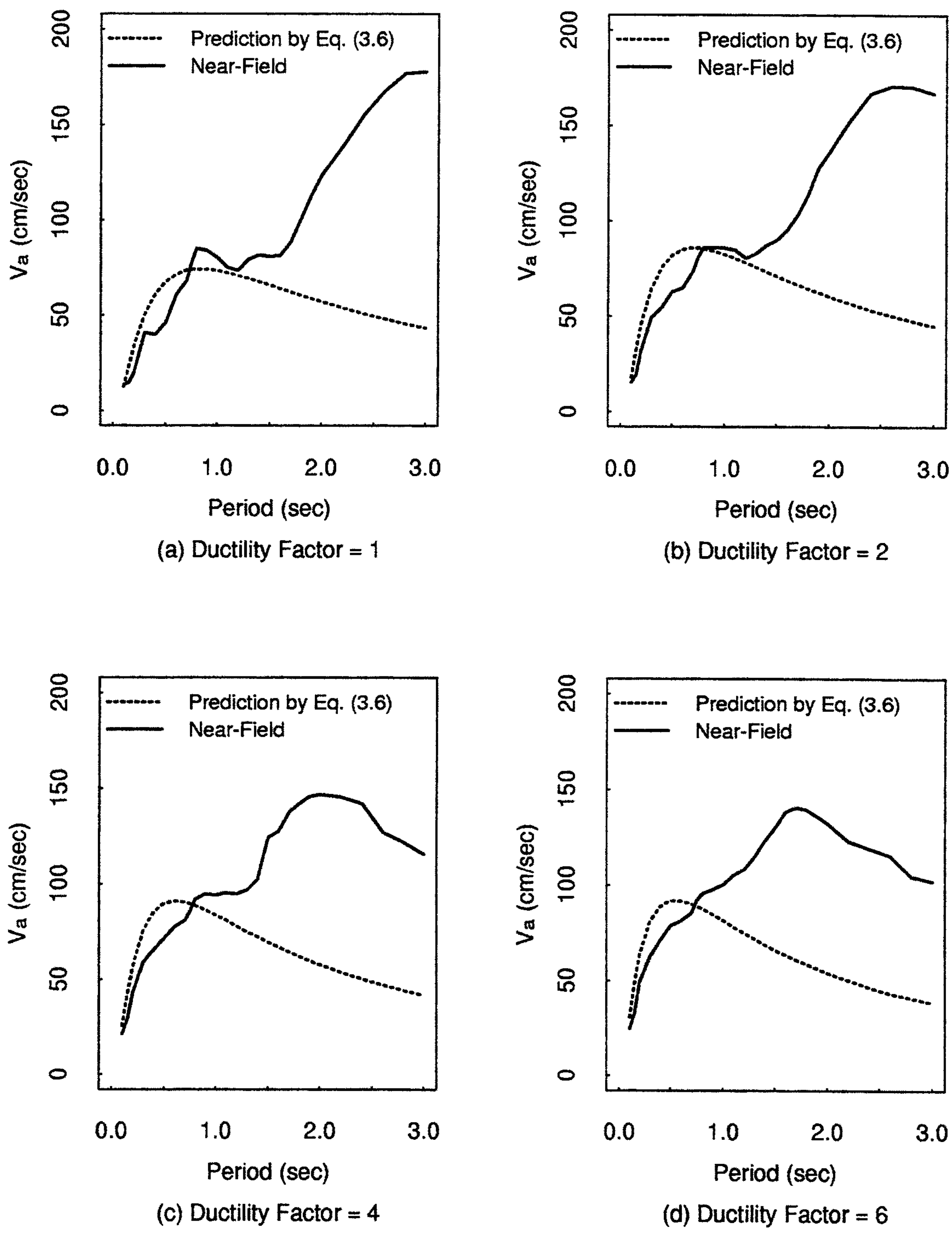

Fig. 4.34 V_a Spectra with Magnitude = 6.5, Distance = 1.3 km – Site Class D (5% Damping, Imperial Valley-El Centro Array Station 6)

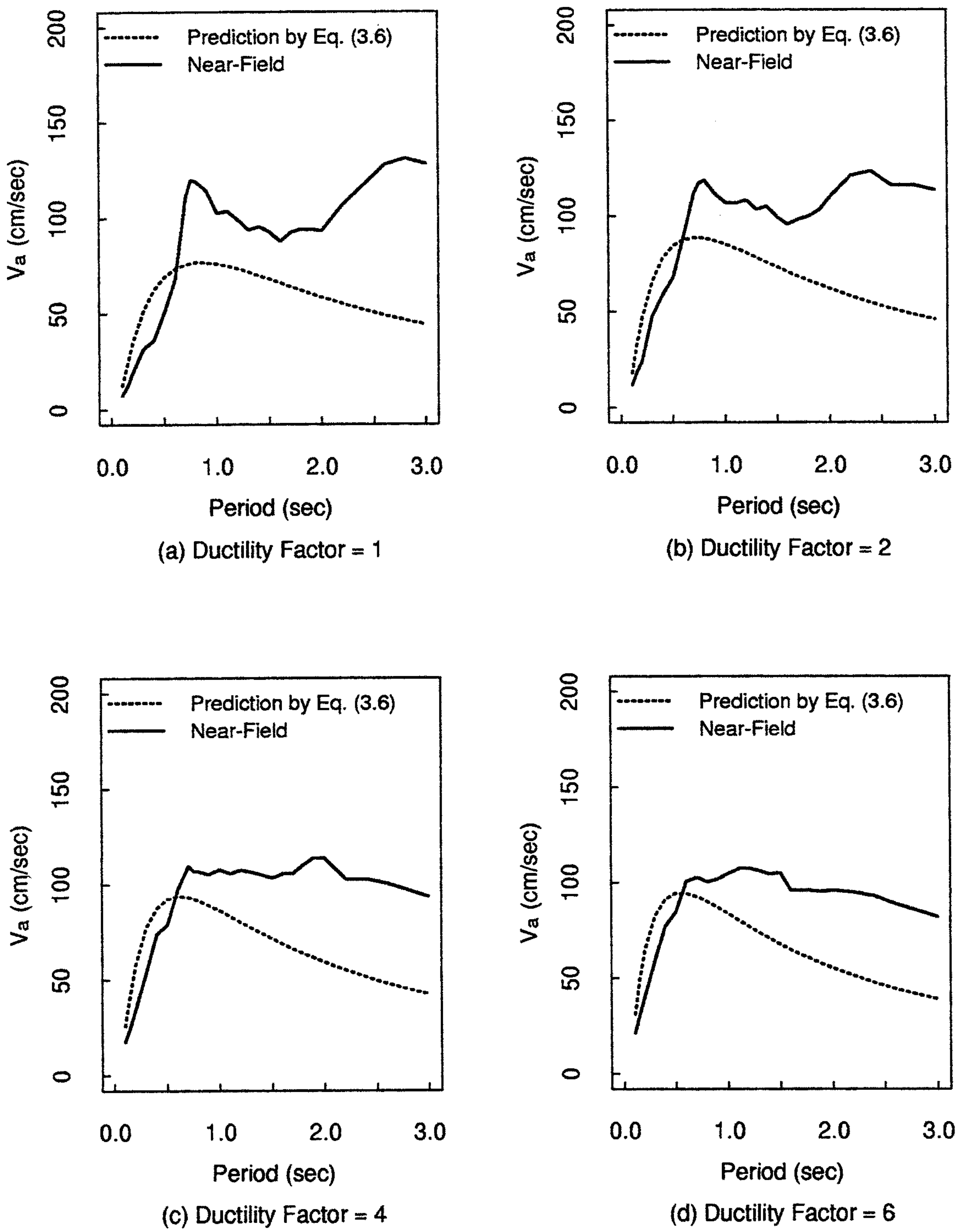

Fig. 4.35 V_a Spectra with Magnitude = 6.5, Distance = 0.6 km – Site Class D (5% Damping, Imperial Valley- El Centro Array Station 7)

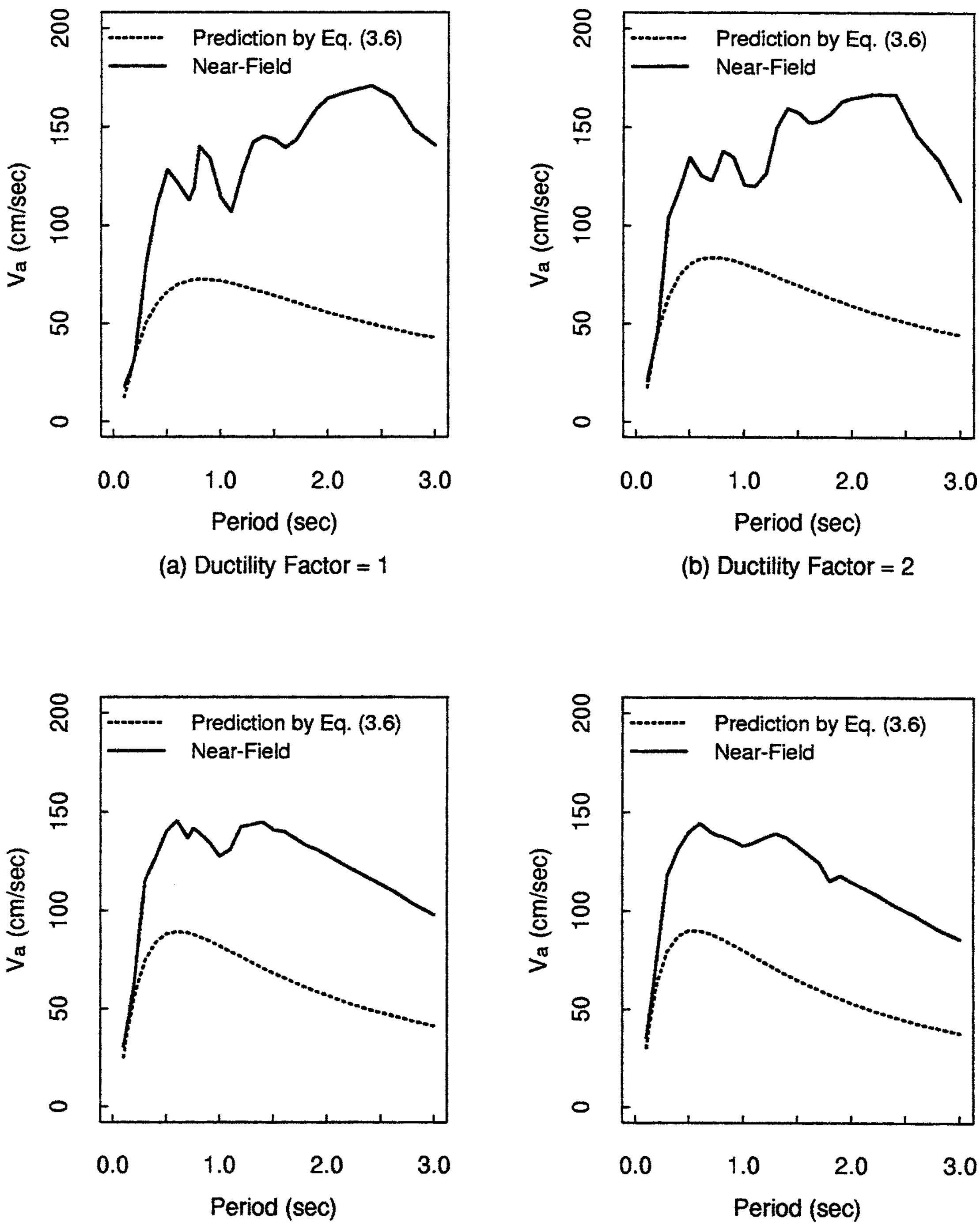

(a) Ductility Factor = 1

(b) Ductility Factor = 2

(c) Ductility Factor = 4

(d) Ductility Factor = 6

Fig. 4.36 V_a Spectra with Magnitude = 6.7, Distance = 1.7 km – Site Class D (5% Damping, Northridge-Sylmar County Hospital Parking Lot)

Appendix A–Strong Ground Motion Database

Site Name	Site No.	AZ1	AZ2	D (km)	Lat. (N)	Long. (W)	Site Class
Kern County, July 21, 1952, M = 7.4							
Pasadena - Athenaeum	CT 475	270	180	109	34.140	118.120	C
Santa Barbara	CT 283	42	132	85.0	34.424	119.701	C
Taft Lincoln School	CT 095	111	21	42.0	35.150	119.460	C
Parkfield, June 28. 1966, M = 6.1							
Cholame-Shandon #5	CT 014	355	85	9.30	35.700	120.328	D
Cholame-Shandon #8	CT 015	50	320	13.0	35.671	120.360	D
Cholame-Shandon #12	CT 016	50	320	17.3	35.636	120.403	C
Cholame-Shandon Tmblor #2	CT 097	295	205	16.1	35.752	120.264	C
San Fernando, February 9, 1971, M = 6.6							
Lake Hughes Sta. 4	CT 126	111	201	19.6	34.650	118.478	D
Lake Hughes Sta. 12	CT 128	21	249	17.0	34.570	118.560	C
Pasadena – Athenaeum	CT 475	0	90	25.7	34.140	118.120	C
Wrightwood	CT 290	25	115	60.7	34.360	117.630	C
Coyote Lake, August 6, 1979, M = 5.8							
Gilroy Array #1	USGS 010	320	230	9.10	36.973	121.572	A+B
Gilroy Array #3	USGS 030	140	050	5.30	36.987	121.536	D
Gilroy Array #4	USGS 040	360	270	3.70	36.005	121.522	D
Gilroy Array #6	USGS 060	320	230	1.20	37.026	121.484	C
Halls Valley	USGS HVR	240	150	30.0	37.338	121.714	C
Imperial Valley, October 15, 1979, M = 6.5							
Aeropuerto Mexicali	USGS 6616	315	045	1.40	32.651	115.332	D
El Centro Bonds Corner	USGS 5054	230	140	2.60	32.693	115.338	D
Calexico Fire Sta.	USGS 5053	315	225	10.6	32.669	115.492	D
Calipatria Fire Sta.	USGS 5061	315	225	23.0	33.130	115.520	D
Cerro Prieto	USGS CPRI	237	147	23.5	32.420	115.301	C
Chihuahua	USGS CHIH	12	282	17.7	32.484	115.240	D
El Centro: Imp. Cnty Cntr FF	USGS ELC0	92	002	7.60	32.793	115.560	D

Coachella Canal #4	USGS CC40	135	045	49.0	33.360	115.590	D
El Centro: Differential Arra	USGS EDA0	270	360	5.10	32.796	115.535	D
El Centro Array #1	USGS 5056	230	140	22.0	32.960	115.319	D
El Centro Array #2	USGS 5115	230	140	16.0	32.916	115.366	D
El Centro Array #4	USGS 0955	230	140	6.80	32.864	115.432	D
El Centro Array #5	USGS 0952	230	140	4.00	32.855	115.466	D
El Centro Array #6	USGS 5158	230	140	1.30	32.839	115.487	D
El Centro Array #7	USGS 5028	230	140	0.60	32.829	115.504	D
El Centro Array #8	--	230	140	3.80	32.810	115.530	D
El Centro Array #10	USGS 0412	050	320	8.5	32.780	115.567	D
El Centro Array #11	USGS 5056	230	140	22.0	32.960	115.319	D
El Centro Array #12	USGS 0931	230	140	18.0	32.718	115.637	D
El Centro Array #13	USGS 5059	230	140	22.0	32.709	115.683	D
Holtville Post Office	USGS HVP0	315	225	7.50	32.812	115.377	D
Parachute Test Site	USGS 5051	315	225	14.0	32.929	115.699	C
Plaster City	USGS PLS0	135	045	32.0	32.790	115.860	D
Superstition Mt.	USGS 0286	135	045	26.0	32.955	115.823	D
Westmoreland Fire Sta.	USGS WSM0	180	090	15.0	33.037	115.623	D

<u>Livermore Valley, January 24, 1980, M = 5.8</u>

Antioch	CDMG 67070	90	360	20.8	38.015	121.813	C
APEEL Array Sta. 3E	CDMG 23573	146	236	40.3	37.656	122.060	C
Fremont – Mission San Jose	CDMG 57064	075	345	33.1	37.530	121.919	C
San Ramon	CDMG 57134	146	236	16.7	37.780	121.980	D
Tracy	CDMG 57063	183	093	28.5	37.766	121.421	D

<u>Livermore Valley, January 27, 1980, M = 5.8</u>

Antioch	CDMG 67070	90	360	20.8	38.015	121.813	C
APEEL Array Sta. 3E	CDMG 23573	146	236	40.3	37.656	122.060	C
Fremont – Mission San Jose	CDMG 57064	075	345	33.1	37.530	121.919	C
Livermore – Fagundes Ranch	CDMG 57T01	90	360	4.00	37.753	121.772	D
Livermore – Morgan Territ. Pk.	CDMG 57T02	355	265	10.1	37.819	121.795	C
San Ramon	CDMG 57134	146	236	16.7	37.780	121.980	D

<u>Westmoreland, April 26, 1981, M = 5.6</u>

Brawley Airport	USGS 5060	135	225	11.2	32.990	115.510	D
Parachute Test Site	USGS 5247	315	225	2.60	32.930	115.700	C
Salton Sea Wildlife Refuge	USGS 5062	315	225	0.60	33.180	115.620	D
Superstition Mtn.	USGS 0286	135	45	9.2	32.950	115.820	C
Westmoreland	USGS 2588	90	180	0.5	33.037	115.623	D

<u>Morgan Hill, April 24, 1984, M = 6.2</u>

Gilroy #1	CDMG 47379	67	337	17.6	36.973	121.572	A+B
Gilroy #2	CDMG 47380	90	0	16.6	36.982	121.556	D
Gilroy #3	CDMG 47381	90	0	16.2	36.987	121.536	D
Gilroy #4	CDMG 57382	270	360	14.5	37.005	121.522	D
Gilroy #6	CDMG 57383	90	0	13.6	37.026	121.484	C
Gilroy #7	CDMG 57425	90	0	15.8	37.033	121.434	D

Halls Valley	CDMG 57191	240	150	0.3	37.338	121.714	D

<u>Palm Springs, July 8,1986, M = 5.9</u>

Desert Hot Spr. F. S.	CDMG 12149	0	90	8.8	33.962	116.509	C
Helmut – Stenson F. S.	CDMG 12331	360	270	45.0	33.729	116.979	D
Indio C. C.	CDMG 12026	0	90	46.2	33.717	116.156	D
Joshua Tree F. S.	CDMG 22170	90	0	29.8	34.131	116.314	C
Murrieta Hot Springs	CDMG 13198	90	0	60.6	33.599	117.132	A+B
Palm Springs Airport	CDMG 12025	90	0	16.1	33.829	116.501	D
Puerta LA. Cruz	CDMG 12168	258	348	81.7	33.324	116.683	C
Riverside Airport	CDMG 13123	180	270	70.3	33.951	117.446	C
Silent Valley P. F.	CDMG 12206	90	0	22.7	33.851	116.852	A+B
San Jacinto V. C.	CDMG 12202	270	360	36.8	33.760	116.960	D
Temecula	CDMG 13172	0	90	70.0	33.496	117.149	D
Winchester - BR	CDMG 13199	90	0	54.9	33.640	117.094	A+B
Winchester - HVF	CDMG 13200	0	90	49.2	33.681	117.056	A+B

<u>Whittier, October 1, 1987, M = 6.0</u>

Alhambra – Fremont Sch.	CDMG 24461	270	180	3.80	34.070	118.150	C
LA Country Club North	CDMG 24389	90	0	28.5	34.063	118.418	D
LA Country Club South	CDMG 24390	90	0	28.3	34.062	118.416	D
LA Hollywd Storage bld. ff	CDMG 24303	90	0	21.2	34.090	118.339	D
Lake Hughes #1	CDMG 24271	90	0	72.3	34.674	118.430	C
Rancho Cucamonga – L&J	CDMG 23497	90	0	43.2	34.104	117.574	C
Sylmar	CDMG 24514	90	0	41.5	34.326	118.444	D
Tarzana	CDMG 24436	90	0	40.3	34.160	118.534	C
17645 Saticoy St. Northridge	USC 03	180	90	40.4	34.209	118.517	D
13232 Kagel Can. Rd. Pacoima	USC 05	45	315	34.6	34.251	118.420	C
9210 Sunland Bvd…Sun Valley	USC 08	310	220	29.6	34.235	118.367	C
Coldwater Cany… Studio City	USC 10	182	92	29.1	34.146	118.413	D
542 N. Buena Vista St., Burbank	USC 12	340	250	23.0	34.168	118.332	D
Mulholland Dr., Beverly Hills	USC 13	9	279	31.1	34.132	118.439	D
Mulholland Dr., Beverly Hills	USC 14	122	32	27.9	34.127	118.405	C
700 N. Faring Rd., LA	USC 16	90	0	30.1	34.089	118.435	C
600 E Grand Ave., San Gabriel	USC 19	180	270	0.8	34.091	118.093	C
4312 S. Grand Ave., LA	USC 22	180	90	16.7	34.005	118.279	D
2369 E. Vernon Ave., LA	USC 25	173	83	12.6	34.004	118.230	D
624 Cypress Ave., LA	USC 33	143	53	10.5	34.088	118.222	C
3035 Fletcher Dr., LA	USC 34	234	144	13.2	34.115	118.244	D
Sunset Blvd., Pacific Palisades	USC 49	190	280	41.1	34.042	118.554	D
Pacific Coast Hwy., Malibu	USC 51	150	60	62.7	34.024	118.787	C
Las Virgines Rd., Calabasas	USC 52	290	200	54.8	34.151	118.696	C
Lst. Can. Rd., Canyon Country	USC 57	0	270	48.0	34.419	118.426	D
New York Ave., La Crescenta	USC 60	180	90	22.4	34.238	118.253	D
Big Tujunga station	USC 61	352	262	25.4	34.286	118.225	C
Angeles Nat. For., Mill Creek	USC 62	0	90	33.9	34.390	118.079	D
Las Palmas Ave., Glendale	USC 63	267	177	17.8	34.200	118.231	C
120 N. Oakbank, Glendora	USC 65	170	80	16.2	34.137	117.882	C
656 S. Grand Ave., Covina	USC 68	105	15	15.8	34.078	117.870	D

Holly Ave., Baldwin Park	USC 69	270	180	6.70	34.100	117.974	C
1271 W. Badillo, Covina	USC 70	0	270	11.7	34.087	117.915	D
1307 S. Orange, West Covina	USC 71	315	225	8.20	34.064	117.952	D
504 Rimgrove Ave., La Puente	USC 72	105	15	11.8	34.026	117.918	D
Colima Rd., Hacienda Heights	USC 73	230	140	11.0	33.990	117.942	D
950 Briarcliff Dr., La Habra	USC 74	90	0	13.5	33.921	117.972	D
E. Joslin St., Sante Fe Springs	USC 77	48	318	8.6	33.944	118.087	D
Castlegate St., Compton	USC 78	0	270	16.5	33.899	118.196	D
12500 Birchdale, Downey	USC 79	180	90	11.9	33.920	118.137	D
6979 Orange Ave., Long Beach	USC 80	10	280	17.3	33.881	118.176	D
21288 Water St., Carson	USC 81	270	180	24.5	33.836	118.239	D
6701 Del Amo, Lakewood	USC 84	90	0	19.4	33.846	118.099	D
5360 Saturn St., LA	USC 91	110	20	22.7	34.046	118.355	D
180 Campus Dr., Arcadia	USC 93	9	279	5.40	34.130	118.036	C
7420 Jaboneria, Bell Gardens	USC 94	297	207	8.50	33.965	118.158	D
1488 Old House Rd., Pasadena	USC 95	90	0	9.7	34.171	118.079	D

<u>Loma Prieta, October 18, 1989, M = 6.9</u>

Anderson Dam: Downstream	USGS 1652	340	250	20.0	37.166	121.628	C
Hollister Airport Diff Array	USGS 1656	255	165	25.4	36.888	121.413	D
Hollister City Hall Annex	USGS 1575	90	180	27.8	36.851	121.402	D
Stanford: SLAC Test Lab	USGS 1601	270	360	35.0	37.419	122.205	D
Hayward City Hall: N. FF	USGS 1129	64	334	58.7	37.679	122.082	C
APEEL Array Sta. 9	USGS 1161	227	137	46.4	37.478	122.321	C
Bear Valley Sta.5	USGS 1474	310	220	53.7	36.673	121.195	C
Bear Valley Sta.7	USGS 1478	310	220	53.7	36.483	121.180	A+B
Bear Valley Sta.10	USGS 1479	310	220	67.3	36.532	121.143	D
Bear Valley Sta.12	USGS 1481	310	220	50.9	36.658	121.249	D
Calasveras Reservoir South	USGS 1687	180	90	36.1	37.452	121.807	C
Cherry Flat Reservoir	USGS 1696	360	270	32.5	37.396	121.756	A+B
Hollister Sago Vault	USGS 1032	360	270	29.9	36.765	121.446	A+B
Sunol Fire Sta.	USGS 1688	180	90	49.9	37.597	121.880	C
Sunnyvale	--	360	270	27.5	37.402	122.024	D
Agnew	CDMG 57066	90	0	27.0	37.397	121.952	D
Capitola	CDMG 47125	90	0	8.60	36.974	121.952	D
Corralitos	CDMG 57007	90	0	0.10	37.046	121.803	C
Coyote Lake Dam: DS	CDMG 57504	285	195	21.7	37.124	121.551	C
Gilroy Array #1	CDMG 47379	90	0	10.5	36.973	121.572	A+B
Gilroy Array #2	CDMG 47380	90	0	12.1	36.982	121.556	D
Gilroy Array #3	CDMG 47381	90	0	14.0	36.987	121.536	D
Gilroy Array #4	CDMG 57382	90	0	15.8	37.005	121.522	D
Gilroy Array #6	CDMG 57383	90	0	19.9	37.026	121.484	C
Gilroy Array #7	CDMG 57425	90	0	24.3	37.033	121.434	D
Gavilon College Geol. Bldg.	CDMG 47006	67	337	10.9	36.973	121.568	C
Halls Valley	CDMG 57191	90	0	29.3	37.338	121.714	D
Hayward BART FF	CDMG 58498	310	220	57.7	37.670	122.086	C
Mission San Jose	CDMG 57064	90	0	42.0	37.530	121.919	C
Monterey City Hall	CDMG 47377	90	0	42.7	36.597	121.897	A+B
Piedmont Jr High School	CDMG 58338	45	315	77.2	37.823	122.233	A+B

San Fran.: Sierra Pt.	CDMG 58539	205	115	67.6	37.674	122.388	A+B
San Fran.: Rincon Hill	CDMG 58151	90	0	78.5	37.786	122.391	A+B
San Fran.: Diamond Heights	CDMG 58130	90	0	75.9	37.740	122.433	C
San Fran.: Airport	CDMG 58223	90	0	63.2	37.622	122.398	D
San Fran.: Pacific Heights	CDMG 58131	360	270	80.5	37.790	122.429	A+B
Saratoga	CDMG 58065	90	0	11.7	37.255	122.031	C
Santa Cruz	CDMG 58135	90	0	12.5	37.001	122.060	C
SAGO south	CDMG 47189	351	261	34.1	36.753	121.396	C
San Jose: Santa Teresa Hills	CDMG 57563	225	315	13.2	37.210	121.803	C
Salinas	CDMG 47179	250	160	31.4	36.671	121.642	D
Woodside	CDMG 58127	90	0	38.7	37.429	122.258	C
Yerba Buena Island	CDMG 58163	90	0	79.5	37.807	122.361	A+B

<u>Petrolia, April 25, 1992, M = 7.1</u>

Eureka – M&W	CDMG 89509	90	0	35.8	40.801	124.148	D
Fortuna: Supermarket FF	CDMG 89486	0	90	13.7	40.584	124.145	C
Petrolia	CDMG 89156	90	0	0.0	40.324	124.286	D
Rio Dell	CDMG 89324	2	272	12.3	40.503	124.100	C
Shelter Cove	CDMG 89530	0	90	32.6	40.026	124.069	C

<u>Landers, June 28, 1992, M = 7.3</u>

Amboy	CDMG 21081	90	0	68.3	34.560	115.743	A+B
Baker	CDMG 32075	140	50	88.3	35.272	116.066	C
Barstow	CDMG 23559	90	0	37.7	34.887	117.047	C
Big Bear Lake – Civic Center	CDMG 22561	270	360	45.4	34.238	116.935	C
Boron	CDMG 33083	90	0	92.4	35.002	117.650	C
Desert Shores	CDMG 12626	90	180	87.3	33.426	116.078	D
Desert Hot Springs	CDMG 12149	90	0	22.5	33.962	116.509	C
Fort Irwin	CDMG 24577	90	0	65.0	35.268	116.684	C
Hemet Fire Station	CDMG 12331	90	0	69.1	33.729	116.979	D
Hesperia	CDMG 23583	90	180	62.6	34.405	117.311	C
Indio – Coach. Canal	CDMG 12026	90	0	54.9	33.717	116.156	D
Indio - Fairgrounds	CDMG 12543	950	185	52.6	33.715	116.221	D
Joshua Tree	CDMG 22170	90	0	11.3	34.131	116.3114	C
Littlerock: Brainard Can.	CDMG 23592	90	180	117.9	34.486	117.98	A+B
Lake Cahuilla	CDMG 12624	94	184	60.1	33.628	116.280	A+B
Mt. Baldy	CDMG 23572	90	180	100.1	34.233	117.661	A+B
Meca - CVWD	CDMG 11625	90	180	77.5	33.564	115.987	D
Palmdale: Black Butte	CDMG 23585	90	180	93.3	34.586	117.728	A+B
Pearblossom: Pallet Creek	CDMG 24463	90	180	112.2	34.458	117.909	A+B
Phelan	CDMG 23597	90	180	77.5	34.467	117.520	C
Palm Springs	CDMG 12025	90	0	36.7	33.829	116.501	D
Pomona	CDMG 23525	90	0	117.6	34.056	117.748	D
Puerta La Cruz	CDMG 12168	90	0	95.0	33.324	116.683	C
Riverside Airport	CDMG 13123	270	180	96.2	33.951	117.446	C
San Bern: E &H	CDMG 23542	90	180	79.9	34.065	117.292	D
Silent Valley	CDMG 12206	90	0	51.3	33.851	116.852	A+B
Snow Creek	CDMG 12630	87	177	37.6	33.888	116.684	A+B
Twentynine Palms	CDMG 22161	90	0	41.9	34.021	116.009	A+B
Wrightwood: Jackson Flat	CDMG 23590	90	180	99.4	34.381	117.737	A+B

Wrightwood: Swarthout Valley	CDMG 23574	90	180	93.1	34.369	117.658	C
Yermo	CDMG 22074	90	0	26.3	34.903	116.823	D

<u>Northridge, January 17, 1994, M = 6.7</u>

Alhambra – Fremont Sch	CDMG 24461	90	360	36.2	34.070	118.150	C
Castaic Old Ridge Rt.	CDMG 24278	90	360	20.8	34.564	118.642	C
Century City - LACC north	CDMG 24389	90	360	17.4	34.063	118.418	B
Lake Hughes #1 fs	CDMG 24271	90	0	36.1	34674	118.430	C
Lake Hughes 4	CDMG 24469	90	0	31.9	34.650	118.478	D
Lake Hughes #4b	CDMG 24523	90	0	32.0	34.650	118.477	D
Lake Hughes #9	CDMG 24272	90	360	25.6	34.608	118.558	A+B
Lake Hughes #12a	CDMG 24607	90	180	21.S	34.571	118.560	C
Littlerock - Brainard Canyon	CDMG 23595	90	180	46.7	34.486	117.980	A+B
Long Beach - City Hall grds.	CDMG 14560	90	360	56.0	33.768	118.196	D
LA - Hollywood stor.blg.	CDMG 24303	90	360	20.0	34.090	118.339	D
Mt. Baldy - Elem. School	CDMG 23572	90	180	72.2	34.233	117.661	A+B
Mt. Wilson	CDMG 24399	90	360	36.5	34.224	118.057	A+B
Phelan - Wilson Ranch Rd.	CDMG 23597	90	180	86.4	34.467	117.520	C
Port Hueneme - NavalLab.	CDMG 25281	180	90	49.8	34.145	119.206	D
Rancho Cucamnga - Deer Can.	CDMG 23598	90	180	80.8	34.169	117.579	A+B
Rancho Palos Verdes	CDMG 14404	90	0	50.8	33.746	118.396	A+B
Riverside Airport	CDMG 13123	270	180	99.8	33.951	117.446	C
Sylmar- Co. Hospital PL	CDMG 24514	90	360	1.7	34.326	118.444	D
TaTzana Cedar Hill Nur. A	CDMG 24436	90	360	3.4	34.160	118.534	C
Wnghtwood - Jackson Flat	CDMG 23590	90	180	65.2	34.381	117.737	A+B
Wrightwood - Nielson Rnch	CDMG 23573	90	180	82.4	34.314	117.545	C
Wrightwood - Swarthout Vly.	CDMG 23574	90	180	72.3	34.369	117.658	C
17645 Saticoy St. Northridge	USC 03	180	90	0.2	34.209	118.517	D
12001 Chalon Rd. LA	USC 15	70	160	12.4	34.086	118.481	C
700 N. Faring Rd, LA	USC 16	0	90	14.1	34.089	118.435	C
8510 Wonderland Ave, LA	USC 17	185	95	15.4	34.I14	118.380	A+B
Willoughby Ave. Hollywood	USC 18	180	90	18.3	34.088	118.365	C
600E.Grand Av., San Gabriel	USC 19	180	270	39.4	34.091	118.093	C
2628 W. 15th. St., LA	USC 20	180	90	26.1	34.045	118.298	D
4312S.Grand Ave, LA	USC 22	180	90	30.4	34.005	118.279	D
2369 E. Vernon Ave, LA	USC 25	180	90	33.8	34.004	118.230	D
624 Cypress Ave., LA	USC 33	53	143	29.4	34.088	118.222	C
3036 Fletcher Dr., LA	USC 34	144	234	26.2	34.115	118.244	D
23536 Catskill Ave., Carson	USC 40	180	90	48.3	33.812	118.270	D
Rancho Palos Verdes	USC 44	5	95	53.1	33.740	118.335	D
148010sage Ave, Lawndale	USC 45	182	92	36.7	33.897	118.346	D
Manhattan Beach	USC 46	0	90	36.1	33.886	118.389	D
Canoga Park	USC 53	196	106	1.6	34.212	118.606	D
3960 Centinela St., LA	USC 54	155	245	22.9	34.001	118.431	D
Canyon Country	USC 57	0	270	11.4	34.419	118.426	D
1250 Howard Rd., Burbank	USC 59	330	60	16.5	34.204	118.302	A+B
New York Ave., La Crescenta	USC 60	180	90	18.8	34.238	118.254	D
Big Tujunga Station	USC 61	352	262	19.9	34.286	118.225	C
3320 Las Palmas Ave., Glendale	USC 63	177	267	22.3	34.200	118.231	C
120 N. Oakbank, Glendora	USC 65	80	170	54.8	34.137	117.882	C
Fairview Ave., El Monte	USC 66	185	95	45.2	34.093	118.019	D

237 Mel Canyon Rd., Duarte	USC 67	90	180	49.3	34.150	117.939	C
656 S. Grand Ave., Covina	USC 68	344	74	58.1	34.078	117.871	D
3699 Holly Ave., Baldwin Park	USC 69	180	270	48.5	34.100	117.974	C
1271 W. Badillo, Covina	USC 70	360	270	54.0	34.087	117.915	D
S. Orange Ave., West Covina	USC 71	315	225	52.1	34.064	117.952	D
504 Rimgrove Ave., La Puente	USC 72	15	105	57.0	34.026	117.918	D
Colima Rd., Hacienda Heights	USC 73	140	230	57.3	33.990	117.942	D
6302 S. Alta Dr. Whittier	USC 75	0	90	48.9	34.015	118.029	C
E. Joslin St., Santa Fe Springs	USC 77	30	120	48.3	33.944	118.087	D
14637 Castlegate St., Compton	USC 78	360	270	44.2	33.899	118.196	D
21288 Water St., Carson	USC 81	180	270	47.4	33.836	118.240	D
Terminal Island	USC 82	330	240	55.8	33.736	118.269	D
Huntington Beach	USC 83	290	200	67.9	33.727	118.044	D
Del Amo Blvd., Lakewood	USC 84	0	90	54.6	33.846	118.099	D
6861 Santa Rita, Garden Grove	USC 85	360	270	64.7	33.790	118.012	D
La Palma Ave., BuenaPark	USC 86	180	90	60.0	33.847	118.018	D
200 S. Flower Ave., Brea	USC 87	20	290	64.9	33.916	117.896	D
2000 W. Ball Rd., Anaheim	USC 88	0	90	66.9	33.817	117.951	D
5360 Saturn St., LA	USC 91	20	110	22.3	34.046	118.355	D
180 Campus Dr., Arcadia	USC 93	9	279	41.9	34.130	118.036	C
7420 Jabonena, BellGardens	USC 94	310	220	41.7	33.965	118.158	D
3620 S. Vermont Ave., LA	USC 96	0	90	28.1	34.022	118.293	D
855 Arcadia Ave., Arcadia	USC 99	172	262	40.1	34.127	118.059	D

Appendix B–Supplemental Plots for Regression Analysis of Pseudo-Velocity

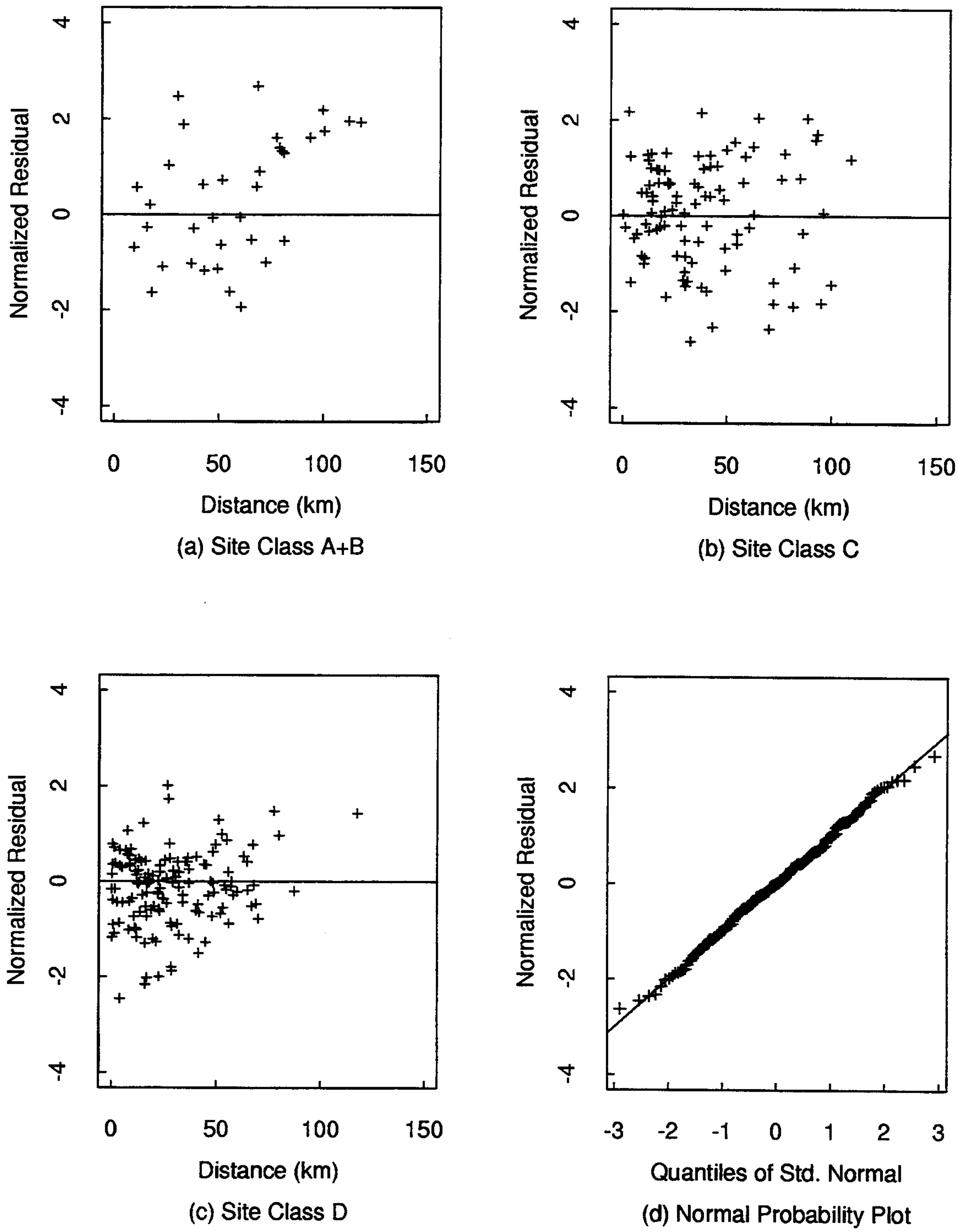

Fig. B.1 Normalized Pseudo-Velocity Residual Plots for $T = 0.5$ sec

(5% Damping)

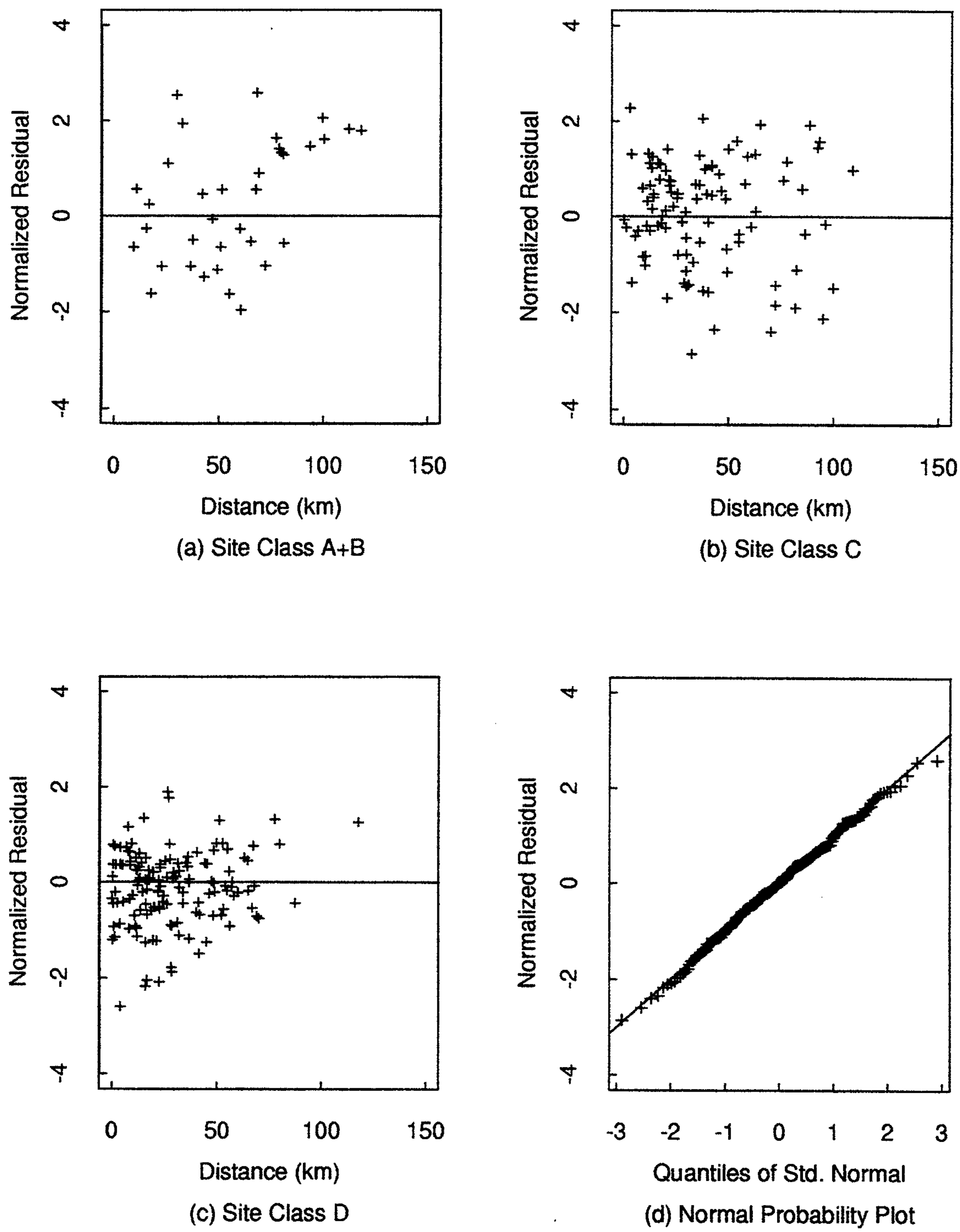

Fig. B.2 Normalized Pseudo-Velocity Residual Plots for $T = 1.0$ sec (5% Damping)

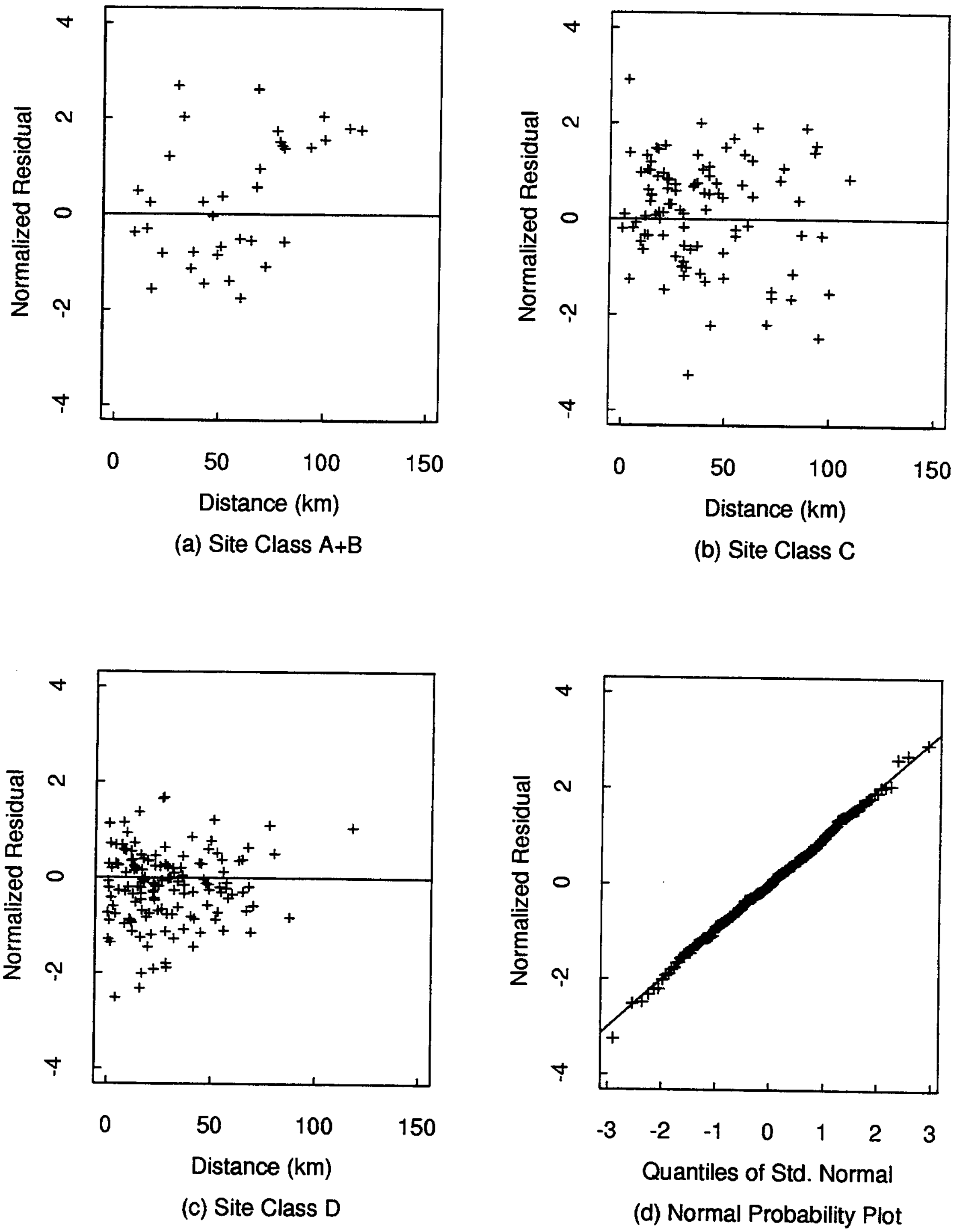

Fig. B.3 Normalized Pseudo-Velocity Residual Plots for $T = 2.0$ sec
(5% Damping)

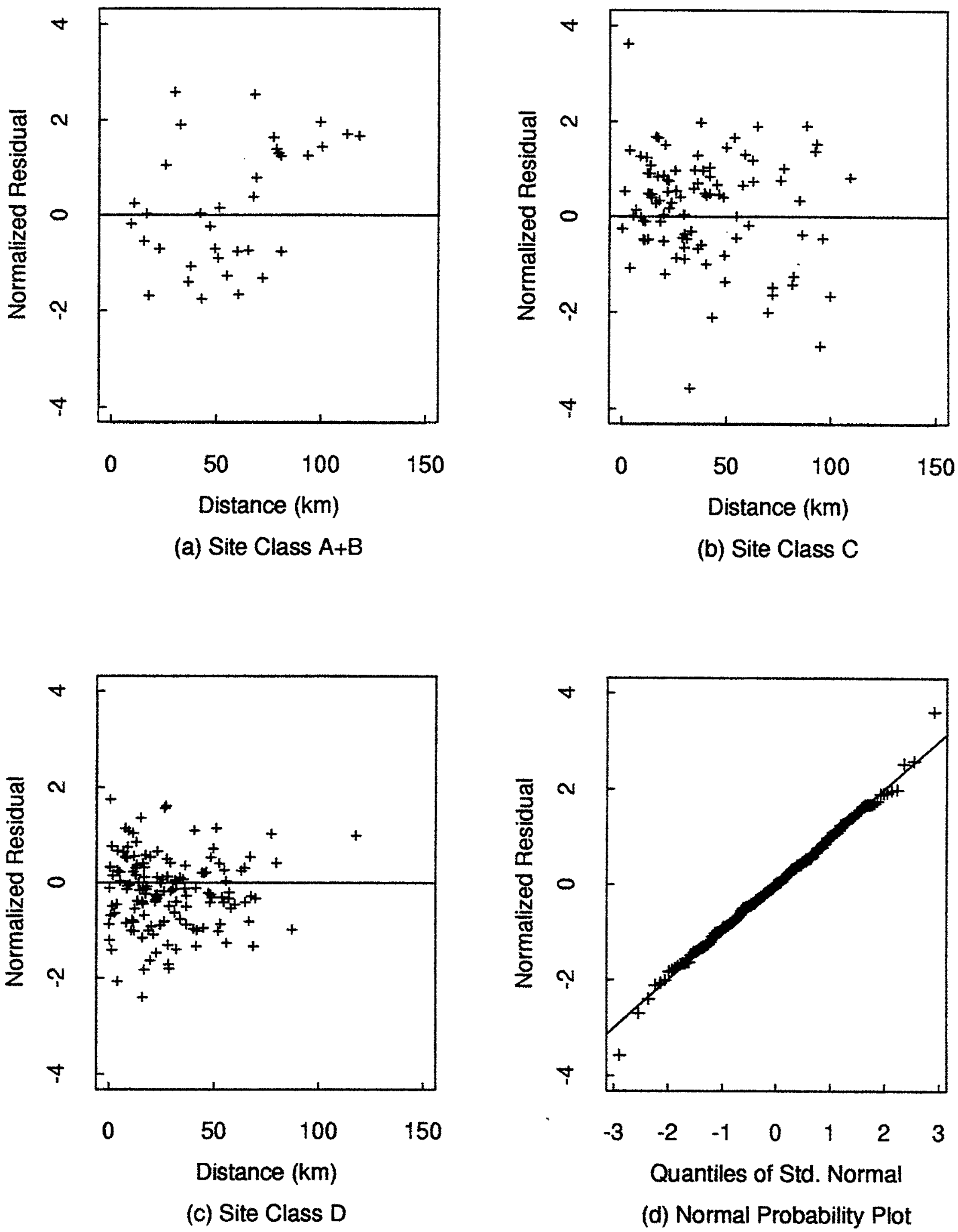

Fig. B.4 Normalized Pseudo-Velocity Residual Plots for $T = 3.0$ sec
(5% Damping)

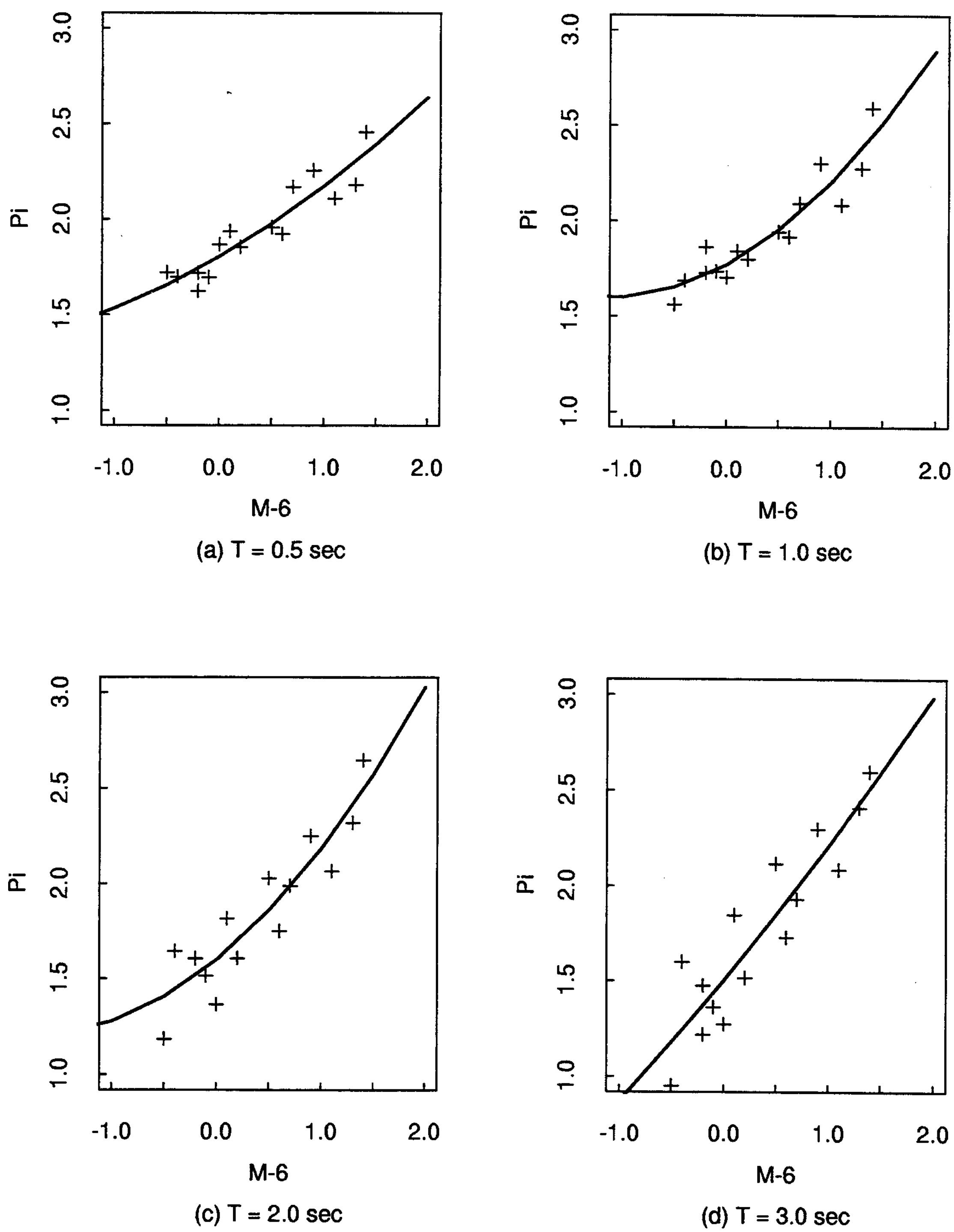

Fig. B.5 Curve-Fitting of P_i versus (M-6) Relationships for V

(5% Damping)

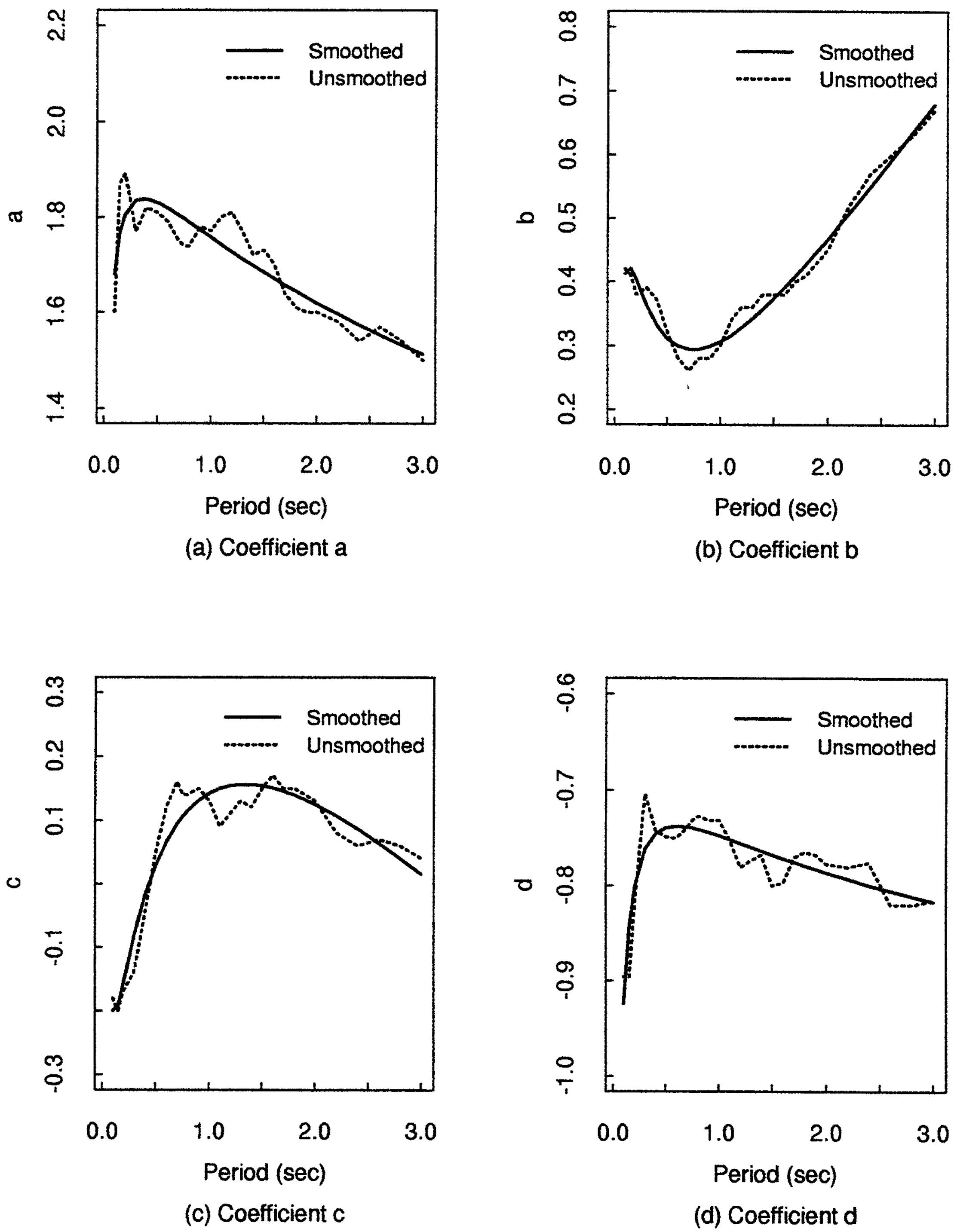

Fig. B.6 Smoothed and Unsmoothed Regression Coefficients for *V*
(5% Damping)

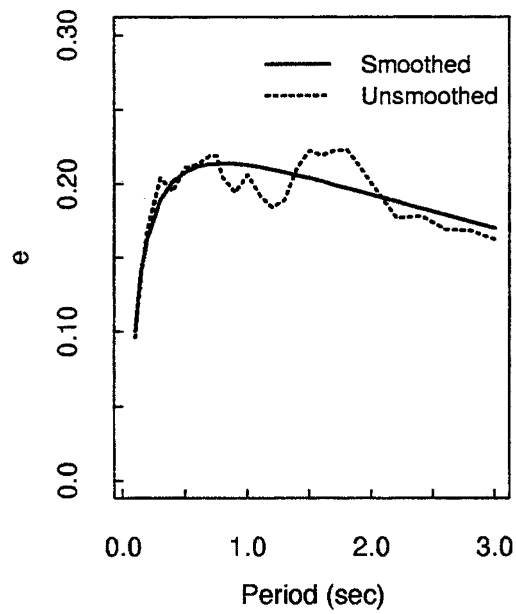

(e) Coefficient e

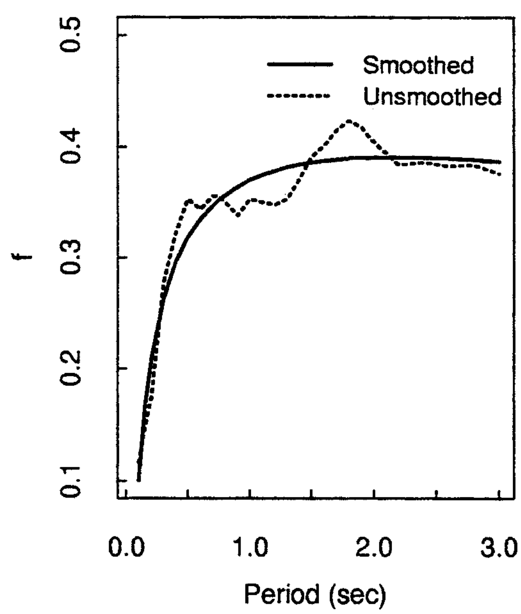

(f) Coefficient f

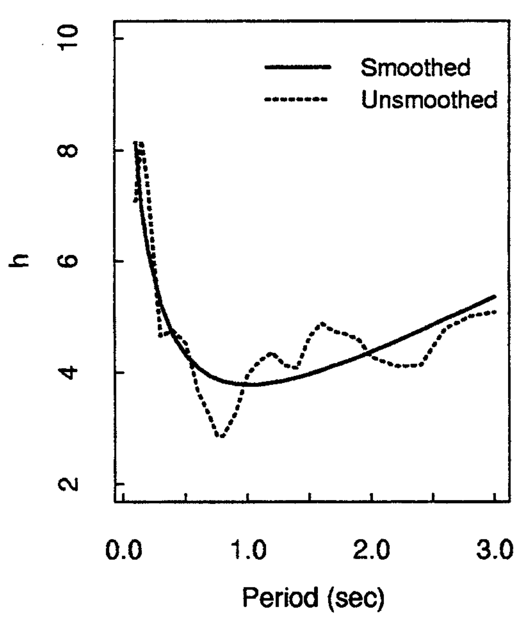

(g) Coefficient h

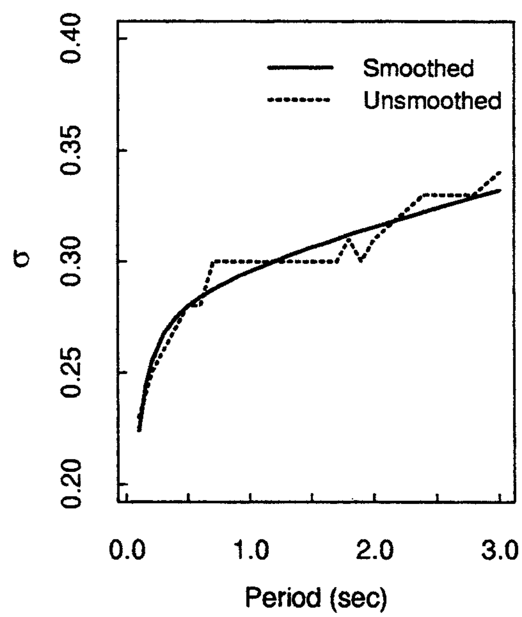

(h) Coefficient

Fig. B.6 Smoothed and Unsmoothed Regression Coefficients for *V*-continued
(5% Damping)

Appendix C–Supplemental Plots for Regression Analysis of Absorbed Energy

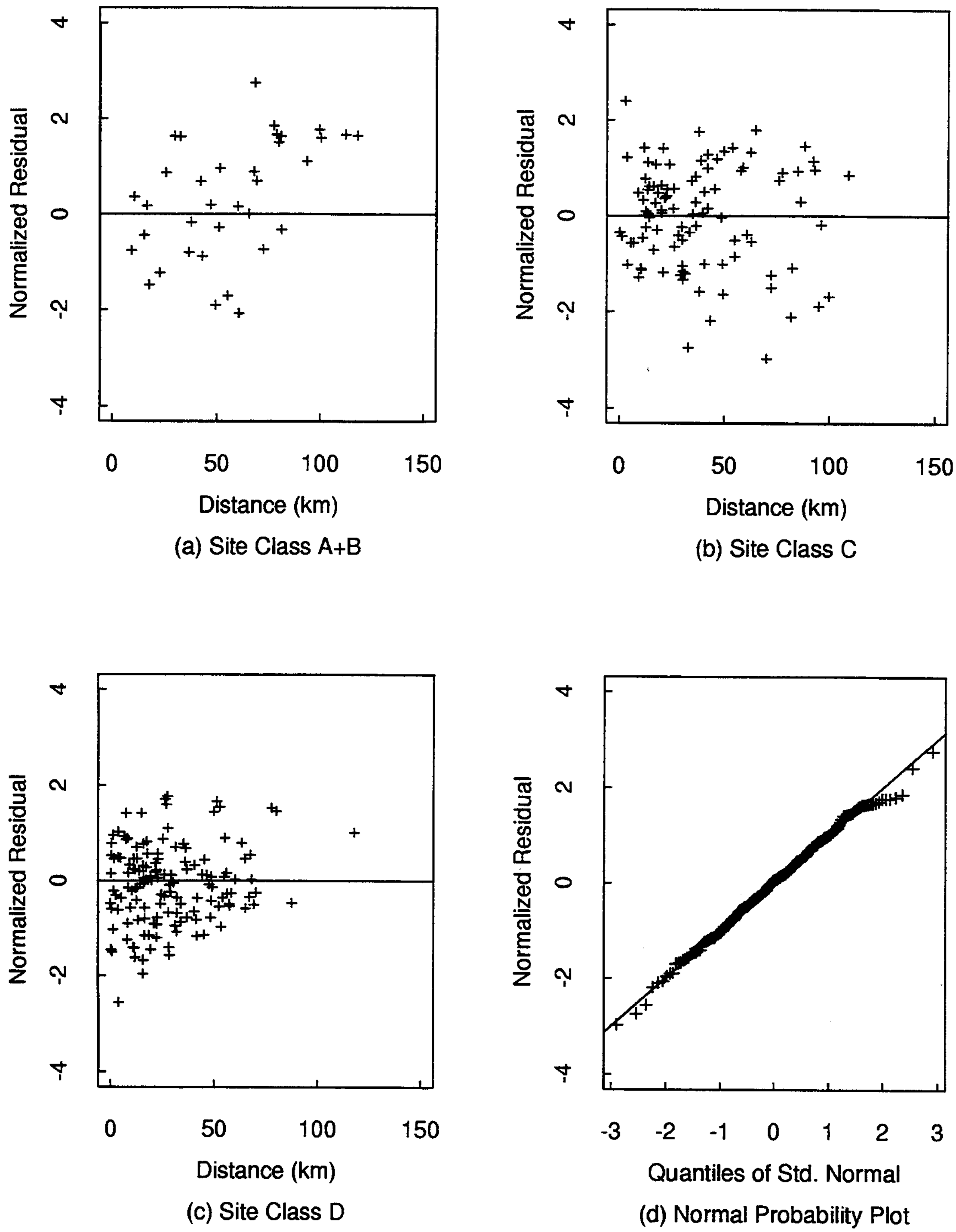

Fig. C.1 Normalized V_a Residual Plots for $T = 0.5$ sec

(5% Damping, Ductility Factor = 4)

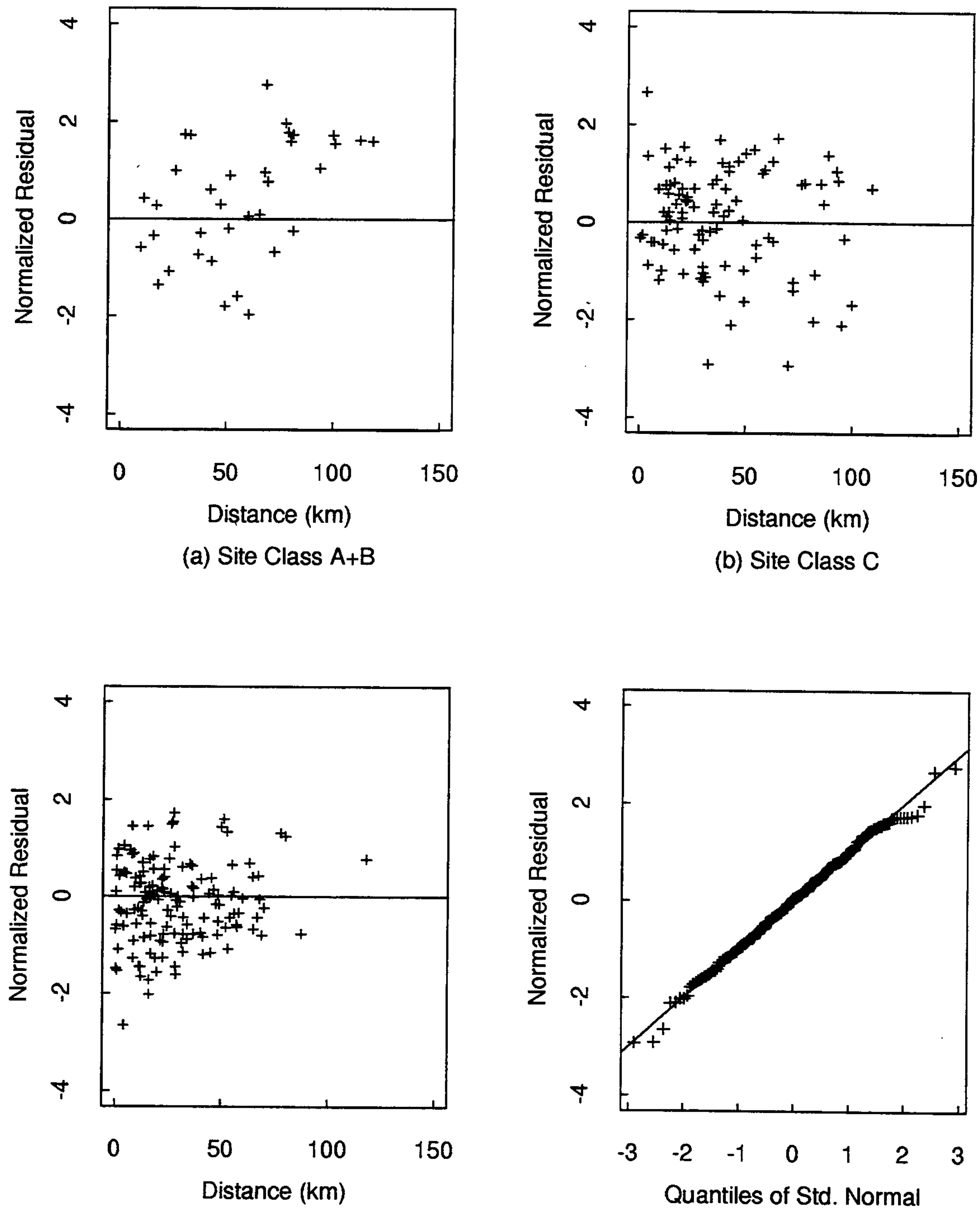

(a) Site Class A+B

(b) Site Class C

(c) Site Class D

(d) Normal Probability Plot

Fig. C.2 Normalized V_a Residual Plots for $T = 1.0$ sec
(5% Damping, Ductility Factor = 4)

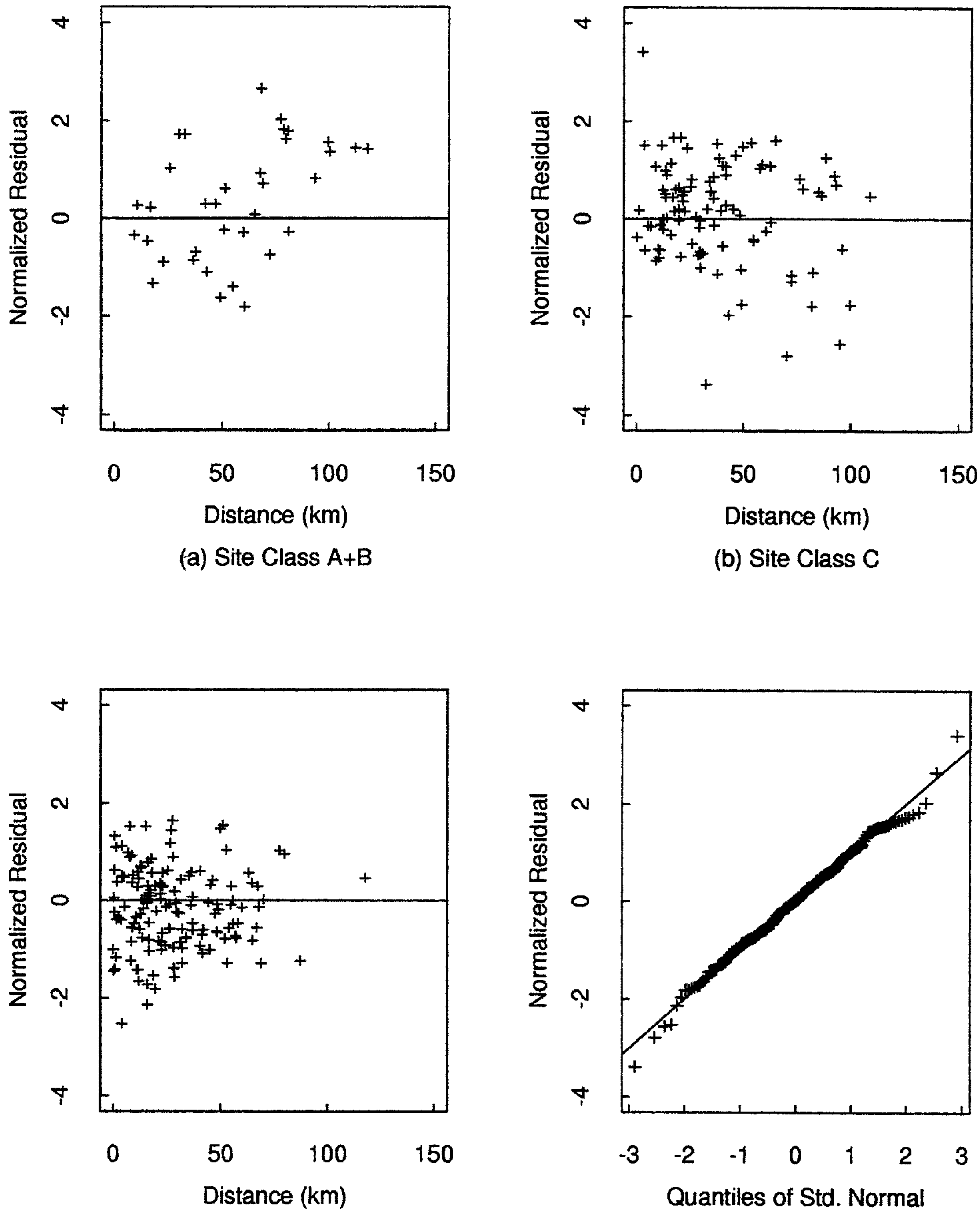

Fig. C.3 Normalized V_a Residual Plots for $T = 2.0$ sec

(5% Damping, Ductility Factor = 4)

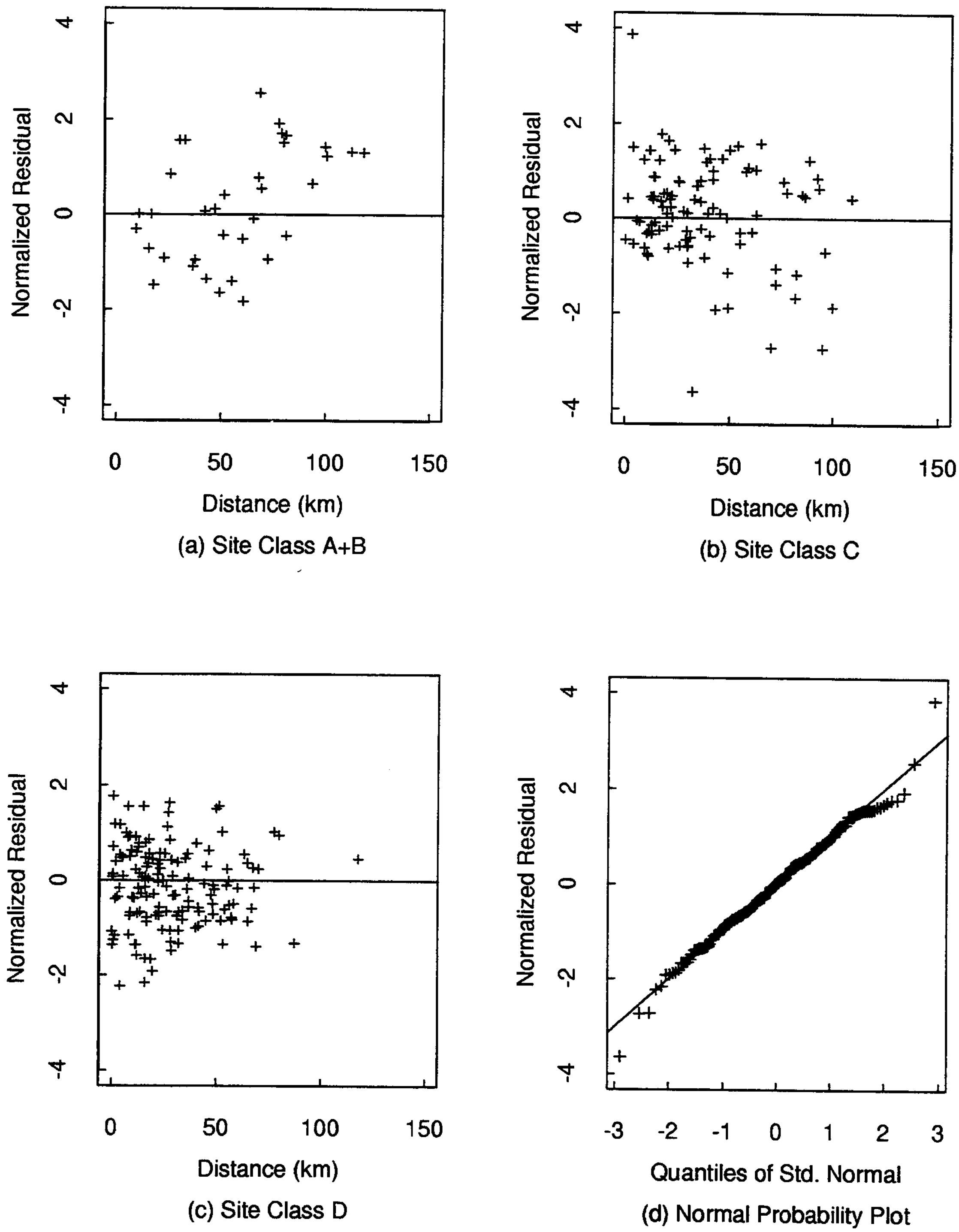

Fig. C.4 Normalized V_a Residual Plots for $T = 3.0$ sec
(5% Damping, Ductility Factor = 4)

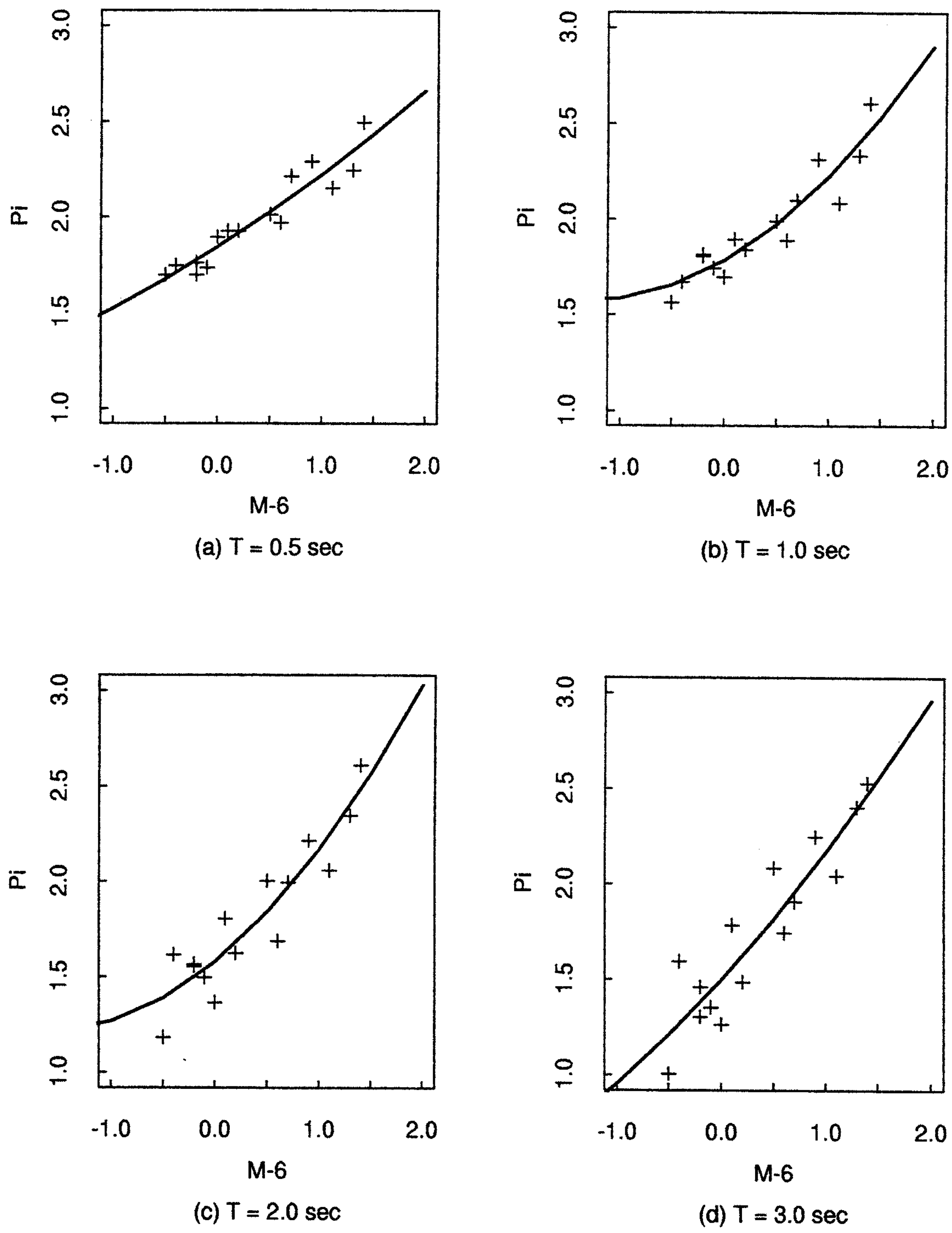

Fig. C.5 Curve-Fitting of P_i versus (M-6) Relationships for V_a

(5% Damping, Ductility Factor = 4)

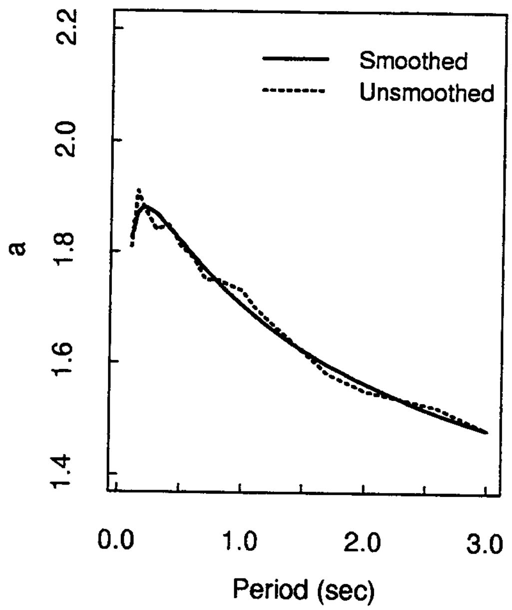

(a) Coefficient a

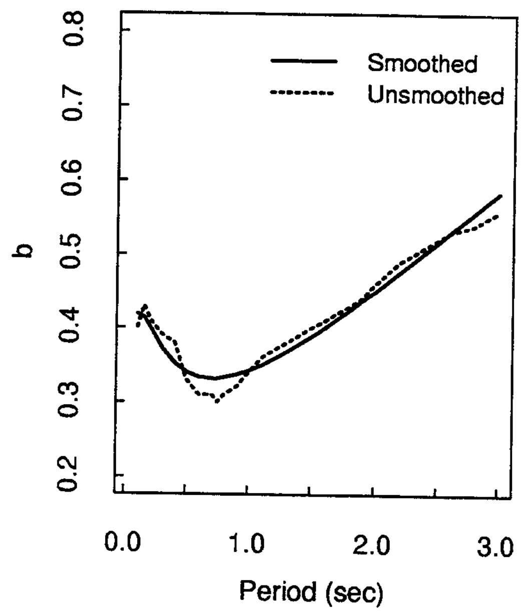

(b) Coefficient b

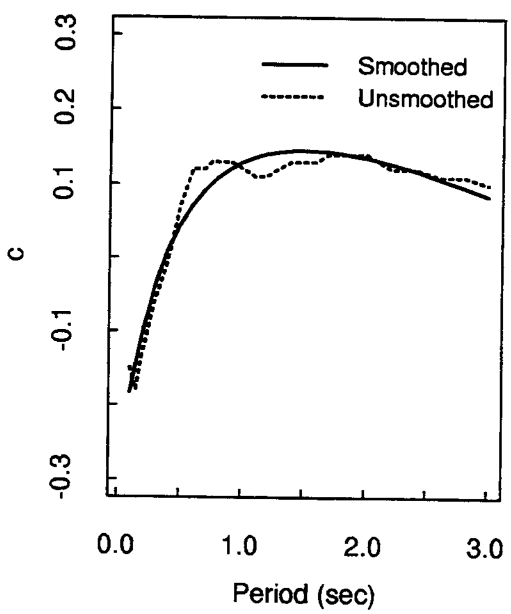

(c) Coefficient c

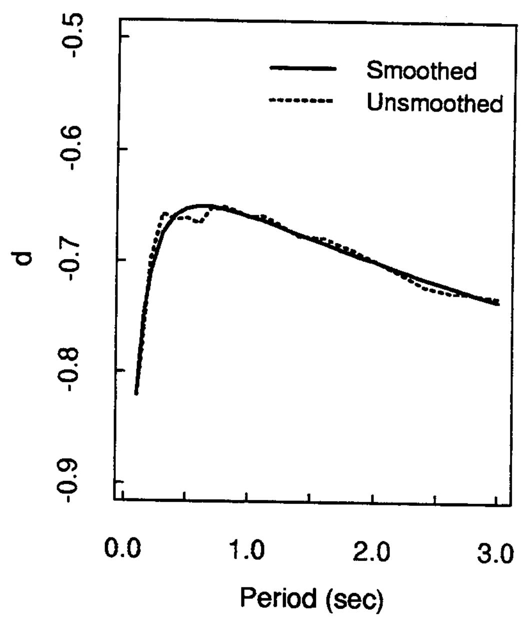

(d) Coefficient d

Fig. C.6 Smoothed and Unsmoothed Regression Coefficients for V_a
(5% Damping, Ductility Factor = 4)

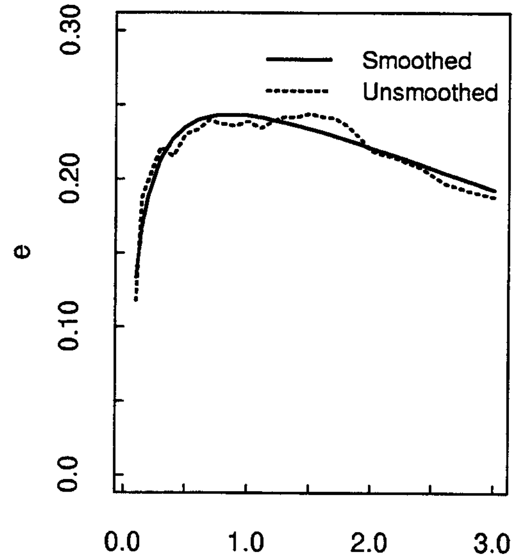

(e) Coefficient e

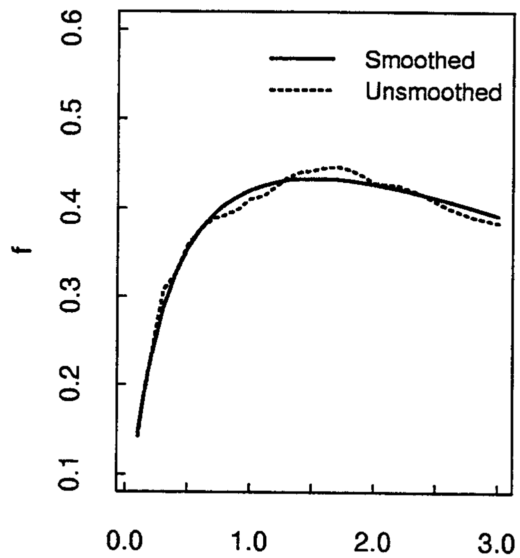

(f) Coefficient f

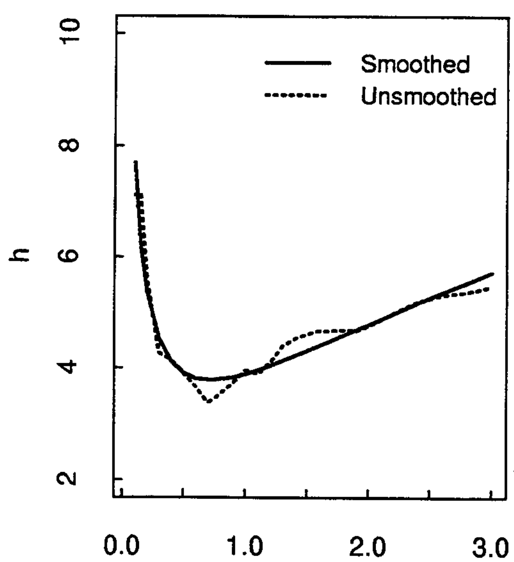

(g) Coefficient h

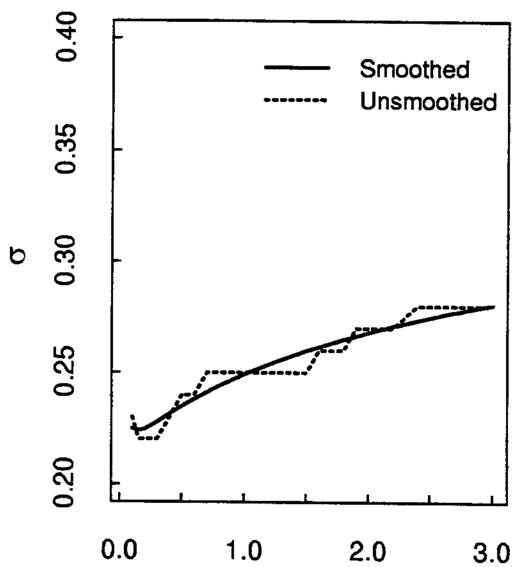

(h) Coefficient

Fig. C.6 Smoothed and Unsmoothed Regression Coefficients for V_a-continued (5% Damping, Ductility Factor = 4)

PEER REPORTS

PEER reports are available from the National Information Service for Earthquake Engineering (NISEE). To order PEER reports, please contact the Pacific Earthquake Engineering Research Center, 1301 South 46th Street, Richmond, California 94804-4698. Tel.: (510) 231-9468; Fax: (510) 231-9461.

PEER 2000/06 *Seismic Evaluation and Analysis of 230-kV Disconnect Switches.* Amir S. J. Gilani, Andrew S. Whittaker, Gregory L. Fenves, Chun-Hao Chen, Henry Ho, Eric Fujisaki. July 2000. $26.00

PEER 2000/04 *An Evaluation of Seismic Energy Demand: An Attenuation Approach.* Chung-Che Chou and Chia-Ming Uang. July 1999. $20.00

PEER 2000/03 *Framing Earthquake Retrofitting Decisions: The Case of Hillside Homes in Los Angeles.* Detlof von Winterfeldt, Nels Roselund, and Alicia Kitsuse. March 2000. $13.00

PEER 2000/01 *Further Studies on Seismic Interaction in Interconnected Electrical Substation Equipment.* Armen Der Kiureghian, Kee-Jeung Hong, and Jerome L. Sackman. November 1999. $20.00

PEER 1999/14 *Seismic Evaluation and Retrofit of 230-kV Porcelain Transformer Bushings*. Amir S. Gilani, Andrew S. Whittaker, Gregory L. Fenves, and Eric Fujisaki. December 1999. $26.00

PEER 1999/12 *Rehabilitation of Nonductile RC Frame Building Using Encasement Plates and Energy-Dissipating Devices.* Mehrdad Sasani, Vitelmo V. Bertero, James C. Anderson. December 1999. $26.00

PEER 1999/11 *Performance Evaluation Database for Concrete Bridge Components and Systems under Simulated Seismic Loads.* Yael D. Hose and Frieder Seible. November 1999. $20.00

PEER 1999/10 *U.S.-Japan Workshop on Performance-Based Earthquake Engineering Methodology for Reinforced Concrete Building Structures.* December 1999. $33.00

PEER 1999/09 *Performance Improvement of Long Period Building Structures Subjected to Severe Pulse-Type Ground Motions*. James C. Anderson, Vitelmo V. Bertero, and Raul Bertero. October 1999. $26.00

PEER 1999/08 *Envelopes for Seismic Response Vectors.* Charles Menun and Armen Der Kiureghian. July 1999. $26.00

PEER 1999/07 *Documentation of Strengths and Weaknesses of Current Computer Analysis Methods for Seismic Performance of Reinforced Concrete Members.* William F. Cofer. November 1999. $15.00

PEER 1999/06 *Rocking Response and Overturning of Anchored Equipment under Seismic Excitations.* Nicos Makris and Jian Zhang. November 1999. $15.00

PEER 1999/05 *Seismic Evaluation of 550 kV Porcelain Transformer Bushings.* Amir S. Gilani, Andrew S. Whittaker, Gregory L. Fenves, and Eric Fujisaki. October 1999. $15.00

PEER 1999/04 *Adoption and Enforcement of Earthquake Risk-Reduction Measures.* Peter J. May, Raymond J. Burby, T. Jens Feeley, and Robert Wood. $15.00

PEER 1999/03 *Task 3 Characterization of Site Response General Site Categories*. Adrian Rodriguez-Marek, Jonathan D. Bray, and Norman Abrahamson. February 1999. $20.00

PEER 1999/02 *Capacity-Demand-Diagram Methods for Estimating Seismic Deformation of Inelastic Structures: SDF Systems*. Anil K. Chopra and Rakesh Goel. April 1999. $15.00

PEER 1999/01 *Interaction in Interconnected Electrical Substation Equipment Subjected to Earthquake Ground Motions.* Armen Der Kiureghian, Jerome L. Sackman, and Kee-Jeung Hong. February 1999. $20.00

PEER 1998/08 *Behavior and Failure Analysis of a Multiple-Frame Highway Bridge in the 1994 Northridge Earthquake.* Gregory L. Fenves and Michael Ellery. December 1998. $20.00

PEER 1998/07 *Empirical Evaluation of Inertial Soil-Structure Interaction Effects.* Jonathan P. Stewart, Raymond B. Seed, and Gregory L. Fenves. November 1998. $26.00

PEER 1998/06 *Effect of Damping Mechanisms on the Response of Seismic Isolated Structures.* Nicos Makris and Shih-Po Chang. November 1998. $15.00

PEER 1998/05 *Rocking Response and Overturning of Equipment under Horizontal Pulse-Type Motions.* Nicos Makris and Yiannis Roussos. October 1998. $15.00

PEER 1998/04 *Pacific Earthquake Engineering Research Invitational Workshop Proceedings, May 14–15, 1998: Defining the Links between Planning, Policy Analysis, Economics and Earthquake Engineering.* Mary Comerio and Peter Gordon. September 1998. $15.00

PEER 1998/03 *Repair/Upgrade Procedures for Welded Beam to Column Connections.* James C. Anderson and Xiaojing Duan. May 1998. $33.00

PEER 1998/02 *Seismic Evaluation of 196 kV Porcelain Transformer Bushings.* Amir S. Gilani, Juan W. Chavez, Gregory L. Fenves, and Andrew S. Whittaker. May 1998. $20.00

PEER 1998/01 Unassigned.